

Electronic Thesis and Dissertation Repository

2-19-2021 10:00 AM

Metallization Process for 3D Printed Electronics: from i3DP II to 3D Co-printing Technology

Junfeng Xiao, *The University of Western Ontario*

Supervisor: Yang, Jun, *The University of Western Ontario*

A thesis submitted in partial fulfillment of the requirements for the Doctor of Philosophy degree in Mechanical and Materials Engineering

© Junfeng Xiao 2021

Follow this and additional works at: <https://ir.lib.uwo.ca/etd>



Part of the [Manufacturing Commons](#)

Recommended Citation

Xiao, Junfeng, "Metallization Process for 3D Printed Electronics: from i3DP II to 3D Co-printing Technology" (2021). *Electronic Thesis and Dissertation Repository*. 7668.
<https://ir.lib.uwo.ca/etd/7668>

This Dissertation/Thesis is brought to you for free and open access by Scholarship@Western. It has been accepted for inclusion in Electronic Thesis and Dissertation Repository by an authorized administrator of Scholarship@Western. For more information, please contact wlsadmin@uwo.ca.

Abstract

3D printing has emerged as a powerful additive manufacturing technique and becomes as a viable alternative to conventional manufacturing processes in an increasing number of applications. Thus, the development of printable materials also continues to expand, while polymers are still the most utilized materials in 3D printing. There is a great advance for developing polymers with versatile mechanical and chemical properties. However, the end-use products are demanding various functions, such as metallization, self-healing, antimicrobial, water treatment, and so on. It is imperative to develop functional 3D printed polymeric materials to achieve enhanced functionalities.

Usually, one polymer can meet one specific application. This has considerably limited the capability of 3D printing technology, especially for the photopolymerization based 3D printing. To overcome the challenges, in this work I have proposed to advance the initiator integrated 3D printing technology to a more universal approach by introducing various active groups into polymer resins to fabricate functional materials and devices, together with a facile post-printing surface modification process. This allows polymeric structure to be metallized for electronics applications.

The strategy of this technology is using a bioinspired approach to engineer seed components into 3D printing resins, which allows the printed structures to possess the ability of functionalization. Dopamine and modified-dopamine are incorporated into water-soluble and lipid-soluble 3D printing resins respectively. After printing, the dopamine-integrated structures serve as active seeds to assist the following metallization process. Naturally derived polyphenols are also integrated into 3D printing resins, providing the customized resin with the capability of metallization, along with other functional properties development. Through secondary reactions, the applications of functional electronics fabrication, water treatment, surface hydrophilization and hydrophobization are demonstrated. Beside materials development, a dual-light 3D printing technology is developed as a 3D co-printing method, which is employed to fabricate 3D printed electronics with a customized 3D printing resin integrated with metal precursors.

In summary, the central strategy is to incorporate active chemical groups with desired functionalities, like high-binding ability, reducing ability, and etc., to develop new 3D printing materials for creation of functional surfaces of the 3D printed objects. This technology allows one 3D printing polymer to possess the capability of providing multiple specific applications through simple post-printing processes.

Keywords

Keywords: 3D printing of functional material, post-printing process, dopamine, water-soluble resin, dopamine methyl acrylamide, phenol, pyrogallol, multifunctional 3D printed electronics, chemical resistance, 3D co-printing.

Summary for Lay Audience

3D printing is becoming an important manufacturing technique to manufacture complex structures that can't be realized by conventional manufacturing processes. Thus, more and more new materials are developed to meet the demands. However, the end-use applications are not always fixed, which is still demanding more development.

Polymers are still the most popular materials in 3D printing industry, while one polymer can often only meet one specific application. This requires development of a variety of new materials, along with corresponding printing techniques to meet the need. This is not only time consuming, but also lead to more technique hurdles, even increase the environmental burden.

A feasible technology is to incorporate active seed components into 3D printing resin. After printing, the printed structure will have functional chemical groups on the surface to develop new functions. In this study, dopamine, modified-dopamine and polyphenols are integrated into different kinds of 3D printing resins. The parameters are optimized not to affect the printability. Finally, newly developed 3D printing materials are able to be metallized or develop various other desired functions.

A dual-light 3D printing technology is also developed in this study, with one light for structure building, the other for conductive traces fabrication. With the unique technology, a 3D co-printing technology is developed for 3D printed electronics application.

Co-Authorship Statement

This doctoral thesis has been carefully prepared according to the regulations for an integrated-article format thesis stipulated by the Faculty of Graduate and Postdoctoral Studies at Western University, and has been co-authored as follows:

Chapter 2: Dopamine assisted metallization process in water-soluble 3D printing resin

All the preparation for experimental testing and set-up was undertaken by J.F. Xiao under the supervision of Dr. J. Yang. Theoretical analyses were conducted by J.F. Xiao under the supervision of Dr. J. Yang. Experimental testing was performed by J.F. Xiao under the supervision of Dr. J. Yang. Chapter 2 was drafted by J.F. Xiao and reviewed by supervision of Dr. J. Yang. A paper co-authored by J.F. Xiao, D.X. Zhang, Q.Q. Guo and J. Yang is to be submitted.

Chapter 3: A modified-dopamine customized UV resin for electroless metallization in 3D printing

All the preparation for experimental testing and set-up was undertaken by J.F. Xiao under the supervision of Dr. J. Yang. Theoretical analyses were conducted by J.F. Xiao under the supervision of Dr. J. Yang. Experimental testing was performed by J.F. Xiao under the supervision of Dr. J. Yang. Chapter 3 was drafted by J.F. Xiao and reviewed by supervision of Dr. J. Yang. A paper co-authored by J.F. Xiao, D.X. Zhang, X.Y. Yin, Q.Q. Guo and J. Yang is to be submitted.

Chapter 4: Metallization and functionalization of 3D printed polymers assisted with polyphenols

All the preparation for experimental testing and set-up was undertaken by J.F. Xiao under the supervision of Dr. J. Yang. Theoretical analyses were conducted by J.F. Xiao under the supervision of Dr. J. Yang. Experimental testing was performed by J.F. Xiao under the supervision of Dr. J. Yang. Chapter 4 was drafted by J.F. Xiao and reviewed by supervision of Dr. J. Yang. A paper co-authored by J.F. Xiao, D.X. Zhang, X.Y. Yin, Q.Q. Guo and J. Yang is to be submitted.

Chapter 5: 3D Co-printing of 3D electronics with a dual light source technology

All the preparation for experimental testing and set-up was undertaken by J.F. Xiao under the supervision of Dr. J. Yang. Theoretical analyses were conducted by J.F. Xiao under the supervision of Dr. J. Yang. Experimental testing was performed by J.F. Xiao under the supervision of Dr. J. Yang. Chapter 5 was drafted by J.F. Xiao and reviewed by supervision of Dr. J. Yang. A paper co-authored by J.F. Xiao, D.X. Zhang, Q.Q. Guo and J. Yang is submitted to *Advanced Functional Materials*.

Acknowledgments

It was a great journey and I will cherish the experiences and memories as Western University. I am grateful to have a great many people who provide encouragement, trust, guidance, joy, and friendship.

Firstly, I would like to sincerely thank my supervisor-Prof. Jun Yang. His encouragement of developing my own thoughts was a big deal for me. I truly appreciate Prof. Jun Yang trust and all the opportunities he provided, which pushed me to explore things that I never thought of before. I also would like to thank my supervisor committees, Prof. G.K. Knopf and Prof. O.R. Tutuna-Fatan, for their co-supervision and guidance.

To my colleagues and friends at Western, I am very fortunate to have met you here. I would like to express my special thanks to Dr. Dongxing Zhang, Dr. Qiuquan Guo, and Dr. Xiangyu Yin, for their stimulating discussions with me, help with experimental setup and general advice. It was my honor to be part of Yang's MEMS team.

Finally, I would like to thank my parents, for always supporting me emotionally and financially. They have encouraged me, stood by my decisions and for that I am eternally gratefully. It simply would not have been possible without you.

Table of Contents

Abstract.....	ii
Summary for Lay Audience.....	iv
Co-Authorship Statement.....	v
Acknowledgments.....	vii
Table of Contents.....	viii
List of Tables.....	xii
List of Figures.....	xiii
Chapter 1.....	1
1 Introduction to 3D printing metallic structures and 3D electronics.....	1
1.1 Introduction of 3D printing technology.....	1
1.1.1 History of 3D printing.....	1
1.1.2 3D printing techniques.....	4
1.2 3D printing of metallic structures.....	11
1.2.1 Direct metal 3D printing.....	12
1.2.2 Indirect metal 3D printing.....	14
1.3 3D printed electronics.....	19
1.3.1 3D printed electronics techniques.....	20
1.3.2 Conductive materials.....	26
1.3.3 Post-treatment process.....	31
1.3.4 Recent progress in 3D printed electronics.....	33
1.4 Challenges and objectives.....	41
1.5 Outline of the thesis.....	45
Chapter 2.....	56
2 Dopamine assisted metallization process in water-soluble 3D printing resin.....	56

2.1	Introduction.....	56
2.2	Experimental section.....	59
2.2.1	Chemicals and materials	59
2.2.2	Preparation of customized 3D printing UV resin	59
2.2.3	Metallization of the 3D printed structures	60
2.2.4	Characterization	61
2.3	Results and discussion	61
2.3.1	Printability of the integrated resin and metallization process	61
2.3.2	Formula optimization of the integrated resin.....	65
2.3.3	Surface morphology of metallic parts.....	68
2.3.4	3D printing of complex metallic structures	68
2.3.5	The applicability of other phenol/polyphenol and water-soluble resin	70
2.4	Conclusions.....	71
	Chapter 3.....	76
3	A modified-dopamine customized UV resin for electroless metallization in 3D printing	76
3.1	Introduction.....	76
3.2	Experimental section.....	77
3.2.1	Chemicals and materials	77
3.2.2	Synthesis of dopamine methyl acrylamide	77
3.2.3	Preparation of customized 3D printing material.....	78
3.2.4	Metallization of the 3D printed structures	78
3.2.5	In situ repairing of metallic structures	80
3.2.6	Characterization	80
3.3	Results and discussion	80
3.3.1	DMA-integrated 3D printing UV resin.....	80
3.3.2	Printability of the DMA-integrated resin.....	81

3.3.3	UV-visible spectrum of DMA-integrated resin	82
3.3.4	Effect of DMA on exposure time during 3D printing.....	83
3.3.5	Confirmation of DMA distributed on the surface.....	84
3.3.6	3D printing of complex metallic structures	87
3.3.7	In situ repairing of metallic structures	90
3.4	Conclusions.....	92
Chapter 4.....		95
4	Metallization and functionalization of 3D printed polymers assisted with polyphenols	95
4.1	Introduction.....	95
4.2	Experimental section.....	97
4.2.1	Chemicals and materials	97
4.2.2	Solubility test	98
4.2.3	Metallization	98
4.2.4	Demonstration of a dual metal actuator	99
4.2.5	Adsorption measurement for water purification.....	100
4.2.6	Surface hydrophilization, hydrophobization and oil-water separation... ..	100
4.3	Results and discussion	101
4.3.1	Lipophilic polyphenols screening	101
4.3.2	Silver reduction with the polyphenol modified resin.....	102
4.3.3	Characterization of the PG-integrated resin.....	105
4.3.4	3D printing of metallic structures	111
4.3.5	In situ repairing of the 3D printed metallic structures	114
4.3.6	Multifunctional 3D printed electronics fabrication.....	116
4.3.7	Water treatment.....	121
4.3.8	Surface hydrophilization.....	124

4.3.9	Surface hydrophobization	125
4.3.10	Oil-water separation.....	126
4.4	Conclusions.....	127
Chapter 5	130
5	3D Co-printing of 3D electronics with a dual light source technology	130
5.1	Introduction.....	130
5.2	Experimental section.....	132
5.2.1	Material preparation.....	132
5.2.2	Setup of 3D Co-printing.....	132
5.2.3	Characterization	134
5.3	Results and discussion	134
5.3.1	Developing material system with metal precursor.....	134
5.3.2	Photoreduction of silver NPs	138
5.3.3	Optimization of conductivity of 3D printed electronics	141
5.4	Demonstrations of 3D printing electronics	146
5.5	Conclusions.....	148
Chapter 6	150
6	Conclusions and future directions.....	150
6.1	Conclusions.....	150
6.2	Future work.....	152
Curriculum Vitae	155

List of Tables

Table 1: 3D printed electronics: materials, 3D printing techniques, and its applications	40
Table 2: Summary of (poly)phenol used in our experiments, including their plant sources and solubility in SR494.	102

List of Figures

- Figure 1-1: Timeline from 1981-2019: invention of different 3D printing technologies, new applications of 3D printing, and some representative work in research. Reprint with permission from ref. [4, 6, 9-18]..... 2
- Figure 1-2: 3D printing process. A digital 3D model can be obtained through CAD software, a 3D scanner, or photogrammetry means. Then the 3D model is transformed to STL file and the printer software generates the G-code file containing geometrical information by a series of 2D layers. Finally, the printers deposit the material in a layer-by-layer manner. Reprint with permission from ref. [21]. 5
- Figure 1-3: (a) Scheme of a top-down configuration SLA printer with a direct writing curing process. A laser scans the surface row by row, until curing the desired layer. Then, the stage moves down until a new layer of resin covers the previous layer again and the laser scans the surface for the curing of the next layer. (b) Scheme of a bottom-up configuration DLP printer with projection technology. In a DMD light system, projection technology allows for curing a whole layer simultaneously. Next, the stage lifts by a defined distance and the curing procedure repeats. Reprint with permission from ref. [3]..... 7
- Figure 1-4: (a) Schematic diagram of FDM. The filament is extruded into the nozzle and is heated to reach semi-liquid state. After that, the material is deposited on the platform or the previous layer. Two nozzles are fed with building material and supporting material, respectively. (b) Schematic diagram of DIW. By movement of the nozzle, structures can be built in a lay-by-layer manner. Reprint with permission from ref. [21]. 9
- Figure 1-5: (a) Schematic of 3DP. Jetting head controlled by a computer dispenses a liquid binder onto the thin layers of powder. Once one layer is formed, the next layer of thin powder is distributed by leveling roller. (b) Schematic of SLS. Instead of the usage of the liquid glue, a laser beam is directed onto the powder layer to sinter or fuse the particles. Reprint with permission from ref. [21]. 10

Figure 1-6: Schematic of Lamination 3D printer. A sheet of material is loaded on the stage, and a laser or a razor is then used to trace the outline of the layer contour. When the excess material is removed, another sheet covers the previous sheet again. Each layer is stacked by adhesive in case of the paper or by welding in case of the metals. Reprint with permission from ref. [3]..... 11

Figure 1-7: Powder bed fusion process. Reprint with permission from ref. [25]. 12

Figure 1-8: DED process using powder or wire. (a) Laser or electron beam sinter or melt process using powder feed. The powder feed is often fed via a nozzle surrounding the beam. (b) Laser or electron beam cladding using wire feed. Reprint with permission from ref. [25]. 13

Figure 1-9: Inkjet metal 3D printing followed by curing, depowdering, and densification steps. Reprint with permission from ref. [31]. 15

Figure 1-10: (a) Metallic nanoparticles suspended in a liquid medium. (b) Organic additives prevent metal nanoparticles contact with each other. (c) Initial contact with neighboring metallic nanoparticles. (d) Parameters of metallic nanoparticle inks. Reprint with permission from ref. [33]..... 16

Figure 1-11: Markforged’s Atomic Diffusion Additive Manufacturing (ADAM) process [34]. 17

Figure 1-12: Schematic illustration of the fabrication of metallic cellular material by i3DP and the subsequent surface initiated atomic transfer radical polymerization (SI-ATRP) assisted ELP. Reprint with permission from ref. [39]. 19

Figure 1-13: Subtractive vs additive manufacturing technology for electronics fabrication. Reprint with permission from ref. [40]. 20

Figure 1-14: Powder bed based printing. (a) 3D printing test rig: (1) powder reservoir, (2) platform, (3) powder feeder, (4) mechanism for application of suspensions, (5) print head, (6) powder head. (b) Enhanced process of 3D printing: (1-3) powder bed-based printing cycle, (4) embedding electrical components, (5) creating conductive paths, (6) connecting a

component to the conductive paths. Aerosol jet printing. (c) Schematic representation of the aerosol jet printing process. (d) Aerosol jet printed interconnection of flipped and embedded QNF-component. Reprint with permission from ref. [43].	22
Figure 1-15: (a) NP inkjet printing system and observation units. Reprint with permission from ref. [45]. (b) Schematic diagram illustrating manufacturing process for the inkjet-printed radio frequency electronics. Reprint with permission from ref. [48].	23
Figure 1-16: (a) Schematic presentation of filament-based direct writing and optical image of the apparatus used (inset). Reprint with permission from ref. [67]. (b) Process of electroless plating. Reprint with permission from ref. [62]. (c) The fabrication process with embedded conductive structures. Reprint with permission from ref. [64].	26
Figure 1-17: Various inks for conductive metals deposition. Reprint with permission from ref. [77].	29
Figure 1-18: (a) The photography of mylti ^{3D} system and (b) schematic of fabrication example. (c) Process steps for fabrication of 3D printed CubeSat module. (d) 3D printed CubeSat module by FDM, CNC routing, and dispenser. Reprint with permission from ref. [93].	34
Figure 1-19: (a) Hybrid SLA/DP system. (b) 555 timer circuit; (c) vertical interconnects; (d) working 3D circuit (yellow LED is on). Reprint with permission from ref. [52].	35
Figure 1-20: Fabrication of flexible electronics by 3D printing technology. (a) A 3D printed part (top) programmed into its temporary state (bottom). (b) Conductive ink coated on the surface. (c) Temperature sensor in its off state (top) and on state (bottom). (d) A printed object with CNTs coating was fixated in a curve state (left). When a voltage was applied, the object recovered to its flat state (right). (e) The object is used to control on and off of the circuit. Reprint with permission from ref. [94].	37
Figure 1-21: (a) 3D MID demonstrator and (b) tank filling sensor. Reprint with permission from ref. [42]. (c) Optical image of an antenna during the printing process. (d) Optical profilometry scans of representative meander lines on ESA1 and SEM image of these features (inset). Reprint with permission from ref. [96].	39

Figure 1-22: 3D printing process of electronics using (a-c) i3DP II and (d) 3D co-printing technology. For i3DP II, (a) initiator-integrated resin is applied into commercial DLP 3D printer, and (b) the functional initiator is distributed throughout the whole UV-cured sample, which can be used in a one-step metallization process. Compared to the metallization process based on dopamine (ci), the printed sample using i3DP II technology can reduce the silver ions in one-step (cii). For 3D co-printing, (d) two lights 3D printing system is proposed: UV light for polymeric structures building and laser for conductive patterns printing..... 44

Figure 1-23: Metallization process for 3D printed electronics: from i3DP II (Phase 1-3) to 3D co-printing technology (Phase 4). 47

Figure 2-1: UV-visible absorbance spectra of water-soluble resins with various (a) dopamine concentration (0 – 250 g/L) and volume percentage (10 and 50 vol%), and (b) volume percentage (0 – 50 vol%) at 150 g/L aqueous dopamine solution. (c) FTIR analysis of the samples printed by dopamine-integrated 3D printing resin. 63

Figure 2-2: Metallization of UV-curing parts with various formulations. (a) 3D model (top) and the UV-curing object (bottom). Different concentrations of dopamine aqueous solution, such as (b) 5 g/L, (c) 10 g/L, (d) 25 g/L, (e) 50 g/L, (f) 150 g/L, and (g) 250 g/L, was used to prepare the UV resin. The cured parts were immersed into 0.1 mol/L AgNO₃ solution for 4 h. (i) and (ii) represent 10 vol% and 50 vol%, respectively. Scale bar: 10mm. 64

Figure 2-3: Metallic objects fabrication via silver deposition process with various AgNO₃: (a) 0.1 mol/L, (b) 0.3 mol/L, (c) 0.5 mol/L, and (d) 0.7 mol/L. Scale bar: 10 mm. 65

Figure 2-4: Metallic samples with various dopamine solution concentrations (50 g/L, 150 g/L, and 250 g/L) and volume/volume percentage (10 vol%, 20 vol%, 30 vol%, 40 vol%, and 50 vol%). 66

Figure 2-5: Thickness of coated silver film with various dopamine concentration: (a) 20 vol%, (b) 30 vol%, and (c) 40 vol%. (d) Sheet resistance and layer thickness obtained at the various dopamine concentration. 67

Figure 2-6: FE-SEM images of the surface with various ELP time: (a) 5 min, (b) 15 min, (c) 30 min, (d) 1 h, (e) 4 h and (f) 12 h. Inset is the enlarged picture. 68

Figure 2-7: Complex metallic architectures printed using dopamine-integrated UV resin. (a) Polymeric and nickel-coated colosseum. (b) Polymeric and copper-coated colosseum. (c) Nickel-coated colosseum morphology in Z direction surface and X/Y direction surface.	69
Figure 2-8: (a-d) The UV cured samples without (top) and with (bottom) silver nitrate treatment. PEGDA mixing with 20 vol% (a) 4-Methylcatechol, (b) 2,3,4-Trihydroxybenzaldehyde, (c) catechin hydrate, and (d) tannic acid, respectively. (e) The UV cured samples using ACOMO with five (poly)phenols: (i) 4-Methylcatechol, (ii) 2,3,4-Trihydroxybenzaldehyde, (iii) catechin hydrate, (iv) tannic acid, and (v) dopamine. Scar bar: 5mm.	71
Figure 3-1: (a) The synthesis of DMA. (b) (i)Dopamine powder (white) and (ii) DMA powder (gray). Homogeneous DMA-integrated UV resins are prepared with: (i) VeroWhite, (ii) Formi Clear, (iii) sResin-PLA, and (iv) BV-002.	78
Figure 3-2: FTIR signals of original resin and DMA-integrated resin.	81
Figure 3-3: The as-cured samples (top) and the samples after silver nitrate treatment (bottom) with different weight percent (from left to right: 0 wt%, 1 wt%, 3 wt%, and 5wt%). The 3D printing material are (a) VeroWhite, (b) Formi Clear, (c) sResin-PLA, and (d) BV-002.	82
Figure 3-4: UV-vis absorbance spectra of DMA-integrated resins with various concentrations (0 – 5 wt%). The inset shows optical image for different concentrations of DMA in UV resins.	83
Figure 3-5: The exposure time for single layer of various DMA concentrations.	84
Figure 3-6: Water contact angel of printed substrates cured by different DMA concentration resins.	85
Figure 3-7: Adhesion forces of (a) none-DMA-added sample and (b) 5 wt% DMA-added sample. Insets are the surface morphology from AFM scanning.	86
Figure 3-8: Complex 3D printing structures and their metallic structures after ELP. (a) Cu-lattice heart and (b) Ni-lattice rabbit.	88

Figure 3-9: Surface morphology for Cu coated substrates printed by UV resin with (a) 3 wt% and (b) 5 wt% DMA.	89
Figure 3-10: SEM used to record the growth of copper particles on the 3D printed object with various ELP time: (a) 6 h, (b) 8 h, (c) 10 h, and (d) 12 h. The inset shows images of the Cu-coated object. (e-g) displays the thickness of the copper film with various reaction time: (e) 8 h, (f) 10 h, and (g) 12 h. (h) Sheet resistance and layer thickness of the deposited on the substrates with different ELP time.....	90
Figure 3-11: In situ repairing of the conductive copper film. (a) Cu-coated bar was used to light LED. (b) After 10 times repairing, the bar can still light LED. The green box shows the 1 st , 5 th , and 10 th repairing experiment as examples. 1-10 indicates the different damaged area.	91
Figure 3-12: Resistance of the Cu-coated bar after different times of in situ repairing.	92
Figure 4-1: Chemical structures of (poly)phenols studied in our study. The name and plant source of all compounds can be found in Table 2.	101
Figure 4-2: PG-integrated UV resins: (a) water-soluble resin, (b) VeroWhite resin, (c) Formi Clear resin, (d) sResin-PLA resin, (e) BV-002, and (f) epoxy resin.	103
Figure 4-3: Digital images of as-cured and AgNO ₃ -treated samples demonstrating versatility of catechol group. Different concentrations of PG (0 - 5 wt%) were added into the (a) VeroWhite, (b) Formi Clear, (c) BV-002, and (d) sResin-PLA, respectively. (e) Different concentrations of Ctl (0-5 wt%) were added into Formi Clear resin.	104
Figure 4-4: The effects of the concentration of AgNO ₃ solution. UV-cured samples with 1 – 5 wt% PG were immersed into 0.1 – 0.9 mol/L AgNO ₃ solution, separately. Scar bar is 5mm.	105
Figure 4-5: UV-vis absorbance spectra of PG-integrated resins with various concentrations (0 – 5 wt%). The inset shows optical image for different concentrations of PG in Formi clear resin.	106

Figure 4-6: The single layer exposure time of various PG concentrations in Formi clear resin. 107

Figure 4-7: Water contact angle of printed substrates cured by different PG concentration resins. 108

Figure 4-8: Tensile strength of the as-printed and post UV-curing samples. 109

Figure 4-9: Measurement of adhesion forces with atomic force microscopy. Force distance curves for (a) the sample without PG and (b) the sample with 1 wt% PG integrated into the resin. 109

Figure 4-10: (a) As-cured sample and the sample with PD were immersed into pH=1, pH=7, and pH=13 solution, respectively. (b) After 7 days, all the samples are treated with 0.1 mol/L AgNO₃ solution. 111

Figure 4-11: 3D printing of complex metallic structures. (a) One part with Ag, Cu, and Ni bridges. (b) Microlattice structure coated with (top to down): Cu, Ni, and Ag. (c1) As-printed Eiffel towers and its metallic structure coated with different metals (top to down): (c2) Cu and Ag, (c3) Ni and Ag, and (c4) Cu, Ni, and Ag. 112

Figure 4-12: Surface morphology for Cu coated substrates printed UV resin with different concentrations of PG: (a) 1 wt%, (b) 3 wt%, and (c) 5 wt%. 113

Figure 4-13: SEM used to record the growth of copper particles on the 3D printed object with various ELP time: (a) 10 min, (b) 30 min, (c) 60 min, and (d) 240 min. The inset image shows the Cu-coated object. (e-g) The thickness of the copper film with various reaction time: (e) 30 min, (f) 60 min, and (g) 240 min. (h) Sheet resistance and layer thickness of the deposited copper layer on the substrates with different ELP time. All samples are printed by Formi Clear with 1 wt% PG. 114

Figure 4-14: In situ repairing of 3D printed metallic structures. (a-d) A metallic structure with three times repairing. (e) After 10 times repairing, the metallic bar is still conductive. 1st, 5th, and 10th repairing processes were shown. NO. 1 – 10 represents different location for

every repairing process. (f) The resistance of the metallic bar after various times repairing.
..... 115

Figure 4-15: Thermo-mechanical response of the polymer-copper-nickel strip. (a) Schematic diagram of the deformation process upon heating. (b) Deformation of the composite strip with perpendicular heating..... 117

Figure 4-16: 3D printed high-resisting electronic. (a) The metallic structure with circuit is used to connect the battery and LED. The heat bed is set as 220 °C. (b) Another printed sample using Asiga clear resin is used to compare with the sample using High Temp resin.
..... 118

Figure 4-17: Temperature distribution of the heat bed. The real temperature is 191.7 °C... 119

Figure 4-18: Stability and flexibility of printed strips. Relative resistance of the conductive strips with various (a) ELD time and (b) bending radius. (c) Lighting LED when twisting. 120

Figure 4-19: 3D printed flexible electronics. (a) Pressure sensor used to detect the arm bending angle. LED lights are used to indicate the bending angle and the corresponding value for different bending angle is shown in the curve graph. (b) Different gestures were designed for different letters. 121

Figure 4-20: (a) Adsorption isotherm plots and curves fitting by Langmuir (solid line) and Freundlich (dot line) models of MB. (b) Adsorption kinetic plots and curve fitting by pseudo-first-order (solid line) and pseudo-second-order (dot line) kinetic models of MB. (c) Time-dependent UV-vis spectra of the MB solution using 3D printed object using PG-integrated resin. (d) Reusability of 3D printed object with PG for MB removal. (e) The photography of the MB solution color change within 240 min..... 123

Figure 4-21: Static water contact angles of printed samples treated with different concentration of DETA (0 – 250 mg/ml)..... 124

Figure 4-22: (a) Preparation process of the hydrophobic surface. (b) Static contact angle of printed samples with various procedures and reaction time. As-printed sample was used as a

control experiment. After 36 h silver nitrate treatment, four samples were immersed into Oct solution for 0h, 12h, 24h, and 36 h, respectively.....	125
Figure 4-23: Stabilized emulsions composed of n-octane, hexane, and toluene could be efficiently separated. Compared with the milky emulsion, transparent water was collected.	126
Figure 4-24: Various applications based on i3DP II.....	128
Figure 5-1: (a) Schematic diagram of home-made 3D printing machine. (b) 3D co-printing process by two laser systems. (c) The laser-reduced mechanism of silver nanoparticles in 3D printed structure during laser scanning process.	133
Figure 5-2: (a) The printed tracks on the cured substrate using ACMO. (b) Processing parameters used for NO. 1 – 7 line.	135
Figure 5-3: SEM images and EDX of silver tracks scanned by different laser power: (a) 5.5W, (b) 4.4W, and (c) 2.75W. The scanning speed is 500 mm/min and the prepared UV resin is based on ACMO.	135
Figure 5-4: The prepared UV resin (PEGDA) with 15 wt% AgNO ₃	137
Figure 5-5: The printed sample with various AgNO ₃ percentage (5 – 20 phr) and materials (PEGDA- 250, PEGDA – 550, and PEGDA- 750): (1)PEGDA250-5%, (2)PEGDA250-10%, (3)PEGDA250-15%, (4)PEGDA250-20%, (5)PEGDA550-5%, (6)PEGDA550-10%, (7)PEGDA550-15%, (8)PEGDA550-20%, (9)PEGDA750-5%, (10)PEGDA750-10%, (11)PEGDA750-15%, and (12)PEGDA750-20%.	137
Figure 5-6: Laser metallization process with various number of scans from top: 10x, 15x, 20x, and 25x, respectively. SEM images and EDX results for silver lines with (b) 10 scans, (c) 15 scans, (d) 20 scans, and (e) 25 scans. (f) The resistance and width of the four silver lines.	139
Figure 5-7: SEM images and EDX element mapping of Ag, C and O with different repeating scans: (a) 10, (b) 15, (c) 20, and (d) 25. 3D printing material is PEGDA750-15%.	140

Figure 5-8: Finite element simulation of laser heating the printed object. (a) Temperature (degree centigrade) changing of samples under different laser powers and irradiation times. 9b) Simulation of temperature profiles as laser scanning speeds of 10 mm/s and 20 mm/s with 5.5 W and 3.85 W inputted power. The radius of laser focusing on the surface is 75 μm .
 142

Figure 5-9: (a) Resistivity of the laser reduced and sintered silver conductive path with different powers, scanning speed, and molecular weight of PEGDA. (b) Resistivity of the silver conductive path on printed sample using PEGDA (750 g mol^{-1}) at 4.95W and 5.5W with various scanning speed. 144

Figure 5-10: The SEM images of sintered Ag nanoparticles with different conditions. (a – f) Ag nanoparticles reduced and sintered by the laser at powers of 2.75 W, 3.3 W, 3.85 W, 4.4 W, 4.95 W, and 5.5 W with scanning speed 500 mm/min. (g – h) Ag nanoparticles reduced and sintered by the laser at scanning speed of 1000 mm/min and 1500 mm/min with 5.5W power. (i) The surface of the sample treated 1 h at 100°C in air. 145

Figure 5-11: 3D printed electronics. (a) 3D printed film with conductive tracks in two different layers connecting a red LED and a green LED to power sources, respectively. (b) A RFID is printed inside a film with a chip on the surface and its 3D model. (c) A printed antenna. d) the resistance between two points. (e) A printed film with RFID, MIM (metal-Insulator-Metal) capacitors, and inductors. (f) A structure connecting different circuits at the different layer. 147

Glossary of Terms

AM	additive manufacturing
SLA	stereolithography
SLS	selective laser sintering
FDM	fused deposition modelling
CLIP	continuous liquid interface production
TPL	two-photon lithography
DLP	digital light processing
DMD	digital mirror device
DIW	direct ink writing
3DP	inkjet 3D printing
DED	direct energy deposition
i3DP	initiator-integrated 3D printing
ELP	electroless plating
DoD	droplet on demand
NPs	nanoparticles
SEM	scanning electron microscopy
DMA	dopamine methyl acrylamide
PD	polydopamine
PG	pyrogallol
Ctl	catechol

Chapter 1

1 Introduction to 3D printing metallic structures and 3D electronics

3D Printing or Additive manufacturing (AM) manufactures parts directly from digital models by using a layer-by-layer material build-up approach. In last few years, 3D printing has been increasingly utilized to fabricate high-value added metallic structures. More specifically, electronic/electrical components through selective metallization process can be deposited and embedded in 3D structures to form multi-functionality products. 3D printing promotes the integrated assemblage and embedded components possible as results of layer-by-layer printing characteristics. Functional elements such as sensors, circuits, and embedded components are now being integrated into 3D-printed products or structures, paving the way for exciting new markets, applications and opportunities.

1.1 Introduction of 3D printing technology

1.1.1 History of 3D printing

3D printing, known more formally as additive manufacturing, has been flourishing since stereolithography (SLA) was first introduced in 1984. As a versatile fabrication process, 3D printing can rapidly convert 3D digital models into physical architectures through progressively adding materials. This technology is usually used to fabricate complex and customizable shapes without a need for traditional molding or machining. After over three decades development, both manufacturing capacity and the diversity of printable materials of 3D printing have improved. Nowadays, 3D printing allows the creation of customized complex components from polymers, metals, ceramics, and even multimaterials. In comparison with the traditional manufacturing process, 3D printing, as a rapid prototyping technique, is more flexible and less wasteful for product designs and reducing the requirement of assembly. These advancements have attracted great attention from the media and the public, and are leading to an increase use in various applications, including automotive, aerospace, and bioengineering [1-3].

The concept of 3D printing can go back to 1970's, but the first experimental 3D printer was dated from 1981. Dr Kodama published a paper of a rapid prototyping system to fabricate parts in a layer-by-layer manner. Using a photosensitive resin, the light-exposed portion can be solidified instantly and plastic models were fabricated in the designed equipment [4]. Three years later, a similar technology, stereolithography, was invented by Charles Hull who founded 3D Systems Corporation [5]. In 1988, Hull and his colleagues developed the first commercial 3D printer, SLA-1 [6]. In the same year, Carl Deckard at the University of Texas brought a patent for selective laser sintering (SLS) in which powder are selectively fused together by a laser [7]. After one year, Scott Crump from Stratasys Inc. filed a patent for fused deposition modelling (FDM) in which filament is melted and extruded through a nozzle to form a pattern [8]. In the 1980s, the three main 3D printing technologies were patented and developed. Figure 1-1 lists the major achievements from the invention of 3D printing to recent years.

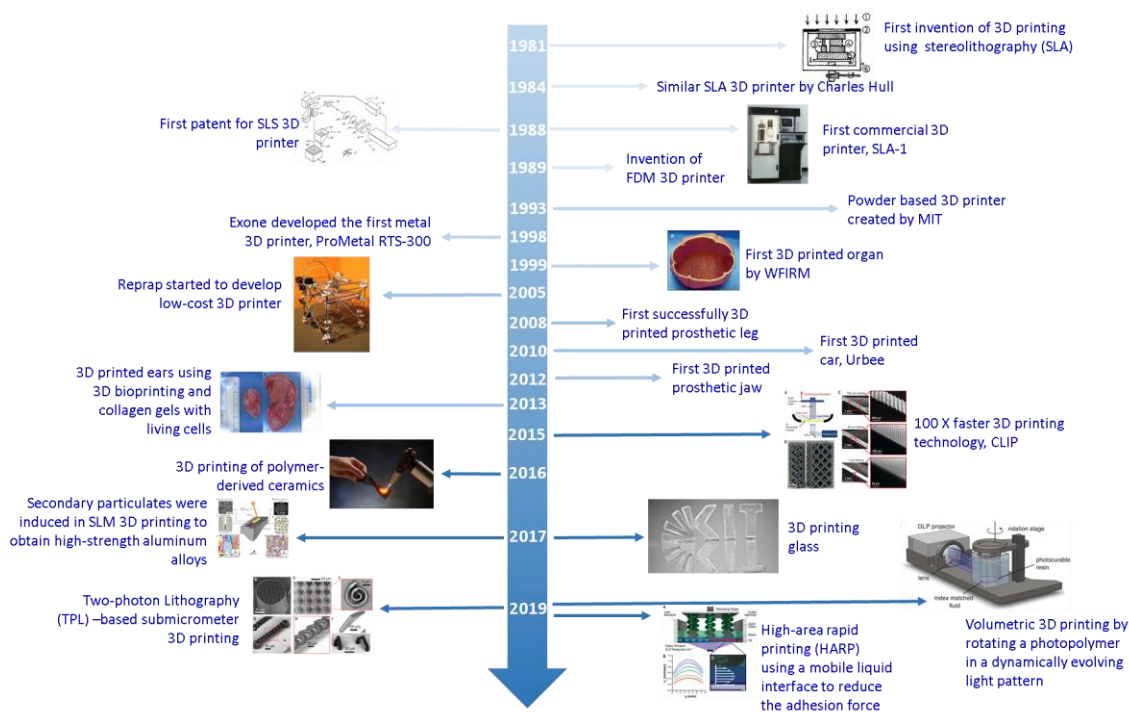


Figure 1-1: Timeline from 1981-2019: invention of different 3D printing technologies, new applications of 3D printing, and some representative work in research. Reprint with permission from ref. [4, 6, 9-18].

In 1993, Emanuel Sachs from MIT patented binder jetting technology which uses a gypsum-type powder and a glycerin/water binder to selectively bond powders together via thermo inkjet print-heads. In 1996, the company Extrude Hone developed this technology to metal objects manufacturing [19]; and later, ExOne spun off from Extrude Hone, focusing on binder jetting of stainless steel and sands for metal casting molds. As the basic 3D printing process was established, a number of areas started to employ this fabrication technique, such as tissue and organ engineering. In 1999, first 3D printed organ was fabricated by scientists from Wake Institute for Regenerative Medicine (WFIRM) and then implanted into the patients [9]. Moreover, in the following 10 years, functional miniature kidneys, biological limbs, and blood vessels were printed by 3D printing. This technology opened up a new era of bio-3D printing fabrication process.

In 2005, Dr. Adrian Bowyer's RepRap project proposed an open-source initiative to create a 3D printer which consists of a self-replicating 3D printer. Most of parts of the 3D printer can be printed by itself [17, 20]. This project led to the wide spreading of desktop 3D printers, and the democratization of manufacturing process became the focus of media.

By the early 2010s, the evolution of 3D printing developed fast, and this versatile and robust technology received a huge amount of attention from academic area as well. The following lists some representative papers since 2015.

In 2015, a 3D printing approach, namely continuous liquid interface production (CLIP), was developed with the printing ability of 100 times faster than that of traditional 3D printing approaches. By forming an oxygen-containing "dead zone" at the bottom of the light-resin reaction area, the fast flow of resin was enabled and can eliminate the repeat replenish and reposition for each layer in CLIP printing process, resulting in a high-speed 3D printing manner [10].

In 2016, Eckel et al. developed a way to make ceramic with complex shape. This invention provides a solution to the long-existed challenge that the extremely high melting point of ceramics brings manufacturing difficulties for 3D printing process. The developed ceramic 3D printing technology can form 3D polymer objects with complex

geometries through preparing UV resin with preceramic monomers, and then printing via an SLA technique. After thermal treatment, complex ceramic parts can be obtained with uniform shrinkage [11].

One year later, 3D printing of transparent glass was created using fused silica glass components in an SLA 3D printer. This method allows the creation of arbitrary microstructure in glass, which widens the 3D printing material types and addresses the problem that the conventional manufacturing process is hard to produce complex glass products [14]. In the same year, a breakthrough technology was progressed in metal 3D printing. Secondary particulates were induced in SLM 3D printing to obtain grain refinement of high-strength aluminum alloys of wrought compositions and some other alloys, which were previously incompatible with 3D printing. This metallurgical approach can be extended to new class of materials, including non-weldable nickel alloys, superalloys and intermetallics [12].

In 2019, high-speed 3D printing has witnessed a burgeoning research interest. Three strategies were applied in stereolithography 3D printing. First, like CLIP, the approach proposed using a mobile liquid fluorinated oil to reduce the adhesion between the printed object and building plate. As the flowing oil cools down the temperature of the print area, continuous and rapid printing process can be achieved regardless of the printing size [13]. Second, high-speed 3D printing based on two-photon lithography (TPL) was achieved via a projection layer-by-layer parallelization. This method increases the throughput up to three orders of magnitude while maintaining submicrometer resolution [15]. Third, Kelly et al. present concurrent printing of all points by rotating a photopolymer with a dynamically evolving light pattern. Only 30 to 120 seconds is required for printing centimeter-scale parts, which is several orders of magnitude faster than those of layer-by-layer approaches [16].

1.1.2 3D printing techniques

3D printing process consists of successive layers of material deposition to fabricate objects from digital data. Through CAD software, a 3D scanner or photogrammetry procedures, a virtual model can be created. Then, it needs to be transformed to an STL

(Standard Tessellation Language or Stereolithography) file, which stores the information for the surfaces of the 3D model file in the form of triangulated sections. Currently, STL file format has been regarded as the gold standard for data conversion between CAD software and 3D printers. In 3D printer software, the STL file can be read and then be converted to a G-code file consisting of 2D cross section layers of the whole object. After slicing process, 3D printer starts depositing the material following a successive sequence of 2D patterns dictated by the G-code file until the desired object is fabricated (Figure 1-2).

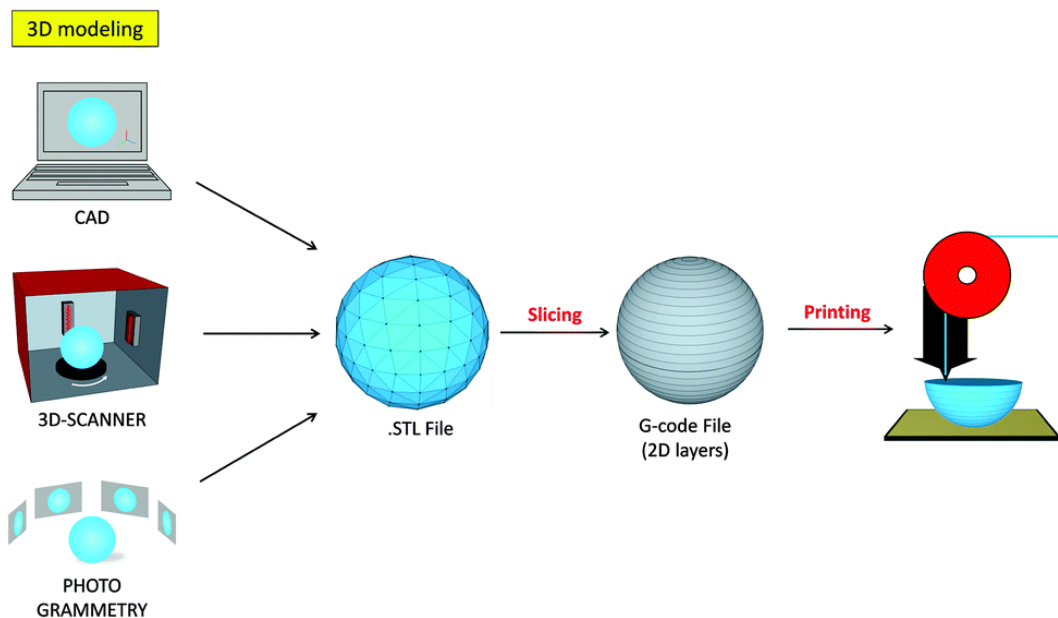


Figure 1-2: 3D printing process. A digital 3D model can be obtained through CAD software, a 3D scanner, or photogrammetry means. Then the 3D model is transformed to STL file and the printer software generates the G-code file containing geometrical information by a series of 2D layers. Finally, the printers deposit the material in a layer-by-layer manner. Reprint with permission from ref. [21].

Several 3D printing techniques have been invented, which can be categorized according to different criteria, ranging from the applications, to the types of materials or the working principles underlying the solidification process. Four main categories are

classified based on their common principle: 1) vat photopolymerization; 2) material extrusion; 3) powder based; and 4) sheet lamination.

Photopolymerization based 3D printing

Among them, vat photopolymerization was the one of the first employed mechanisms for 3D printing. This technology uses the UV light to solidify the liquid polymer through a chain reaction on photopolymer solution. Then, the solidified layer is immersed for curing successive sequencing of 2D layers, which are built one on top of the other. After the entire object printing, the uncured resin is removed, and post treatment may be applied to obtain the desired mechanical properties. There are several different approaches to vat photopolymerization, including stereolithography (SLA) and digital light processing (DLP). As shown in Figure 1-3a [3], an SLA 3D printer contains a tank of liquid photopolymer, a UV laser beam, a scanner system that controls the X-Y movement of the laser beam, and a building plate that permits movement in Z axis. DLP 3D printers also consist of resin vat, UV laser beam, and movable platform, while a digital mirror device (DMD) is used to project one image of each layer [3]. As millions of mirrors that can be controlled in DMD, DLP 3D printing process allows the curing of a complete layer at once, greatly reducing the printing time.

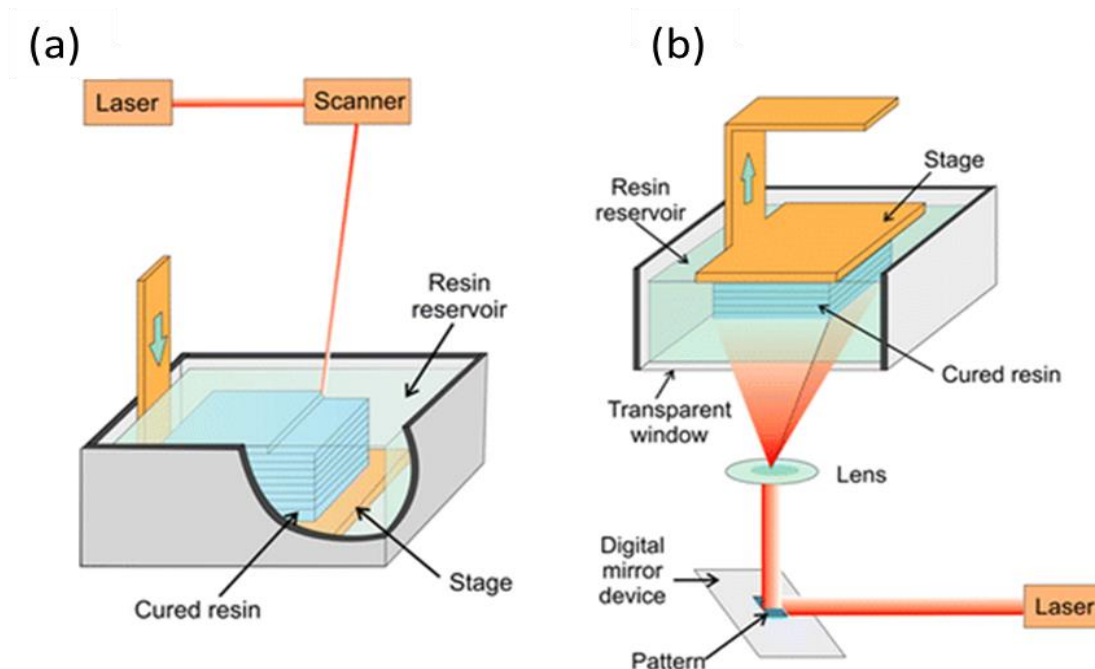


Figure 1-3: (a) Scheme of a top-down configuration SLA printer with a direct writing curing process. A laser scans the surface row by row, until curing the desired layer. Then, the stage moves down until a new layer of resin covers the previous layer again and the laser scans the surface for the curing of the next layer. (b) Scheme of a bottom-up configuration DLP printer with projection technology. In a DMD light system, projection technology allows for curing a whole layer simultaneously. Next, the stage lifts by a defined distance and the curing procedure repeats. Reprint with permission from ref. [3].

Also, there are two configurations of vat photopolymerization based 3D printers, including top-down set-up and bottom-up set-up. Figure 1-3a shows a scheme of a top-down setup, in which the stage is located just below the resin surface. Subsequent layers are built on the top of the previous solidified layer, and the stage lowers further into the resin by a defined distance. The UV light irradiates the liquid resin again for the curing of the next layer until the whole the 3D object is printed. The top-down configuration is the most common configuration for vat photopolymerization, but brings disadvantages including the size of the vat limiting the height of the printed object, the minimum volume of the resin, and extensive cleaning procedures, making bottom-up configuration

an attractive alternative. The bottom-up set-up has the same components as the top-down one; however, the building plate is suspended above the resin reservoir and a transparent window is employed as the bottom of the resin vat (Figure 1-3b). In this way, polymerization of the resin occurs beneath the previous layer, and the movable stage raises, with the liquid resin filling the gaps between the printed parts and bottom of the vat. The required volume of the liquid resin in this setup can be minimized, and the irradiated surface does not be exposed to the oxygen. The printed object using bottom-up always has smoother surface [22].

Extrusion based 3D printing

Different from vat photopolymerization process, material extrusion method deposits material directly from a nozzle head dispenser. The most common extrusion-based 3D printing approach is FDM, which builds an object with a continuous filament in a layer-by-layer fashion. The filament is heated at the nozzle and transformed to semi-liquid state. Then, the semi-liquid material is extruded on the top of the previous printed layer, and solidifies and integrates with the surrounding materials. Thermoplastic filament such as acrylonitrile butadiene styrene (ABS), polylactic acid (PLA), polycarbonate (PC) and nylon are usually employed [23]. Different nozzles can be used for varying materials deposition during a single printing process. Figure 1-4a demonstrates the working scheme of FDM 3D printer, whose building and supporting materials can be printed simultaneously. Based on the similar principle, direct ink writing (DIW) can print a much wider variety of materials in a form of highly viscous “ink”, ranging from plastics, metal, and ceramic to living cells (Figure 1-4b). However, DIW puts specific demands on the ink properties. The types of material and viscosity as well as particles dimension and distribution should be optimized to meet the requirements of DIW 3D printer. Ideally, they should remain shape after deposition and even self-support when printing spanning features. To harden the printed object and improve its mechanical properties, a post-treatment process is always necessary.

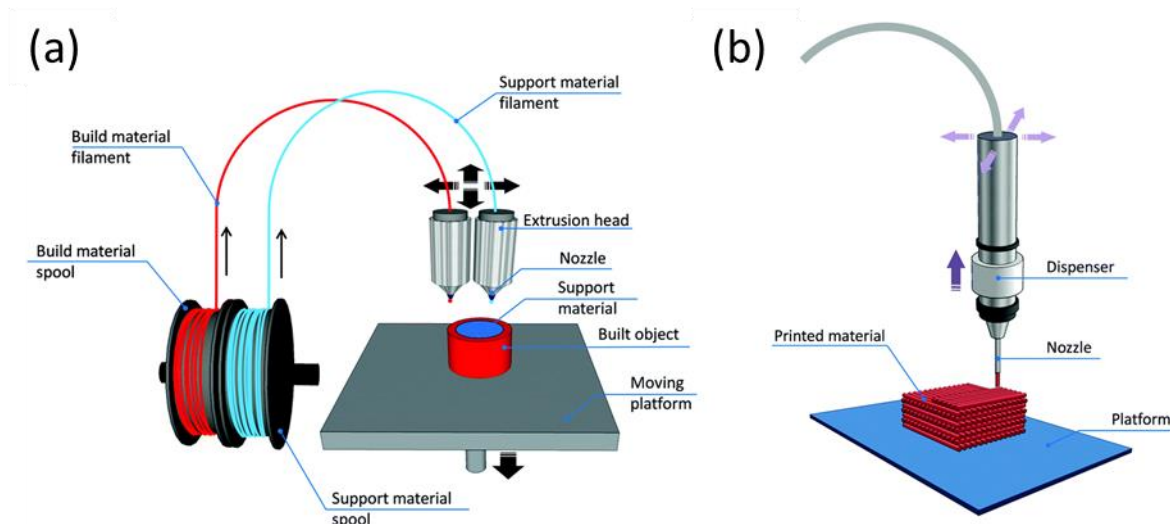


Figure 1-4: (a) Schematic diagram of FDM. The filament is extruded into the nozzle and is heated to reach semi-liquid state. After that, the material is deposited on the platform or the previous layer. Two nozzles are fed with building material and supporting material, respectively. (b) Schematic diagram of DIW. By movement of the nozzle, structures can be built in a lay-by-layer manner. Reprint with permission from ref. [21].

Powder based 3D printing

Powder based 3D printing uses particulates to build parts with arbitrary geometrical complexity. There are two powerful and versatile 3D printing techniques applied to powder based material systems: SLS and inkjet 3D printing (3DP). SLS is a 3D printing process in which thermal energy (laser beam, electron beam, etc.) selectively fuses powder material, while 3DP uses liquid glue to bind the powder particles (Figure 1-5). Once one layer is solidified, the build platform is lowered to allow for distribution of the next layer of powder through rollers or squeegees. Compared to the vat photopolymerization and material extrusion AM techniques, powder-based 3D printing provides an approach that the uncured powder can function as a support material to support complex parts. All non-bonded powder can be reused for another object printing, resulting in a great reduction of printing cost. Currently, particulate forms of polymer, ceramics, metals, and composites are readily available [24].

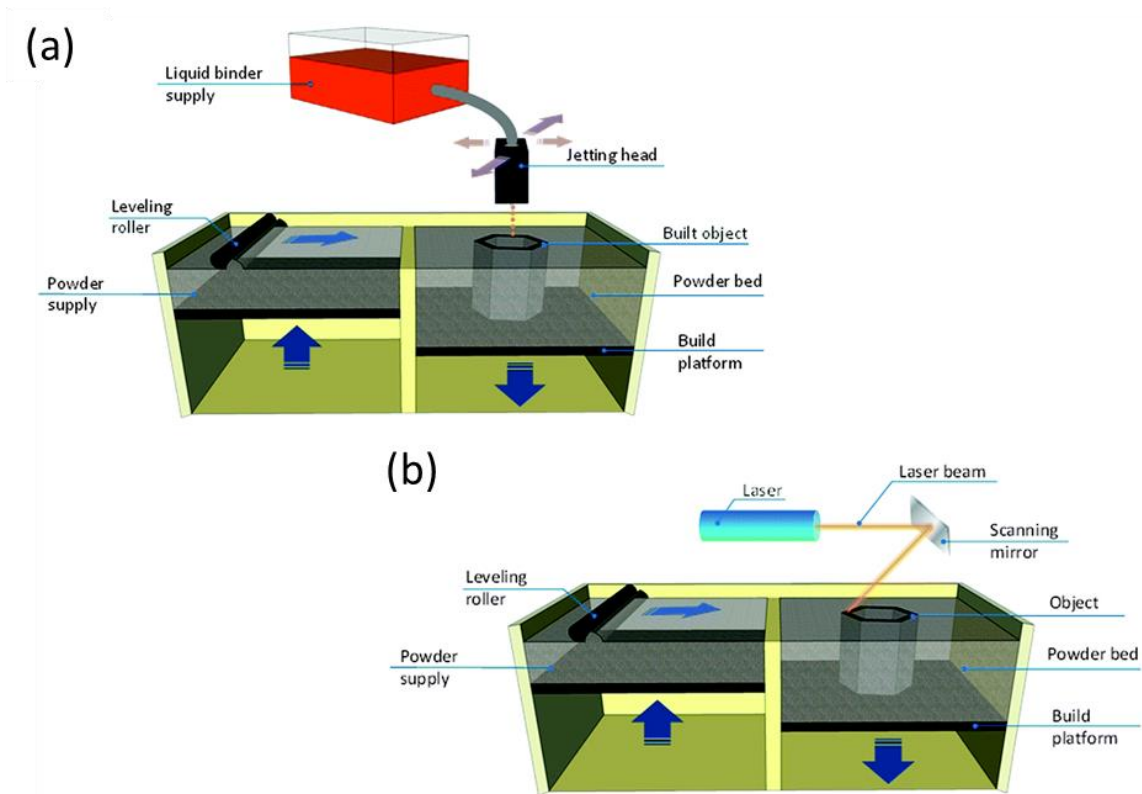


Figure 1-5: (a) Schematic of 3DP. Jetting head controlled by a computer dispenses a liquid binder onto the thin layers of powder. Once one layer is formed, the next layer of thin powder is distributed by leveling roller. (b) Schematic of SLS. Instead of the usage of the liquid glue, a laser beam is directed onto the powder layer to sinter or fuse the particles. Reprint with permission from ref. [21].

Lamination

Lamination is an additive manufacturing process in which sheet materials (paper, plastic and metal) are stacked together using adhesives or welding techniques. As shown in Figure 1-6, the layer of sheet material is loaded onto a stage and then a laser or blade traces the designed cross-section to define the pattern of the layer according to the CAD file. After the excess of materials is removed, a second sheet material covers the previous layer and again is traced. These steps are repeated many times to produce the final 3D object.

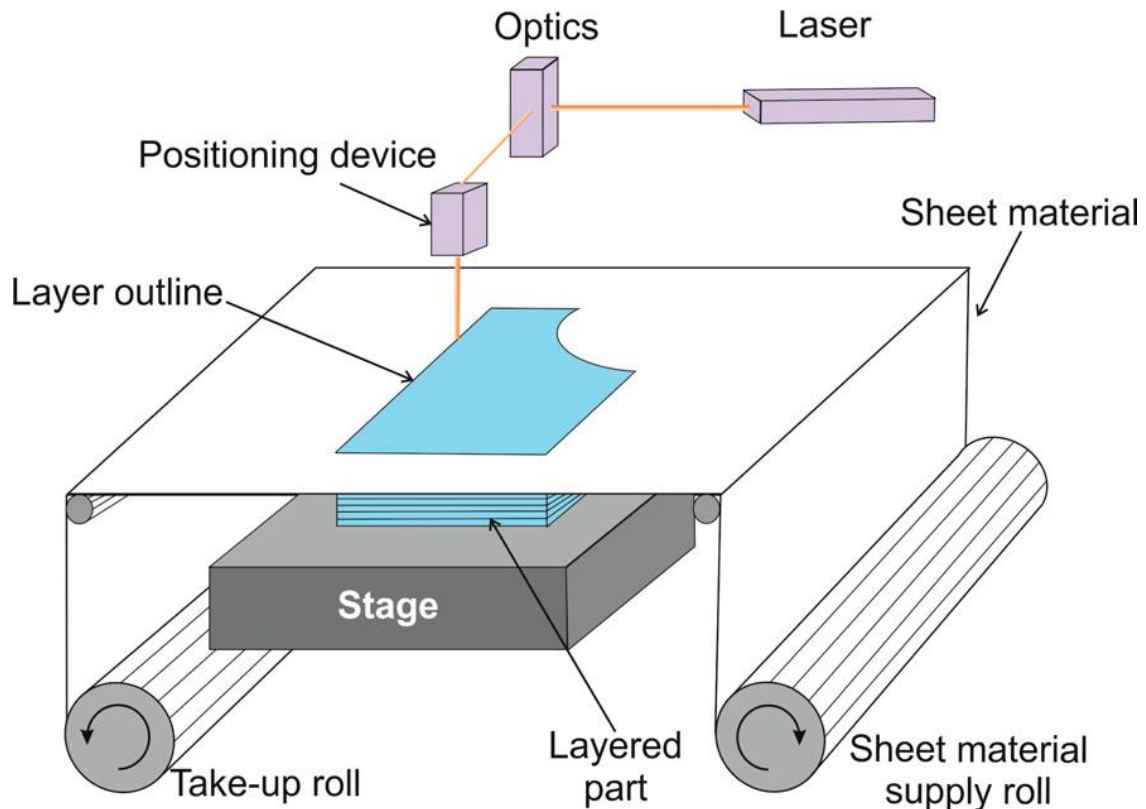


Figure 1-6: Schematic of Lamination 3D printer. A sheet of material is loaded on the stage, and a laser or a razor is then used to trace the outline of the layer contour. When the excess material is removed, another sheet covers the previous sheet again. Each layer is stacked by adhesive in case of the paper or by welding in case of the metals. Reprint with permission from ref. [3].

1.2 3D printing of metallic structures

3D printing of metallic structures, or metal 3D printing, is witnessing significant advances. Maturation of both research-grade and commercial 3D printing techniques during the past two decades, along with an increased capacity of equipment and materials, have spurred significant interests across aerospace, oil & gas, marine and automobile applications. Thus, it is regarded as the most promising technology which is widely adopted in mainstream manufacturing. Metal 3D printing can mainly be classified as direct and indirect metal 3D printing. For the former methods, metallic structures are directly manufactured through 3D printing metallic materials with the assistance of a high-energy power source. Currently, two main categories are involved: powder bed

systems and direct energy deposition (DED), according to material feed stock, energy source (electron beam, laser, etc.), build volume, etc. Indirect metal 3D printing approaches work for pre-metallic materials and mainly include inkjet printing, DIW, FDM and surface metallization. Post sintering process is always required to get the printed objects metallized and further improve their mechanical properties.

1.2.1 Direct metal 3D printing

Figure 1-7 is a schematic fusion process of a powder bed system. Thin layers of very fine powders are spread and packed on a platform, and the powders are fused together selectively with a high energy source beam. Normally, laser or electron beam is adopted according to the melting point of working materials, and electron beam can provide higher fusion temperature. Then, subsequent layer of powders is rolled on the top of previous layer, and scanning process is repeated until the final structure is completed. If necessary, further processing, such as coating, sintering, infiltration, or polishing, is applied. Powder size and distribution determine the density of the final object. Powder bed system can be used for polymers, metals, and alloys powders. Taking the laser-based approach for example, during SLS process, the laser does not fully melt the powders and the induced local temperature on the surface results in fusion of the powders at the molecular level.

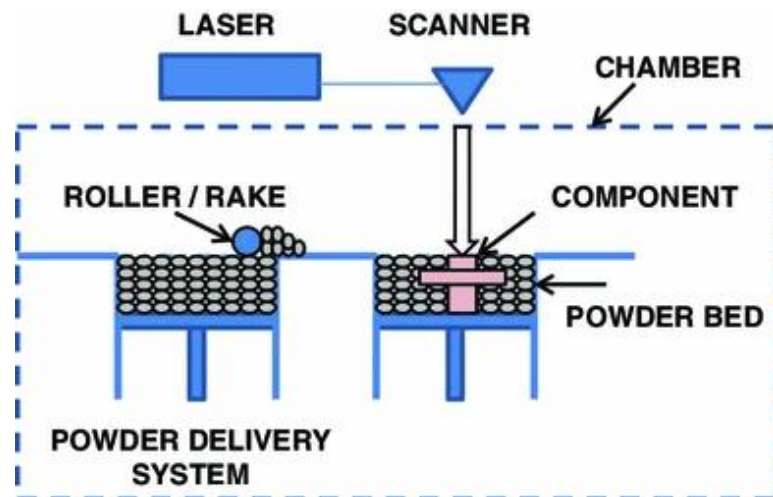


Figure 1-7: Powder bed fusion process. Reprint with permission from ref. [25].

Powder feed system and wire feed system all belong to DED category, which uses a laser or electron beam directly to melt a feedstock material (powder or wire), as shown in Figure 1-8. DED is also known as direct metal deposition (DMD), laser engineered net shaping (LENS), direct light fabrication (DLF), laser solid forming (LSF), and wire arc additive manufacturing (WAAM) [26-28]. A source of energy is directly focused on a small region, and the feedstock material is deposited and fused into the working area and then solidified after scanning of the energy beam [29]. DED using powder/wire exists the ability of high printing speed (10 kg/h for WAAM [27]) and very large building area (up to 6 x 1.4x1.4 m [30]). As this 3D printing process is formulated around the deposition, there is no need for building plate. In addition, DED is also applied to add value to other components by repairing the damaged parts, adding new features to an existing part with new material which serves as optimization of the surface quality. However, compared to SLS or SLM, the printed parts have lower surface quality and lower accuracy, and less complex parts can be manufactured. Therefore, DED is always used for a large part with low complexity. Also, DED can improve printing speed and reduce cost, and provides excellent mechanical properties and accurate composition control.

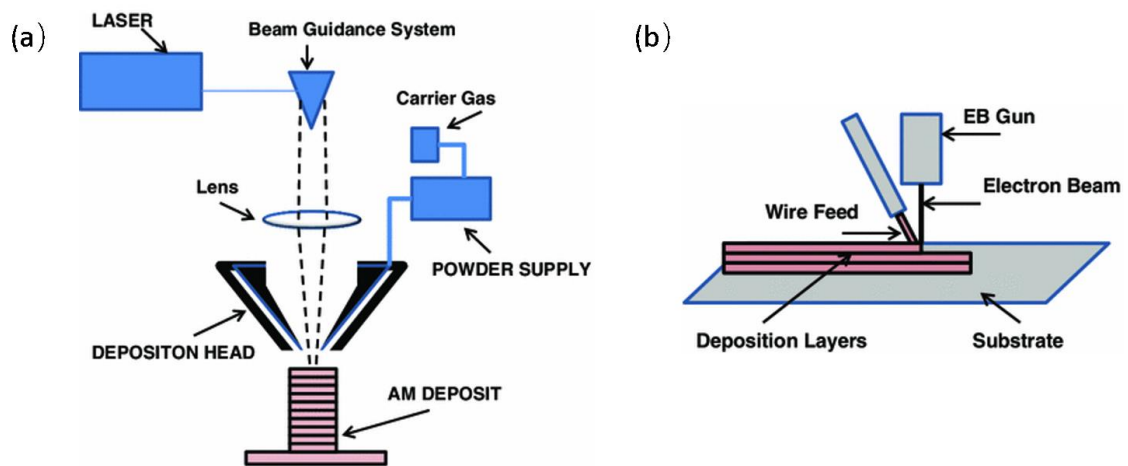


Figure 1-8: DED process using powder or wire. (a) Laser or electron beam sinter or melt process using powder feed. The powder feed is often fed via a nozzle surrounding the beam. (b) Laser or electron beam cladding using wire feed. Reprint with permission from ref. [25].

DED systems use materials in the form of powder/wire which is similar to FDM but with an extremely higher energy for metal melting. Therefore, powder/wire feed systems can be helpful for filling cracks and metal parts repairing where powder fusion process is limited. In addition, DED process using power or wire allows for both multi-material and multi-axis deposition, and easily works with subtractive processes to complete machining.

1.2.2 Indirect metal 3D printing

Due to limitations of direct metal 3D printing in high cost, oxidation induced by the laser, and residual stresses in the printed parts, indirect metal 3D printing methods are also developed for the fabrication of metallic structures.

Inkjet metal 3D printing

Inkjet metal 3D printing extrudes a suitable binder from an ink-jet printer head directly to the selective area, creating a rare metal/binder structure which is subsequently sintered at high temperature to remove the binder and sinter the metal powder (Figure 1-9). In ink-jet print heads, liquid binders are pulsed from an orifice in a reservoir containing the binder. These binders usually exist a low surface tension which allows spreading of micro- and nano-size droplets on the printed surface. As the build progresses, the layers of powder materials are selectively bonded together into the desired shape. After printing, the box may be heated to cure the binder, and then the printed part is removed from the powder bed. The printed object is at this point not suitable for end-use and then use a post-process to achieve desirable mechanical properties.

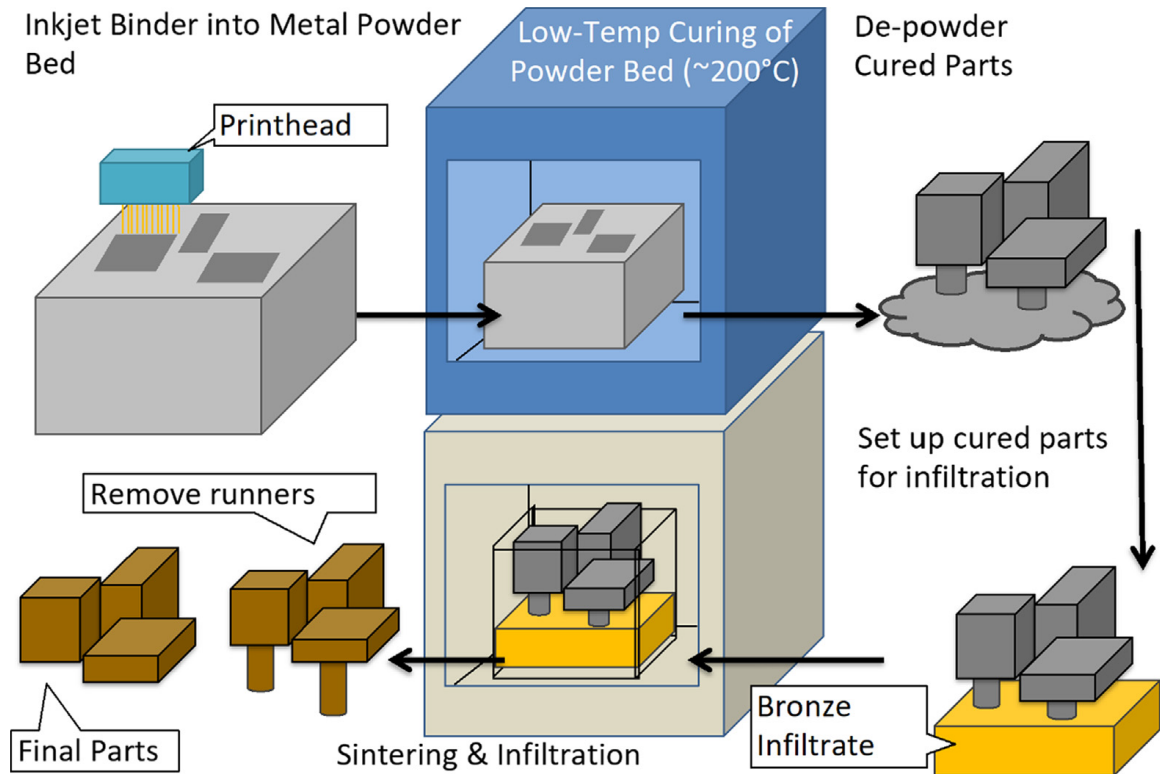


Figure 1-9: Inkjet metal 3D printing followed by curing, depowdering, and densification steps. Reprint with permission from ref. [31].

Inkjet technology has the widest selection of materials of all 3D printing techniques because it is compatible with virtually any powder materials. Another advantage is that the building process occurs at room temperature without gas protection, avoiding oxidation, residual stress, and phase changes of the surrounding powders. During inkjet process, as there is no significant heating occurring, printed parts do not undergo thermally-induced stresses and distortions, so it is practical to print overhanging features [32]. In addition, various densities with controlled porosity can be achieved using inkjet metal 3D printing.

DIW of metallic structures

DIW is also used for metallic structure building through extrusion of metallic inks on a substrate layer-by-layer to make a 3D part. The metallic ink is prepared by mixing micro- or nanoparticles to the polymer solution, which are applied in DIW to print a metal-polymer composite 3D part. Similar to inkjet metal printing, a post-treatment is required

to pyrolyze the polymer and sinter metal particles. Although this method is successful, it is difficult to produce many layered and complex structures due to sagging of inks under their own weight. So, the stability of the metallic ink should be considerable enhanced. In general, metallic inks are suspensions of metallic nanoparticles in liquid mediums (Figure 1-10a), and individual metallic nanoparticle is encapsulated in a layer of insulating organic additives and stabilizing agents (Figure 1-10b). Both the organic additives and stabilizing agents are used to prevent agglomeration of metallic particles. After sintering process, the metallic nanoparticles can contact each other (Figure 1-10c). The detailed parameters of metallic nanoparticle inks can be found in Figure 1-10d.

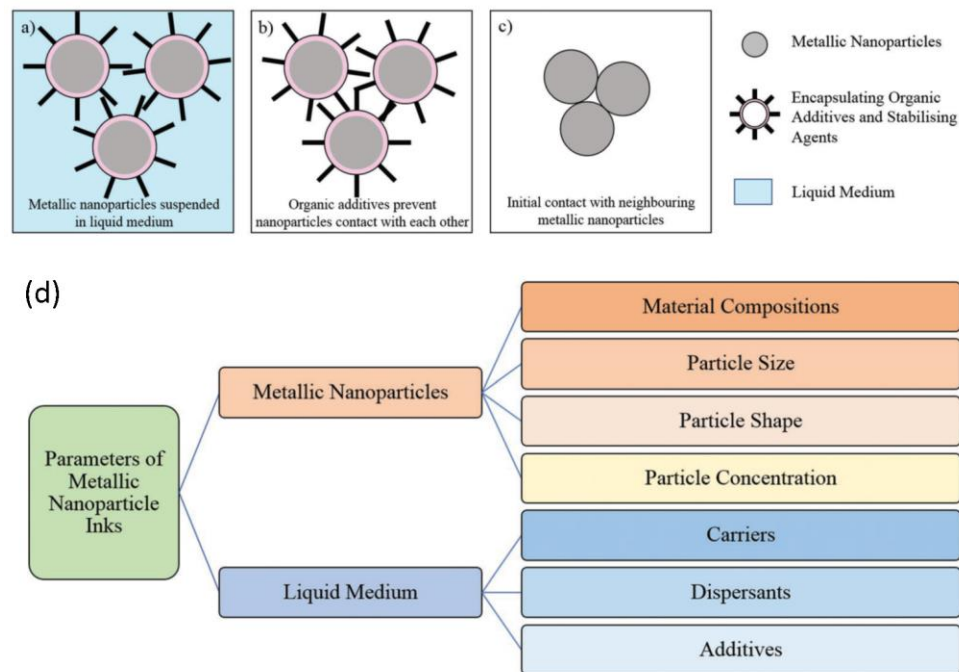


Figure 1-10: (a) Metallic nanoparticles suspended in a liquid medium. (b) Organic additives prevent metal nanoparticles contact with each other. (c) Initial contact with neighboring metallic nanoparticles. (d) Parameters of metallic nanoparticle inks. Reprint with permission from ref. [33].

FDM-based metal 3D printing

Recently, MarkForged launched one commercial 3D metal FDM printer, Metal X (Figure 1-11) [34]. The working scheme of metal FDM process is the same as plastic based

FDM, but the filament is a combination of thermoplastic polymer and metallic particles. After the part is built, it is placed into the oven to burn out the remaining plastic and sinter the metal particles. This metal filament extrusion process benefits from FDM advantages, such as high precision and low-cost.

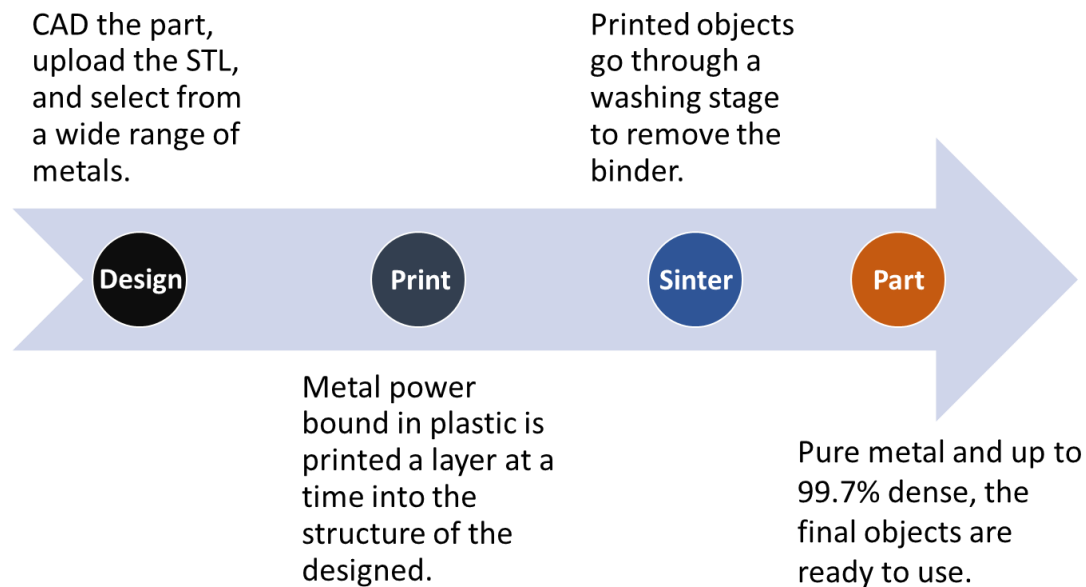


Figure 1-11: Markforged’s Atomic Diffusion Additive Manufacturing (ADAM) process [34].

Surface metallization

Direct metal 3D printing approaches enable the creation of large building areas of certain metallic materials, but a high resolution is difficult to achieve, let alone the expensive equipment, rigorous operation, and limited working materials. While indirect metal 3D printing approaches provide cost-effective methods for fabricating metal structures, the most significant challenge is the inability to predict the large amount of distortion that occurs during metals sintering process, which lowers overall accuracy of the printed object. Moreover, the printed object after the heating process tends to leave small voids and bubbles inside the 3D structures, which has a negative impact on the final object mechanical properties and porosity. All these uncertainties of the accuracy and

mechanical properties limit the practical applications. Therefore, several surface metallization methods, such as sputtering, vacuum metallization, and plating have been demonstrated using 3D structures and objects.

Among these methods, electroless plating (ELP) is a simple wet chemical process, which is more cost effective and suitable for metal deposition onto polymeric materials. In our lab, an initiator-integrated 3D printing (i3DP) approach [35-38] was developed to address the above challenges by integrating 3D printing with an initiator-assisted surface modification technique. As demonstrated in Figure 1-12 **Error! Reference source not found.**, by directly 3D printing an initiator-integrated UV-curable resin, the highly cross-linked networks of 3D printed architectures will be fully integrated with the initiator. Then, surface-initiated atomic-transfer radical polymerization (SI-ATRP) will enable the following polyelectrolyte-brush-assisted ELP, resulting in high-quality metallic microarchitectures. Compared with the conventional electroless metallization process, which can dramatically damage the polymer surface due to the pretreatment of chemical etching, the instinctive polyelectrolyte brushes induced by i3DP can not only retain the structure resolution, but also maintain the properties of constituent materials. Therefore, with the i3DP-assisted technique, the metal structure is conformal to the high-resolution polymer core, leading to a high-resolution structure simultaneously. In addition, the coating thickness can be controlled precisely through the metal coating time. Together, the well-controlled meta-structure can be fabricated.

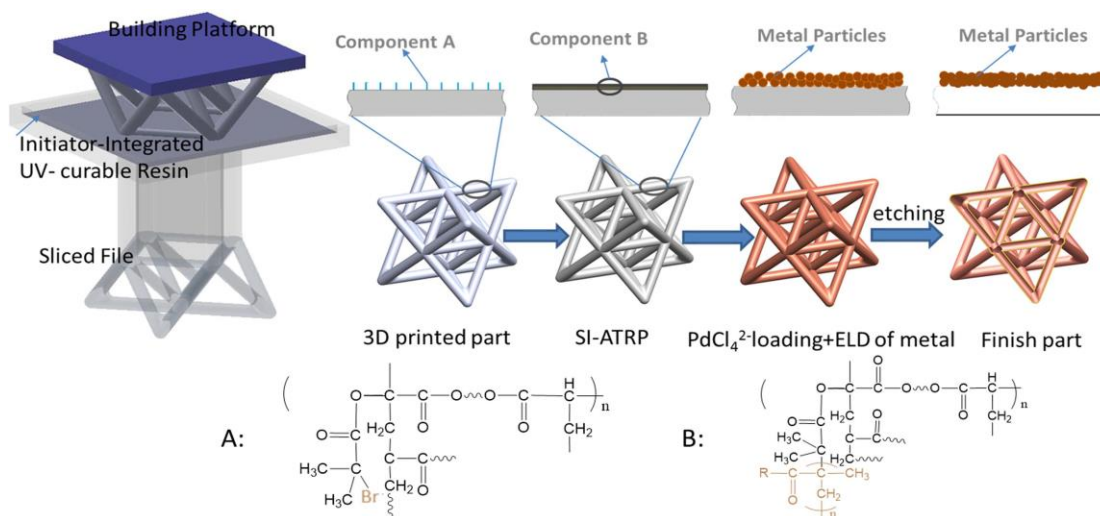


Figure 1-12: Schematic illustration of the fabrication of metallic cellular material by i3DP and the subsequent surface initiated atomic transfer radical polymerization (SI-ATRP) assisted ELP. Reprint with permission from ref. [39].

1.3 3D printed electronics

The production of modern state-of-the-art electronics has become complicated with the cost growing exponentially, and low-cost with high resolution manufacturing process are key attributes for future electric devices. It is known that photolithography as a common method has been widely used to produce electronics, but it limits some cutting-edge applications that require complicated 3D geometries. Moreover, conventional photolithography patterning of electronics involves multiple processes, such as vacuum depositions and etching, leading to high overall cost and chemical wastes of photoresist, organic solution and etchants. The main difference between conventional subtractive and 3D printing process for electronics fabrication can be found in Figure 1-13. 3D printing methods become alternatives due to their natural advantages in manufacturing highly complex configurations. 3D printing approaches can also facilitate complex topology optimizations through theoretical modeling, and the functionality can be tailored by various structural parameters, such as sensors and EMI shielding. Thus, various functional 3D electronics via 3D printing techniques have been vigorously investigated.

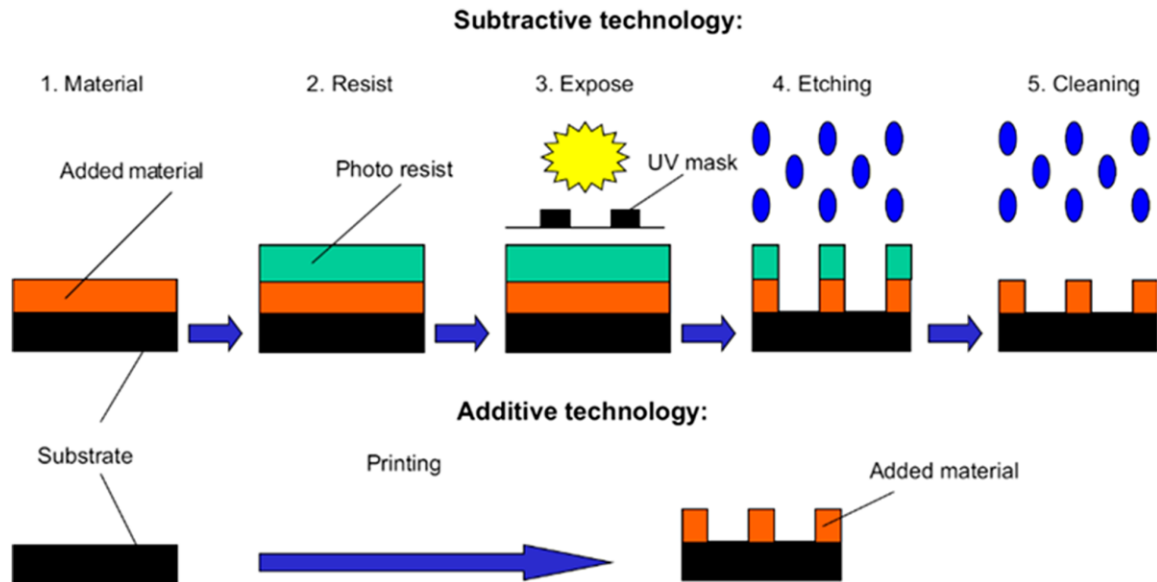


Figure 1-13: Subtractive vs additive manufacturing technology for electronics fabrication. Reprint with permission from ref. [40].

The fabrication freedom offered by 3D printing has been explored in the context of 3D electronics integration, referred to as 3D printed electronics. In comparison with time-consuming traditional 2D bread-boarded fabrication, the cooperation of 3D printing techniques with electrical components placement and electrical interconnect deposition has raised a new revolution for rapid fabrication of electronics. Other than new and reactive functional materials development, the functionalization of the printed substrates with unusual geometries instead of the conventional planar circuit boards is still a challenge. It is expected that the developed 3D printing technologies for electronics may eventually be used to make end-use parts and thus provide better customization. In this section, techniques, printing materials, post-treatment, and the recent advances are reviewed.

1.3.1 3D printed electronics techniques

Currently developed approaches of 3D printing electronics are dominated by the deposition of conductive materials onto the surface of the dielectric substrates, or embedment of conductive materials within the 3D printed insulating matrix, or coating a metal layer on the substrates.

Binder deposition

Hoerber et al. demonstrated a developed building process for 3D printed electronics based on conductive binder deposition [41]. Here, a powder bed-based 3D printer shown in Figure 1-14a was used. A powder feeder deposited a thin layer of metal powder, and the print head was used to apply the binder to connect the electrical components to form conductive circuit. To create a conductive pattern, low-viscous (20 cPs) ink with silver nanoparticles get drawn into the powder and form an incoherent structure. A Surface Mount Technology (SMT) resistor can be placed into the cavity, which was then buried into the powder bed. Also, generating a connection between conductive paths and the SMT have to be developed (Figure 1-14b step 6).

Aerosol jet printing

Aerosol jet printing can be used for electronics fabrication from different functionalized inks. Due to the silver ink having a viscosity of 50 to 100 cPs, one conductive layer can be deposited on the surface, avoiding the seeping of the ink caused by the high surface roughness of the powders. Depending on the nozzle geometry, a line width $<100\ \mu\text{m}$ up to 10 mm of the deposited ink can be printed. A component having 24 leads (pitch of $800\ \mu\text{m}$) was embedded with silver path (Figure 1-14d). Moreover, a focal length of the aerosol beam and a high nozzle stand-off allow printing on complex 3D surfaces [42]. Both these two methods required thermal postposing to evaporate the solvent and improve the contact between metal particles.

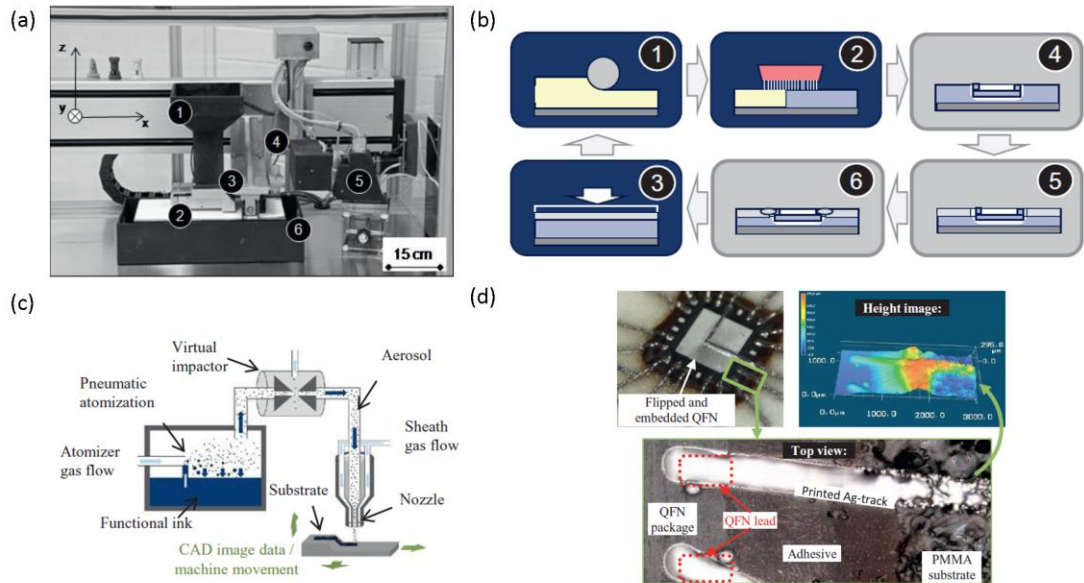


Figure 1-14: Powder bed based printing. (a) 3D printing test rig: (1) powder reservoir, (2) platform, (3) powder feeder, (4) mechanism for application of suspensions, (5) print head, (6) powder head. (b) Enhanced process of 3D printing: (1-3) powder bed-based printing cycle, (4) embedding electrical components, (5) creating conductive paths, (6) connecting a component to the conductive paths. Aerosol jet printing. (c) Schematic representation of the aerosol jet printing process. (d) Aerosol jet printed interconnection of flipped and embedded QFN-component.

Reprint with permission from ref. [43].

Extrusion methods

Material extrusion method is a straightforward approach and has been used for a wide range of materials, to create 3D electronics with conductive components embedded. Inkjet printing, filament-based direct writing, and FDM are representatives and have been adapted to print 3D electronics over the last several years. For example, through a droplet on demand (DoD) method, inkjet printing can eject the inks containing conductive nanomaterials from the printheads of a large number of small nozzles. Upon contacting with substrate, the ink can be immediately solidified by infrared light or heating because increasing the temperature can accelerate the evaporation of solvent, and then increase the viscosity of the ink, leading to the solidification of the droplets with a smaller

diameter and higher growth rate of conductive traces [44]. By this method, microstructures including metal micro pillar arrays, micro helices, micro zigzags and micro bridges can be printed on plastic substrates, shown in Figure 1-15a [45, 46]. Similarly, inks containing photo-curable oligomers, photoinitiator and metal NPs can be solidified by light. The LED-based light is inexpensive, compact and efficient, and can sinter the metal inks meanwhile curing the photopolymer, which means one apparatus has two functions - printing conductive and nonconductive materials simultaneously [47]. Compared to heating-based method, light curing is more flexible to control the printing resolution and surface quality. RMS roughness by light-based method can reach $0.4 \mu\text{m}$ (Figure 1-15b) [48]. However, inkjet printing is limited to fabricate 3D electronics with low conductivity and low aspect ratio owing to the dilute nature of the used inks. As wet inkjet printing, the satellite drop formation and non-uniform drop drying also cause inhomogeneous features [49].

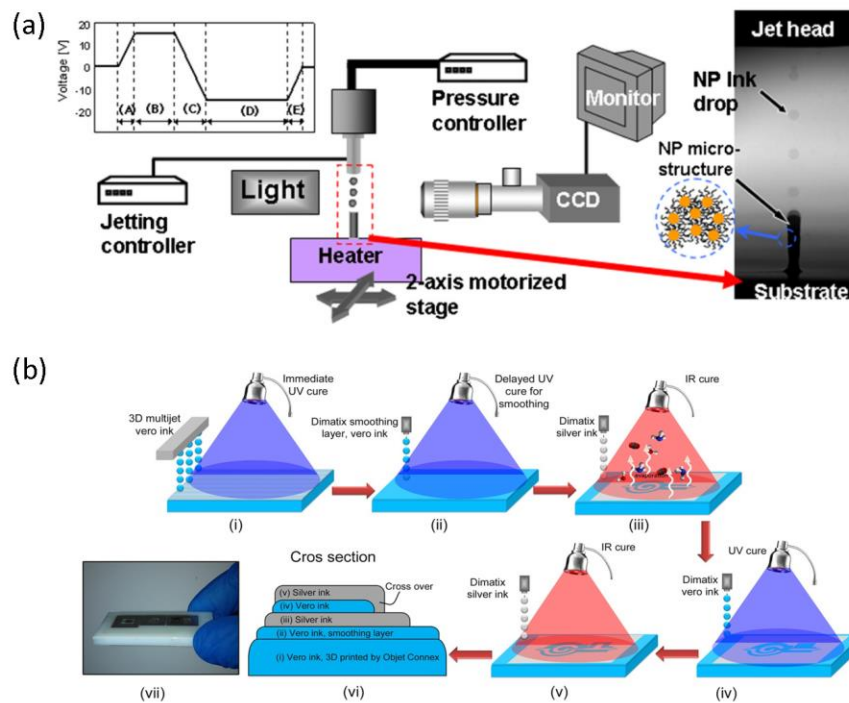


Figure 1-15: (a) NP inkjet printing system and observation units. Reprint with permission from ref. [45]. (b) Schematic diagram illustrating manufacturing process for the inkjet-printed radio frequency electronics. Reprint with permission from ref. [48].

Direct writing of concentrated conductive materials is applied to overcome above limitations [50, 51]. Mixing in an organic solvent, the conductive inks are first loaded into a syringe barrel, and the syringe is mounted onto the 3-axis stage to extrude ink filament either in- or out-of-plane (shown in Figure 1-16a). The printing resolution depends on the nozzle diameter, applied pressure, printing speed and loading of conductive materials. To date, $\sim 2 \mu\text{m}$ conductive traces can be achieved by a $1 \mu\text{m}$ nozzle at modest speeds. Wicker and co-workers built a hybrid 3D printing system via integrating filament-based direct writing within an SLA apparatus, and this system has created a series of 3D printed electronics, such as conformal 555 timer [52], Hall effect sensor [53], even a game die toy [54].

Conductive materials are also prepared in filament shape by melt blending, and then used in FDM approaches. For example, commonly used filament material – PLA can be mixed with metal NPs [55], carbon black (CB) [56], carbon nanotubes (CNTs) [57] or graphene [58] to synthesize conductive filament, and the percentage of the effective conductive components can be prepared as high as 40 wt% [57]. With the assistance of low-cost multi-material FDM 3D printer, it is able to produce highly customised and functional elements. Especially, FDM printer that has multiple nozzles can extrude nonconductive and conductive components simultaneously onto the same subject, thus, the conductive parts and matrix part can be produced in a single build process without complex and expensive facilities, allowing the fabrication of highly complex volumetric sensors and electronics. To date, liquid sensors, flex sensors, capacitive buttons, and ‘smart’ vessel have been printed by FDM [56, 57]. In addition, the flexibility of 3D printing process also benefits the design and optimization process when developing new electronics and sensors.

Other than directly introducing conductive components during 3D printing process, post-treatment process also enables the addition of conductive materials. Some researchers have explored the feasibility of depositing metal, namely metallization process, onto the 3D printed structures via ELP [59] or electroplating process [60]. The metallization process typically involves steps of surface roughening, surface activation, and ELP/electroplating. Here, roughened surface is necessary to increase the attachment

chance of catalysts to the polymer surface. Sputtering and etching step are two common approach used to surface treatment [59, 61]. Since different polymer materials will have different abusability to catalysts, it is able to selectively metallize the object which is printed by multi-materials FDM printer (Figure 1-16b) [62, 63].

Model based methods

Another simple approach is fillings of liquid metal paste into the internal channels to form metallic elements/interconnects. Hybrid extrusion printer, which integrated inkjet printing manner and thermal extrusion manner, was developed to printed embedded electronics as shown in Figure 1-16c. Benefiting from the high printing resolution, a variety of microelectronics components, such as capacitors, inductors, and resistors were produced. A polymeric “smart cap” with an embedded inductor-capacitor (LC) tank sensor was demonstrated by cooperating with different electrical components for food safety detection [64]. In addition, through infiltration of a dispersion of silver NPs and chemical sintering, a porous 3D printed object can be conductive [65]. Based on this method, the functionalities of the 3D printed electronics would be largely extended by material selection. Recently, flexible 3D objects can be printed with a DLP printer using a family of flexible and stretchable UV resin. After immersed into silver NPs solution and sintered by HCl vapor, the flexible 3D printed electronics were made with excellent mechanical and electric repeatability [66].

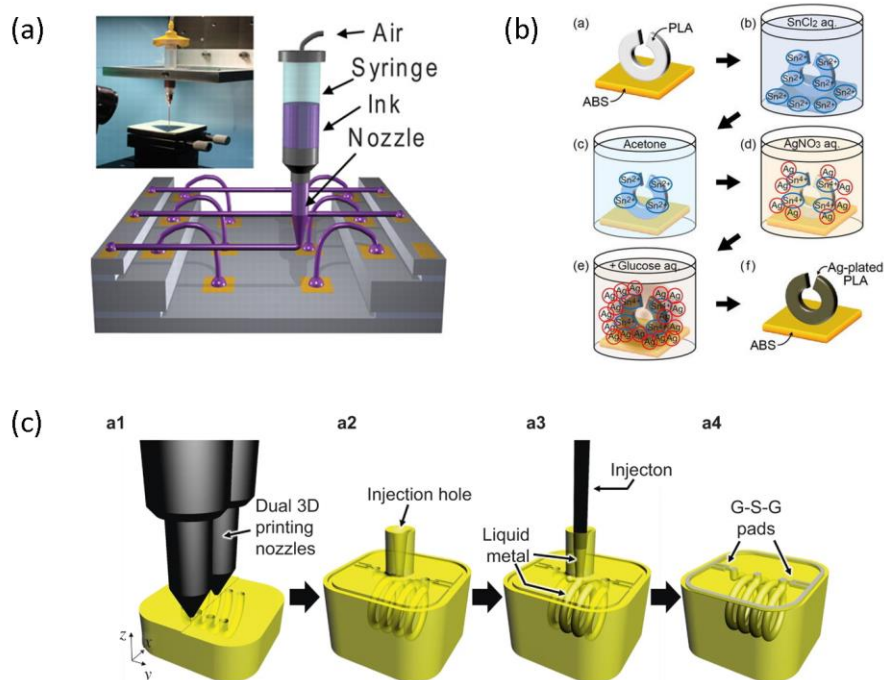


Figure 1-16: (a) Schematic presentation of filament-based direct writing and optical image of the apparatus used (inset). Reprint with permission from ref. [67]. (b) Process of electroless plating. Reprint with permission from ref. [62]. (c) The fabrication process with embedded conductive structures. Reprint with permission from ref. [64].

Conductivity can also be achieved when metal precursor is induced to the printing material. For example, silver NPs can be reduced on the substrate, which is printed using the mixture of polyethylene glycol diacrylate (PEGDA) and silver nitrate, by heating or UV irradiation. The in situ generation of the metal NPs enables the formation of volumetric circuits, and the density and morphology of metal NPs can be further optimized by improving the material formulation and processing parameters [68, 69].

1.3.2 Conductive materials

Up to now, a series of conductive materials have been developed to be compatible with the 3D printing approaches, including metal nanoparticles (NPs), metal nanowires (NWs), CNTs, graphene, conductive polymers as well as organometallic compounds and the relative complexes. The materials can be deposited as solids, pastes, inks, thermoplastic,

etc. that can regulate the flow of the conductive materials. Different 3D printing processes work for different printing materials, depending on the printing principle, required conductivity of the electronics, printing resolution and the post-treatment process. In this section, we focus more on the commonly used metal NPs and NWs, graphene, CNTs and conductive polymer.

Metal NPs and NWs

To obtain an effective electrical conductivity for 3D printed electronics, silver and gold are the mostly used conductive ink formulation, due to their high natural conductivity and resistance to oxidation. Owing to the high cost of silver and gold, cheaper metals are used as alternatives, such as aluminum, copper and nickel. Two main approaches are currently employed to make metal NPs, namely top-down method and bottom-up method. The former one involves breaking the bulk metal into small particles, including mechanical grinding, laser ablation, electro-explosion of a metal wire, plasma excitation of metal plates, while the latter is mainly based on the reaction of a metal precursor with a reducing agent as well as the decomposition of metal salts and organometallic compounds (carbonyldibenzylidene acetonates, acetyl acetonates, complexes of metals with fatty acids). Compared with the top-down approach, the bottom-up approach can yield a great variety of dispersions with various characteristics (such as size distribution, morphology, stability, etc.) through controlling the process parameters, such as the types of reducing agent, the concentration of the reagents, temperature, pH and the rate of reagent addition.

A major challenge for these metals is how to avoid oxidation under ambient conditions. For example, rapid oxidation of aluminum in air will form a thin nonconductive Al_2O_3 layer [70]. Compared with aluminum, copper undergoes a less oxidation process. A proper protective layer can also assist copper with long-term stability, such as by coating protective polymers [71], alkanethiols [72], amorphous carbon, graphenes [73], inorganic materials [74], or by introducing other metals (such as Ti, Pd, Al, or Cr) [75] to minimize the penetration of oxygen.

Another long-existed challenge is the aggregation and sedimentation of the metal NPs dispersed within the ink formulation, although various dispersing agents are developed to prevent aggregation. Figure 1-17 shows commonly used conductive ink types for circuits printing. The listed ink formulas generally work with appropriate stabilizer and the composition, which are determined by the process requirement and target property, such as drying time, large-scale production and environmental issue. For example, despite of having a fast drying time, methyl-ethyl-ketone (MEK) flaws in generating a strong odor which cannot fulfill the requirements of volatile organic compounds (VOC) legislation [76]. Other solvents (ether alcohols, diols and triols, cellosolves, and aliphatic ether acetates) were developed to replace MEK. Among them, slow evaporating solvent - butyl carbitol is more widely used since it hardly generates defects and bubble during the evaporation, and it also has a robust shelf life of inks because of its stability. However, it comes with another problem that the presence of the insulating stabilizer affects the purity of the conductive constituent, leading to a lower conductivity. Therefore, the organic additives should be removed from the printed patterns to allow physical contact between metal NPs through post-treatment sintering.

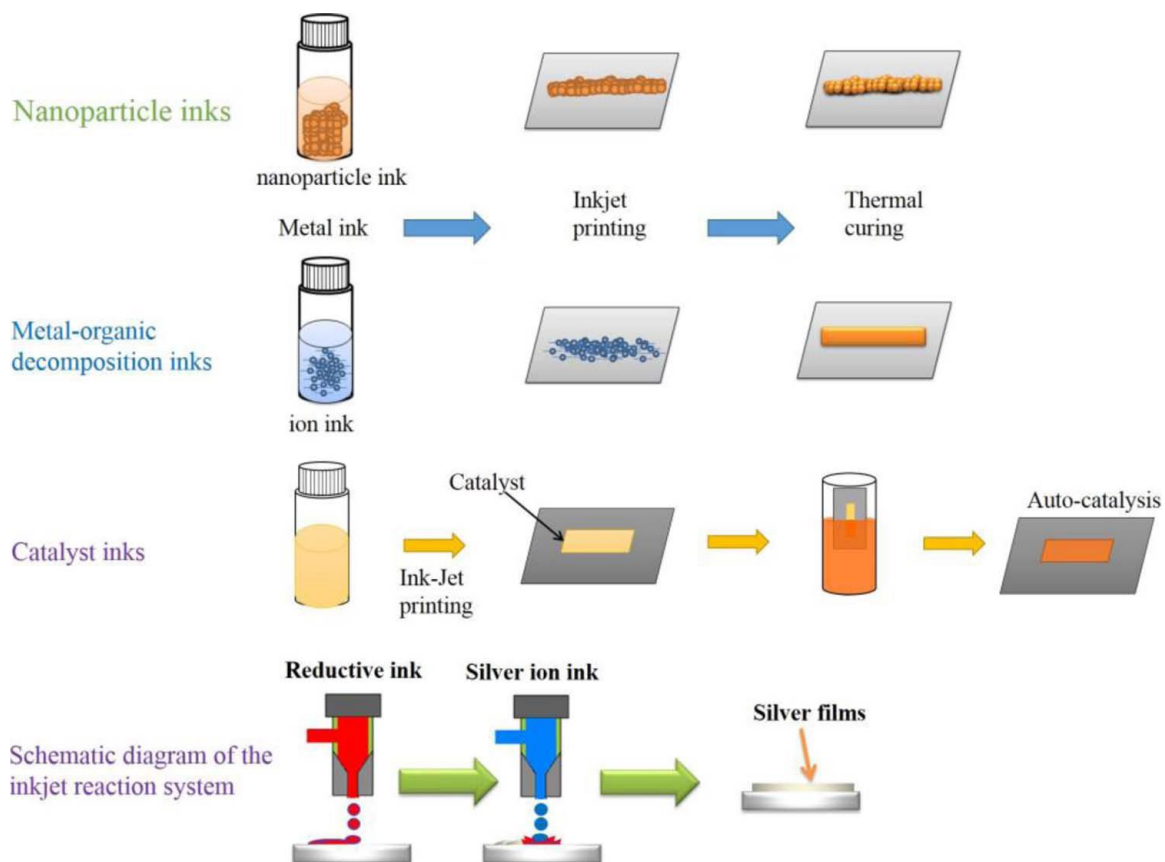


Figure 1-17: Various inks for conductive metals deposition. Reprint with permission from ref. [77].

CNTs and graphene

Carbon-based conductive materials are another family of conductive nanomaterials for printing conductive tracks, for instance CNTs and graphene. They are being used widely due to their excellent electronic, mechanical, optical, and thermal properties. Two-dimensional graphene sheet is characterized by a high intrinsic conductivity, and CNTs possess metallic or semiconducting behavior [78]. The conductivity of individual metallic CNTs is comparable to that of metals. Moreover, although van der Waals force would cause the graphene and CNTs to stick together and further clog the nozzles [79], graphene and CNTs are compatible with 3D printing approaches after proper treatment, such as being dispersed by solvent composition, dispersants or additives [80]. For example, in an inkjet printing fashion, the CNTs/graphene ink can be dispersed evenly in an organic solvent forming a conductive mixture. Typical organic solvents are

dimethylformamide (DMF), isopropyl alcohol, and N-methyl-2-pyrrolidone. Because the CNTs are hydrophobic, dispensing agents, such as Triton X-100, Tween 20 and Tween 80 and sodium cholate, are required to prepare the printable ink [81]. Depending on the working viscosity of the corresponding printing techniques, the contents of CNTs in ink is 0.01 – 10 g/L. Moreover, nitric acid in post-treatment process is commonly used to eliminate the influence of the junction points between CNTs on the final electrical performance [82].

As for graphene, dispersions of pristine graphene are usually prepared in water or organic solvents. Ideal organic solvents, including N-methylpyrrolidone and DMF are used in graphene-based ink formula, and ethylene glycol or glycerol are used to adjust the viscosity. In order to obtain a proper dispersion, the concentration of graphene ink is normally prepared as 0.11 – 9 g/L, thus, it usually requires to repeat several printing layers to get conductive tracks [83-87]. Graphene flakes easily agglomerate in solutions due to the strong inter-sheet van der Waals forces, thus while ink with graphene oxide (GO) containing epoxide, -OH, and -COOH groups is stable in water and polar organic solvents. However, for the GO-based ink formula, an additional reduction process is required to restore the electrical properties of the printed ink [86, 88].

Conductive polymers

Compared with the aforementioned two types of conductive materials, conductive polymers have a better mechanical stability and adhesion to the substrates. Conductive polymers such as poly(3,4-ethylenedioxythiophene) (PEDOT), polypyrrole (PPy) and polyaniline (PANI) have been used in 3D printed electronics [89]. In the presence of a conjugated pi-electron system throughout the polymer, printed tracks from conductive polymer is conductive, and generally, these polymers have lower conductivities than metallic inks. However, since post-printing treatment are rarely required, conductive polymers have a better processability for 3D electronics fabrication.

1.3.3 Post-treatment process

Post-treatment process is applied to improve the conductivity either through removing the insulating materials to expose the conductive patterns or improve the morphology of the conductive constitute by thermal heating or light/laser sintering. Removing insulated materials can be achieved by decomposition, desorption, or evaporation of the organic additives, aiming to enhance the contact between NPs. For the aspect of improving conductivity, high-conductively constitute can be selected and deposited (e.g. copper, silver, gold, and nickel). The following lists some post-treatment processes which are commonly used in 3D printing electronics.

Thermal sintering. The common method of sintering conductive patterns is heating the 3D printed object. Since high surface-to-volume ratio and enhanced self-diffusion of surface atoms result in a drastic decrease in their melting point, it is possible to achieve their fusion at temperatures much lower than the melting point of the bulk metal.

However, conventional thermal sintering is incompatible with most of polymers due to the decomposition when applied high temperature (normally > 150 °C), Thus, avoiding destruction of the polymer substrate concerns a lot when developing thermal-related post-treatment process.

Photonic sintering. During photonic sintering, energy can be delivered to the targeted material in a light-thermal reaction manner by using resources such as flash lamps or laser beam. When the light reaches the surface of printed layer, rapid heating starts to react with material, and then generate and sinter NPs. Effective sintering of the printed tracks can be achieved without damaging the 3D structures by adjusting the wavelength, energy, and duty cycle of the light.

Efficient sintering relies on the match between the light wavelength and the spectral absorption peaks of the metal inks. For example, silver NPs below 50 nm in diameter have an adsorption peak at around 400 nm [90], thus UV \sim 400 nm is much suitable to apply sintering process. Since UV curing techniques are applied to most commercial resin in SLA, 3D printing process using UV irradiation works for both the procedures of

converting UV-curable resin into 3D structure and sintering of silver NPs ink into conductive tracks. This 3D printed electronics process simplifies the machine configurations and vastly speeds up the fabrication process as no additional postprocesses are required, which also offers a convenient route to print electronics with large number of conductive layers [47].

Intense pulsed light (IPL), which uses visible light (such as Xenon lamps), is also a commonly used light sintering method. Short intense pulse irradiates on the printed ink, which generates rapid localized heat through photonic absorption. Currently, IPL is used to sinter the inkjet-printed conductive inks, and it can reduce the ink and sinter the conductive material in just a few milliseconds. However, IPL would lead to a destruction of the conductive patterns due to its characteristic of extreme rapid heating and cooling [91, 92].

IR sintering demonstrates a very fast approach to sinter metal inks and enhance the conductivity. From a technical point of view, IR sintering is compatible with existing 3D printing techniques. However, owing to the induced high thermal stress during the process, only high temperature resistance polymers can be processed in this system, but power and lamp distance could be adjusted to reduce the substrates temperatures.

Chemical sintering. The approach of chemical sintering is based on the addition of chemical agents to a printed ink to render the polymeric surface conductive. Some deposition material requires the removal of stabilizers via oxidation and decomposition, but most of the chemical sintering are based on destabilization of the stabilizing layer by dissolving or detachment of the chemical molecules. For instance, after dipping a porous 3D printed object in a dispersion of silver NPs, conductive percolation paths within the 3D structures are generated by exposing to HCl vapour [65]. The advantages of the chemical sintering are their low-temperature sintering process and simplicity without the need for costly equipment and high energy consumption.

ELP and electroplating process. The plating-based process is intended as a low-cost alternative to current hybrid 3D printing for 3D printed electronics. With many of the common 3D printing techniques using polymers, a simple solution to metallize the

surface of the 3D printed object is ELP or electroplating process. As most 3D printed polymeric objects can be metallized through ELP or electroplating, it makes possible to combine the high spatial resolution of the 3D printed structures with the functional properties of the coated metallic layer. A typical ELP process involves surface roughening, surface activation and ELP. Immersing into strong oxidizing solution, the surface of the polymeric object would be etched away to a certain degree, making the surface rough and hydrophilic. The increase of the roughness also increases the attachment chance for the catalyst seed deposition. Followed by dipping into the metal salt solution with reducing agent, a layer of metal can be coated to the polymeric surface. Different 3D printing material have various solubility in some specific solution. For example, in a chrome-sulfuric etchant, almost the whole surface of ABS was eaten away leaving a coarse morphology after 10 min etching, while only microholes can be observed in the surface of PETG, PLA, and PC. Based on this finding, 3D printed electronics embedded complex circuits can be manufactured by combining the dual-material 3D printing technologies and selective electroless plating [59, 62].

Electroplating has also been applied to 3D printed objects. Compared with ELP, electroplating is faster and has the ability to selectively deposit different layer thickness or materials on the same object. In electroplating metal ions transfer from the anode to the cathode, forming a metal layer to improve strength and conductivity. However, all area needed to be plated should be electrically connected to the cathode. This may require additional ELP to prepare the surface [59] or choose conductive filament to pattern circuitry [60].

1.3.4 Recent progress in 3D printed electronics

Embedded electronics

Through embedding electrical components into 3D structure, the printed part can be electronic functionality. Owing to the layer-based 3D printing technology, a single object with embedded components can be achievable: at the given layer, building process is stopped for placing electronical components. Generally, the embedded electronics can greatly decrease the mass and reduce assembly complexity. A hybrid 3D printer, multi^{3D}

system, which includes two FDM systems, a CNC (computer numerical control) router and a dispenser for conductive ink deposition, has been developed to print a part with multi-materials and multifunctionalities (Figure 1-18a-b). This system allows embed wires and components on a one structure to realize mechanical, electrical, and electromagnetic functionality. Figure 1-18c shows the printing process of the multi^{3D} system and a 3D CubeSat Trailblazer part embedded electronics has been successfully made [93].

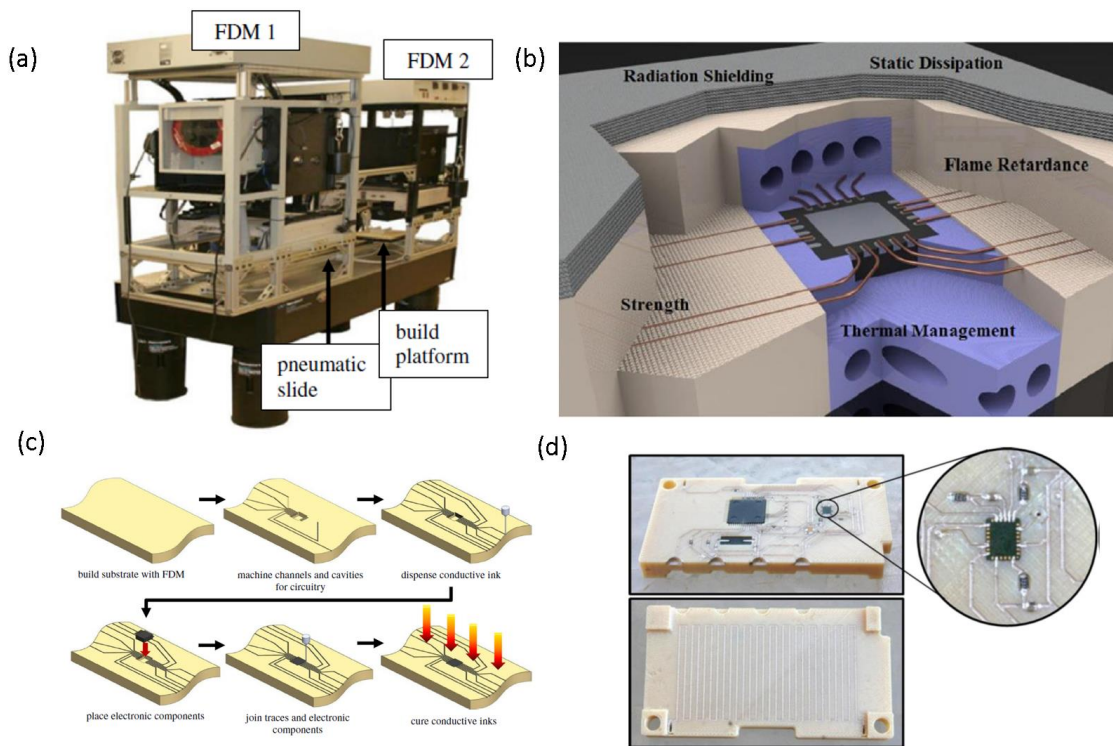


Figure 1-18: (a) The photography of mylti^{3D} system and (b) schematic of fabrication example. (c) Process steps for fabrication of 3D printed CubeSat module. (d) 3D printed CubeSat module by FDM, CNC routing, and dispenser. Reprint with permission from ref. [93].

Besides FDM, SLA can also incorporate with a digital projector to produce a functional 3D structure with embedded electrical components. As shown in Figure 1-19a, a hybrid SLA/DLP system was made by integrating a 3D Systems SLA 250/50 machine and an nScript micro-dispensing pump. A corresponding process was developed to

fabricate 2D and 3D monolithic structures with embedded conductive tracks. The whole process involved multiple starts and stops of SLA process, removing the uncured resin, inserting electrical components, and conductive ink deposition and curing by laser. Functional 3D 555 timer circuit have been fabricated by this system (Figure 1-19b-d). Couple the 3D micro-dispensing DP system for conductive traces deposition with the manufacturing flexibility of SLA machine, this method enabled 3D printed electronics fabrication. However, many of the process are manual, which is not efficient and as well as affects the quality of the printed object.

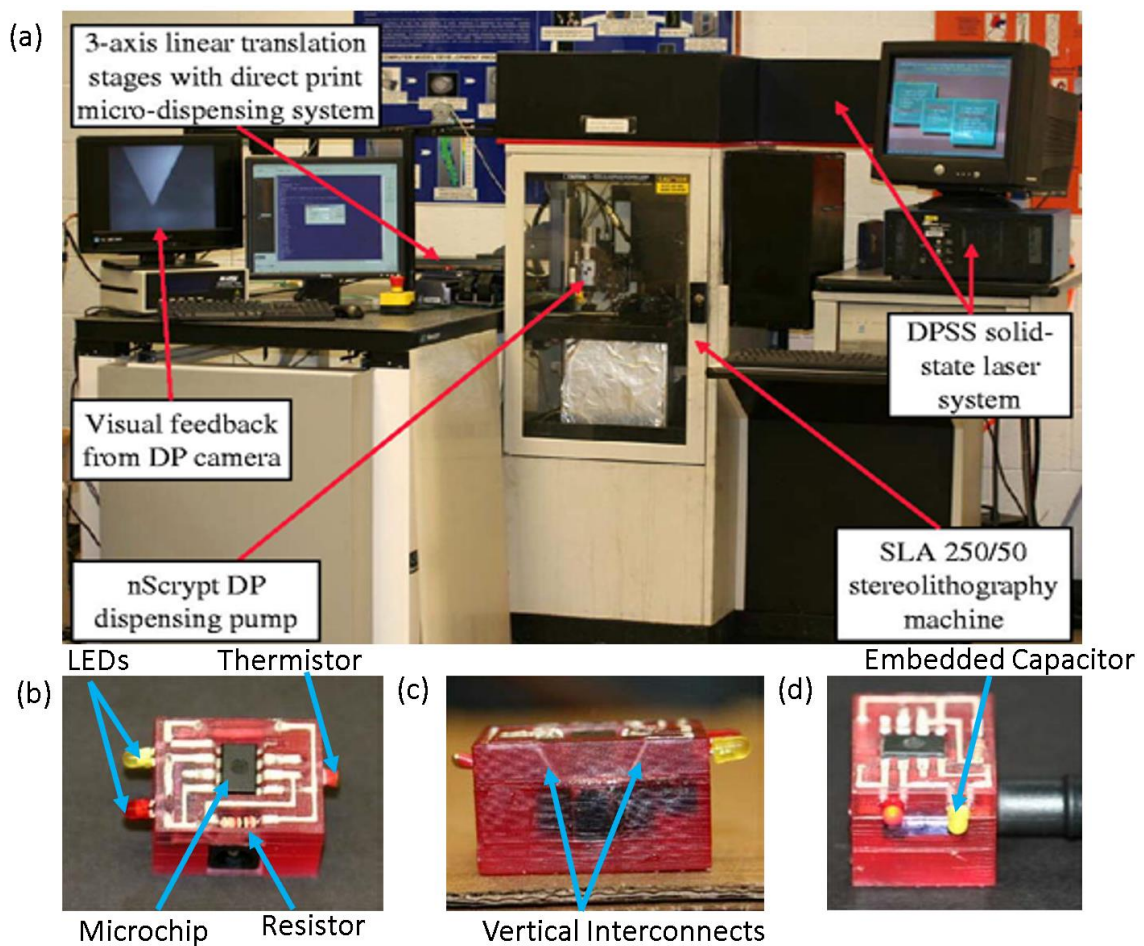


Figure 1-19: (a) Hybrid SLA/DP system. (b) 555 timer circuit; (c) vertical interconnects; (d) working 3D circuit (yellow LED is on). Reprint with permission from ref. [52].

Flexible electronics

Flexible electronics are not only capable of portable functions but also can be used to monitor human health information. Recently, 3D printing technology is employed for flexible devices fabrication with complicated geometries. 3D printed flexible electronics possess complicated geometries with precisely prescribed microarchitectures and excellent mechanical property.

To endow 3D printed electronics with excellent flexibility, flexible material for 3D printing should be developed. For example, polycaprolactone (PCL) macromonomers were synthesized via the chemical reaction of isocyanatoethyl methacrylate and PCL10K. After printed, these 3D printed flexible electronics were coated with conductive materials, such as CNT or silver particles (Figure 1-20a,b). The printed structure exhibits shape-memory behavior. Upon increasing the temperature, it recovered from the temporary shape to the original shape, as shown in Figure 1-20c in which it was used to turn on and off the LEDs. Moreover, when a layer of CNT was applied to the surface in a horse shoe pattern, the CNTs can convert the electrical energy to heat, inducing the deformation of the whole structure (Figure 1-20d,e). The 3D printed electronics comprising shape-memory materials are advantageous as their behavior can be controlled, which would expand the application of 3D printed electronics toward simple actuators.

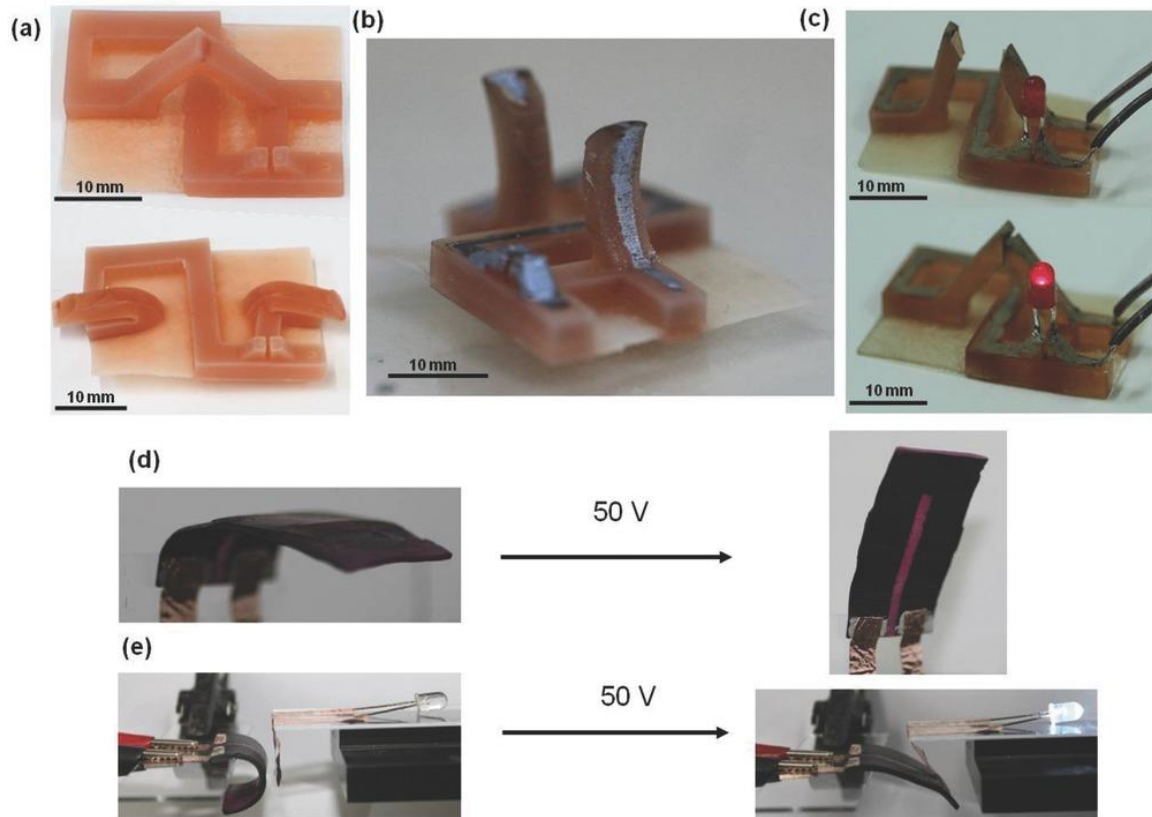


Figure 1-20: Fabrication of flexible electronics by 3D printing technology. (a) A 3D printed part (top) programmed into its temporary state (bottom). (b) Conductive ink coated on the surface. (c) Temperature sensor in its off state (top) and on state (bottom). (d) A printed object with CNTs coating was fixated in a curve state (left). When a voltage was applied, the object recovered to its flat state (right). (e) The object is used to control on and off of the circuit. Reprint with permission from ref. [94].

Conformal electronics

3D printing is capable of printing complex and conformal electronics with a suitable manufacturing technique. The aerosol jet printing has successfully been demonstrated as a powerful method to deposit conductive materials on a conformal 3D printing structure. Figure 1-21a illustrates a molded interconnect devices (MIDs) demonstration part. Aerosol jet deposited silver particles on the surface to form a 3D circuit, and then the conductive trace was sintered to give the desired properties. All these processes are

digitally driven. Figure 1-21b is a tank filling sensor. Two capacitive sensor circuits were printed on the tank. When water is pumped into the tank, the sensor measured the water level and lighted LEDs to indicate the fill level [41].

With precise control of the location, geometries and thickness of the deposit, the printed conductive patterns can insure optimum antenna performance. Some commercial mobile device antennas, such as the NFC, LTE, GPS, and BT, have been fabricated through the aerosol jet process. According to the tests, they are in the same level with other production methods [95].

Other than aerosol jet printing, filament-based direct writing also used for conformal printing. Conductive ink was deposited onto the convex and concave surface of hemispherical glass substrates. Figure 1-21c displays a representative antenna (ESA1) printed on the surface of the hemisphere glass. The cross-section of the printed lines is characterized by an optical profilometry scan of two lines located ten horizontal are segments from the base, as shown in Figure 1-21d. The inset illustrates a scanning electron microscopy (SEM) image of the segments, revealing the high resolution of the printed line. Their bandwidth approaches the fundamental limit for their size, improving nearly an order of magnitude over rudimentary monopole antenna designs [96].

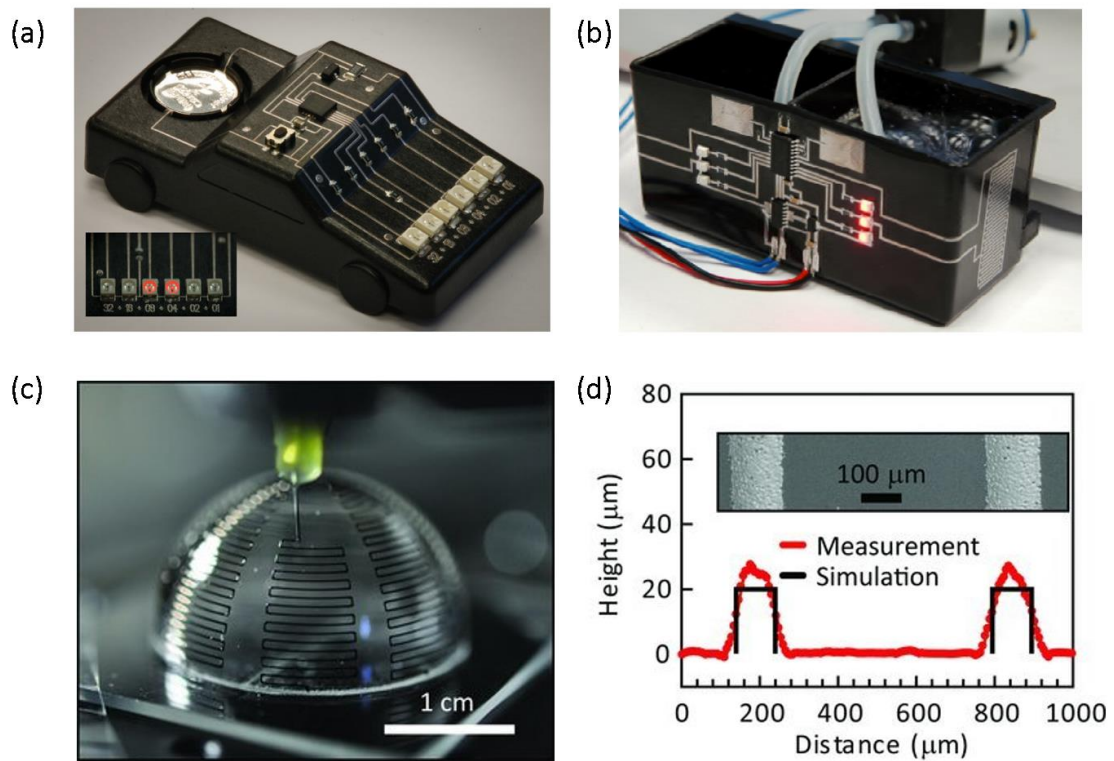


Figure 1-21: (a) 3D MID demonstrator and (b) tank filling sensor. Reprint with permission from ref. [42]. (c) Optical image of an antenna during the printing process. (d) Optical profilometry scans of representative meander lines on ESA1 and SEM image of these features (inset). Reprint with permission from ref. [96].

Table 1-1 summarized the recent advances related to 3D printing electronics.

Nonconductive Material		Conductive Material				Resistivity/sheet resistance /resistance	Applications	Ref.
Material	3D printing technique	Material	3D printing technique	Post-printing treatment				
Photocure-polymer	SLA	silver ink	direct writing	laser annealing	$2.7 \times 10^{-7} \Omega \text{ m}$	555 timer, Hall effect sensor, and a game die toy	[52, 97]	
/	/	gold ink	inkjet	laser annealing	$2.5 - 9.1 \times 10^{-2} \Omega \text{ cm}$	3D micro-wire, -wall and pocketed wire	[44]	
/	/	gold ink	inkjet	low-temperature sintering	$2.4 \mu\Omega \text{ cm}$	metal pillar arrays, helices, zigzag and micro bridges	[45]	
/	/	silver ink	e-jet	thermal annealing	$3 \times 10^{-7} \Omega \text{ m}$	arrays of pillars, walls, helical structures and arch-like bridges	[46]	
Photocure-polymer	inkjet	silver ink	inkjet	photothermal sintering	$0.48 \mu\Omega \text{ m}$	electrical tracks and two-wheeled robotic car	[47]	
Photocure-polymer	inkjet	silver ink	inkjet	thermal annealing	$1 \times 10^7 \text{ S m}^{-1}$	inductors, capacitors, and radio frequency filter	[48]	
Photocure-polymer	inkjet	silver ink	inkjet	thermal annealing	$0.34 \Omega \text{ cm}$	vertical metal wire	[98]	
/	/	CNT/PLA filament	FDM	/	2350 S m^{-1}	liquid sensors	[57]	
PLA	FDM	CB/PLA filament	FDM	/	0.09 ohm m^{-1}	flex sensors, capacitive buttons, and 'smart' vessel	[56]	
rubber/PVA filament	FDM	graphene nanoflasks and oxide ink	inkjet	chemical and thermal sintering	$4.47 \times 10^4 \text{ S m}^{-1}$	antenna and strain sensor	[99]	
PLA	FDM	conductive filament	FDM	/	$0.014 \Omega \text{ cm}$	resistor, inductor, capacitor, and high-pass filter	[58]	
PLA	FDM	/	/	ELP	$0.7 \Omega/\text{sq}$	toroidal inductor	[100]	
Photocure-polymer	inkjet	silver ink	injection	/	$2.8 \times 10^5 \text{ S m}^{-1}$	capacitors, inductors, resistors, LC tanker, and wireless-resonant sensors	[64]	
flexible filament	FDM	Galinstan metal	injection	/	$3.46 \times 10^6 \text{ S m}^{-1}$	earable smart device for core body temperature detection	[101]	
silicon	direct writing	silver ink	direct writing	/	$1.31 \times 10^{-6} \Omega \text{ m}$	bionic ear	[102]	

Table 1: 3D printed electronics: materials, 3D printing techniques, and its applications

1.4 Challenges and objectives

Although 3D printing provides a powerful and unprecedented manufacturing method for creating sophisticated, customized, and cost-effective structures, it is still limited by the lack of printable materials and functionalities of the 3D printed devices. To date, standard 3D printing techniques have advanced so that a wide range of materials including polymers, metals, and ceramics can be printed, while polymers are the most utilized materials in a variety of applications. However, for developing 3D printing technologies for fabrication of functional devices, metallic parts or electrical conductivity are often required. Therefore, it is imperative to consider developing compatible technologies for manufacturing the polymer-metal structures.

Direct metal 3D printing including SLS and SLM is a commonly used 3D metallic parts fabrication approach. Due to the local fusion process of metal powder with diameters in the tens of micrometers, objects with sub-millimeter resolution are hard to make. The component size is restricted by the chamber size and considerable effort is required for application design and setting process parameters. Also, the requirements of the homogeneous diameter of metal powders and a high intensity of energy for metal powder fusion are contributing to a high cost of direct metal 3D printing.

An alternative solution for creating metallic part is indirect metal 3D printing, which can be compatible with most existing 3D printing technologies. A classic formulation for indirect metal 3D printing materials mainly consists metal powders, polymers, solvents, and additives. Polymers are important components in 3D conductive material formulation to promote a good dispersion and prevent agglomeration of solid metal powders. Depending on the types of 3D printing technologies and the final application, the materials must meet certain requirements (such as viscosity, surface tension, etc.) to be 3D printable. For this reason, some additives are required to adjust the rheological characteristics. To obtain higher conductivity, all the polymers and additives should be removed by sintering process, allowing welding the solid metal particles. Although indirect metal 3D printing enables creating metallic structures based on the existing cost-effective 3D printing technologies, the generation of voids is inevitable during sintering

process, significantly influencing the conductivity performance of the final parts. Additionally, due to the disappear of polymers and additives, the unpredictable shrinkage rate can significantly affect the accuracy and resolution.

Besides metal and metal composites printing, a simple solution is to metallize only the surface of the printed objects through a chemical reaction, where only interfacial properties are required. Metallization of polymer substrate has advantages with respect to its ability to generate uniform coatings with low cost and simple equipment. However, the conventional metallization process has suffered from environment-unfriendly processes, and the inherent difficulties in controlling these multiple processes. Additionally, a main challenge of polymer metallization process comes from their low chemical affinity with various metals, making it necessary for surface activation treatment to develop the metal-polymer bonding.

Moreover, surface metallization of printed objects is either lacking effective approach for patterning coating or relying on costly patterning apparatus, such as photolithography or laser-induced activation, limiting the creation of metallic circuitry in a freeform manner. Although hybrid 3D printing process can print simultaneously conductive and nonconductive within one structure, the efficiency, cost and the problems brought from dissimilar materials deposition hinder the 3D printed electronics fabrication.

To settle the challenges mentioned above, a majority of efforts have focused on developing specific printing strategies together with different types of materials, which is quite insufficient and costly. In this work, special attention is being given to new material system development with unique functionalities specially enabled by 3D printing technology. Specifically, we are focusing on the functional 3D printable materials along with surface modification to make 3D printed objects desired functions and properties. Following this thinking, integrating active components into 3D printing has proven to be a successful approach for preparing functional 3D printing material. Through selecting different additives in the existing 3D printing material, a robust additive can induce various surface modification for several surface properties, which improves the efficiency of the functional object fabrication without specific printing strategies development.

Therefore, our objective in this work is to further advance the new initiator integrated 3D printing technology (i3DP II) into a more universal functionalization technique, by integrating various functional additives into 3D printing resin, together with versatile yet simple post-processing techniques to make functional 3D printed objects. Figure 1-22a-c illustrates 3D printing process using initiator-integrated resin and metallization process of the 3D printed objects. Mixing with suitable initiator, the developed 3D printing material can be compatible with the existing 3D printing techniques and the 3D printed samples can be obtained after repeat UV-curing process (Figure 1-22a). As the initiators are directly introduced into the printing liquid resins, the initiators would be distributed throughout the solidified parts, allowing metal deposition on the surface (Figure 1-22b). Also, Figure 1-22cii shows the metallization process of 3D printed objects with initiators. The catechol groups growing on the surface are used to reduce the silver ions in one-step. Compared to the commonly used dopamine method (Figure 1-22ci), polymerization of dopamine is not required in i3DP II, simplifying the metallization process.

Here, a big challenge comes from the compatibility of the functional additive with the existing 3D printing materials, due to the poor solubility of additives in 3D printing materials. With a proper combination of additives with 3D printing materials, the newly developed materials can be used to print functional 3D objects while remaining the advantages of the original 3D printing materials. Inspired by the functionality of the dopamine, some initiators with similar chemical structures can be screened. Additionally, chemical modification of the additives can be a powerful tool when the types of the additives are limited.

Simultaneously, we also pay attention to the development of selective metallization process. Through integrating metal precursors into 3D printing material, UV light converts liquid 3D printing resin into solid object consisting of successive layers and selective laser scanning allows the in-situ generation of conductive metal particles. As conductive patterns are achieved during printing process, highly selective circuits embedded in 3D structures can be fabricated based on a 3D co-printing process (Figure 1-22d).

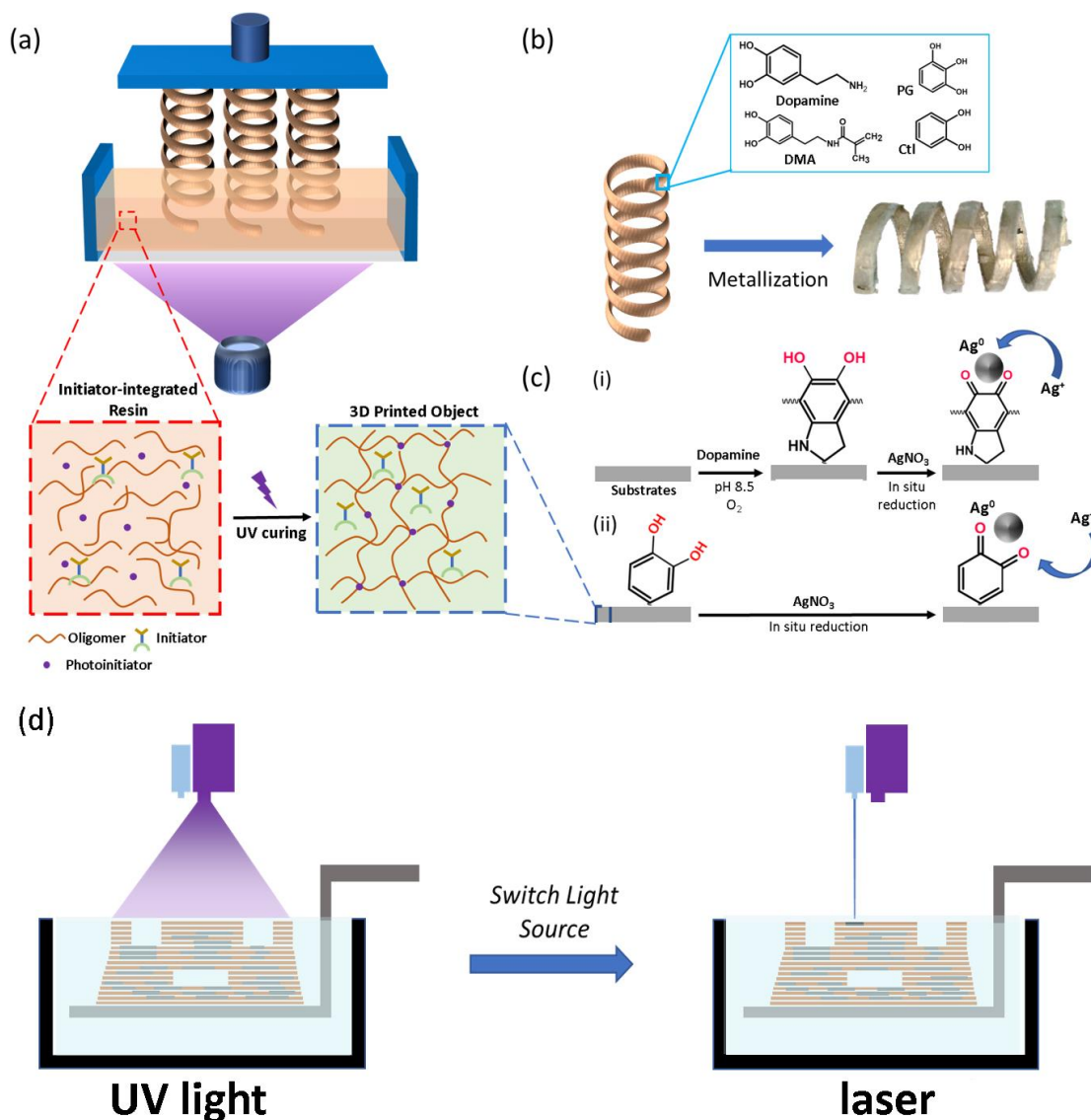


Figure 1-22: 3D printing process of electronics using (a-c) i3DP II and (d) 3D co-printing technology. For i3DP II, (a) initiator-integrated resin is applied into commercial DLP 3D printer, and (b) the functional initiator is distributed throughout the whole UV-cured sample, which can be used in a one-step metallization process. Compared to the metallization process based on dopamine (ci), the printed sample using i3DP II technology can reduce the silver ions in one-step (cii). For 3D co-printing, (d) two lights 3D printing system is proposed: UV light for polymeric structures building and laser for conductive patterns printing.

Therefore, the research in this study focused on the new 3D printing functional materials through selection of proper additives. Based on the functional surface of the 3D printed object, various properties can be obtained from post-printing modification and the usage of new 3D printing technique.

1.5 Outline of the thesis

The dissertation will be organized as follow:

In the Chapter 1, we have reviewed 3D printing history, the state-of-the-art 3D printing technologies, 3D printed electronics including printing techniques, conductive materials, and post treatment, and finally, identified the research opportunities and objectives.

To upgrade our developed i3DP technology, bio-inspired initiators - molecules that contain catechol groups - are chosen to optimize the process, namely i3DP(II). In the Chapter 2, dopamine was first studied due to its hydrophilic nature. Dopamine-integrated water-soluble UV resin was developed. The catechol groups work as a seed layer to induce the surface reactions, making a part with high-quality surface functionality. In this chapter, the functionality of making metallic structures from dopamine was successfully proved.

Aiming to comply the dopamine with a wide variety of 3D printing materials, modified-dopamine - dopamine methyl acrylamide (DMA) was synthesized in Chapter 3. The introducing of methacrylate group changes the hydrophilic nature of dopamine, making it compatible with most used acrylic-based UV resin. DMA also contains catechol groups and enables the printed object redox active, allowing silver ions reduction. The formation of thin silver film catalyzes ELP to form robust metal layers (such as Ag, Cu and Ni). The proposed method schematically provides a universal solution to combine the functionality of catechol groups from dopamine with the merits of 3D printing techniques. Moreover, as the synthetic dopamine is distributed throughout the whole 3D printed parts, locally repairing of the induced metal layer is possible.

So far, we have demonstrated the functionalities of catechol groups. In Chapter 4, we further optimized the initiator by using plant phenol and polyphenols to expand the

applicability of the initiators to a wider range of 3D printing materials, which possess a remarkable abundance of catechol and gallol functional groups are promising alternatives to dopamine. Through screening the natural phenol and polyphenols, there are two phenols existing a good solubility in acrylic-based resin. This newly developed material can introduce the catechol groups into most commercial 3D printing UV resins and enable creation of multifunctional printed objects without no critical condition.

On the basis of initiator-integrated 3D printing materials, in Chapter 5, we focus more on developing a selective metallization technology, 3D co-printing. Coupling dual light sources with a 3D printing UV resin with metal precursor, conductive patterns embedded 3D structures can be fabricated. Without multiply materials deposition and post treatment process, 3D co-printing provides an efficient and inexpensive method for 3D printed electronics, and can even be applied to generate different sizes of metal particles in 3D printed structures.

Here, Figure 1-23 summarises the different research phases in my study. In Phase 1, dopamine was chosen to replace the initiator from i3DP and mixed with water-soluble resin due to the hydrophilic nature of the dopamine. However, most commercial photocurable 3D printing materials are acrylic resins. To improve the applicability of i3DP II, modified-dopamine with increased solubility in acrylic resins was synthesized through introducing methacrylate group in Phase 2. Additionally, natural polyphenols provide abundant catechol-based initiators and two initiators (pyrogallol and catechol) were chosen in Phase 3 because of their high solubility in 3D printing materials with minimized effects on the printability of the integrated resins. As the existence of the powerful initiators on the 3D printed structures, multiply functionalities can be achieved after various secondary reactions. In Phase 4, 3D co-printing system was proposed to realize selective metallization. In our study, one additional laser was employed to generate conductive traces. This developed 3D printing system allows a simple and efficient approach to manufacture 3D printed electronics.

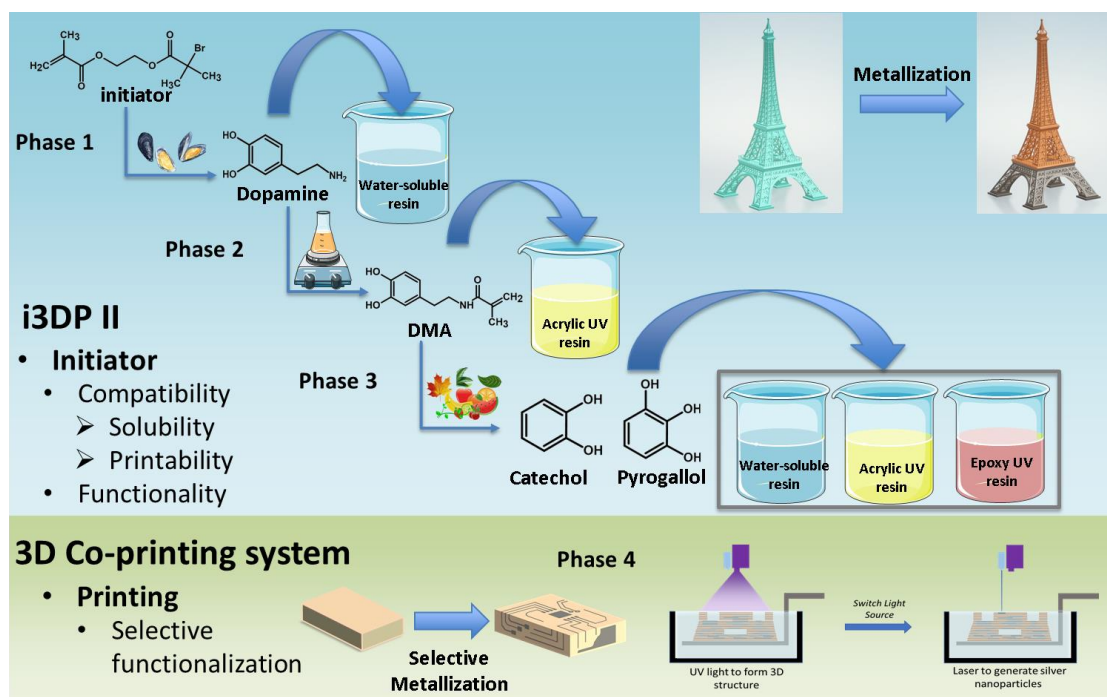


Figure 1-23: Metallization process for 3D printed electronics: from i3DP II (Phase 1-3) to 3D co-printing technology (Phase 4).

In Chapter 6, we conclude the strategies of metallization of the 3D printed objects and their applications in electronics, and give perspectives on future research.

References

1. Lecklider, T., *3D printing drives automotive innovation*. Technology, 2019. **4**: p. 3D.
2. Joshi, S.C. and A.A. Sheikh, *3D printing in aerospace and its long-term sustainability*. Virtual and Physical Prototyping, 2015. **10**(4): p. 175-185.
3. Gross, B.C., et al., *Evaluation of 3D Printing and Its Potential Impact on Biotechnology and the Chemical Sciences*. Analytical Chemistry, 2014. **86**(7): p. 3240-3253.
4. Kodama, H., *Automatic method for fabricating a three - dimensional plastic model with photo - hardening polymer*. Review of Scientific Instruments, 1981. **52**(11): p. 1770-1773.
5. Hull, C.W., *Apparatus for Production of Three-Dimensional Objects by Stereolithography*. United States Patent, Appl., No. 638905, Filed, 1984.
6. Hull, C.W., *The Birth of 3D Printing*. Research-Technology Management, 2015. **58**(6): p. 25-30.
7. Beaman, J.J. and C.R. Deckard, *Selective laser sintering with assisted powder handling*. 1990, Google Patents.
8. Crump, S.S., *Apparatus and method for creating three-dimensional objects*. 1992, Google Patents.
9. Atala, A., et al., *Tissue-engineered autologous bladders for patients needing cystoplasty*. The Lancet, 2006. **367**(9518): p. 1241-1246.
10. Tumbleston, J.R., et al., *Continuous liquid interface production of 3D objects*. Science, 2015. **347**(6228): p. 1349-1352.
11. Eckel, Z.C., et al., *Additive manufacturing of polymer-derived ceramics*. Science, 2016. **351**(6268): p. 58-62.
12. Martin, J.H., et al., *3D printing of high-strength aluminium alloys*. Nature, 2017. **549**(7672): p. 365-369.
13. Walker, D.A., J.L. Hedrick, and C.A. Mirkin, *Rapid, large-volume, thermally controlled 3D printing using a mobile liquid interface*. Science, 2019. **366**(6463): p. 360-364.
14. Kotz, F., et al., *Three-dimensional printing of transparent fused silica glass*. Nature, 2017. **544**(7650): p. 337-339.

15. Saha, S.K., et al., *Scalable submicrometer additive manufacturing*. Science, 2019. **366**(6461): p. 105-109.
16. Kelly, B.E., et al., *Volumetric additive manufacturing via tomographic reconstruction*. Science, 2019. **363**(6431): p. 1075-1079.
17. Su, A. and S.J. Al'Aref, *Chapter 1 - History of 3D Printing*, in *3D Printing Applications in Cardiovascular Medicine*, S.J. Al'Aref, et al., Editors. 2018, Academic Press: Boston. p. 1-10.
18. Reiffel, A.J., et al., *High-Fidelity Tissue Engineering of Patient-Specific Auricles for Reconstruction of Pediatric Microtia and Other Auricular Deformities*. PLOS ONE, 2013. **8**(2): p. e56506.
19. Sachs, E.M., et al., *Three-dimensional printing techniques*. 1993, Google Patents.
20. Jones, R., et al., *RepRap – the replicating rapid prototyper*. Robotica, 2011. **29**(1): p. 177-191.
21. Ambrosi, A. and M. Pumera, *3D-printing technologies for electrochemical applications*. Chemical Society Reviews, 2016. **45**(10): p. 2740-2755.
22. Melchels, F.P.W., J. Feijen, and D.W. Grijpma, *A review on stereolithography and its applications in biomedical engineering*. Biomaterials, 2010. **31**(24): p. 6121-6130.
23. Weng, Z., et al., *Mechanical and thermal properties of ABS/montmorillonite nanocomposites for fused deposition modeling 3D printing*. Materials & Design, 2016. **102**: p. 276-283.
24. Shirazi, S.F.S., et al., *A review on powder-based additive manufacturing for tissue engineering: selective laser sintering and inkjet 3D printing*. Science and Technology of Advanced Materials, 2015. **16**(3): p. 033502.
25. Frazier, W.E., *Metal Additive Manufacturing: A Review*. Journal of Materials Engineering and Performance, 2014. **23**(6): p. 1917-1928.
26. Wu, B., et al., *A review of the wire arc additive manufacturing of metals: properties, defects and quality improvement*. Journal of Manufacturing Processes, 2018. **35**: p. 127-139.
27. Cunningham, C.R., et al., *Invited review article: Strategies and processes for high quality wire arc additive manufacturing*. Additive Manufacturing, 2018. **22**: p. 672-686.
28. Ngo, T.D., et al., *Additive manufacturing (3D printing): A review of materials, methods, applications and challenges*. Composites Part B: Engineering, 2018. **143**: p. 172-196.

29. Gibson, I., D. Rosen, and B. Stucker, *Directed Energy Deposition Processes*, in *Additive Manufacturing Technologies: 3D Printing, Rapid Prototyping, and Direct Digital Manufacturing*, I. Gibson, D. Rosen, and B. Stucker, Editors. 2015, Springer New York: New York, NY. p. 245-268.
30. *Largest Metal 3D Printed Available*. Available from: <https://www.sciaky.com/largest-metal-3d-printer-available>.
31. Mostafaei, A., et al., *Binder jet 3D printing – Process parameters, materials, properties, and challenges*. Progress in Materials Science, 2020: p. 100707.
32. Mostafaei, A., et al. *Binder Jet Printing of Partial Denture Metal Framework from Metal Powder*. 2017.
33. Tan, H.W., et al., *Metallic Nanoparticle Inks for 3D Printing of Electronics*. Advanced Electronic Materials, 2019. **5**(5): p. 1800831.
34. *MarkForged metal FDM printer*. Available from: <https://markforged.com/3d-printers/metal-x>.
35. Dongxing, Z., et al., *Hierarchical metal/polymer metamaterials of tunable negative Poisson's ratio fabricated by initiator-integrated 3D printing (i3DP)*. Nanotechnology, 2018. **29**(50): p. 505704.
36. Dongxing, Z., et al., *Development of ultralight, super-elastic, hierarchical metallic meta-structures with i3DP technology*. Nanotechnology, 2017. **28**(45): p. 455708.
37. Zhang, D., et al., *Initiator-Integrated 3-D Printing of Magnetic Object for Remote Controlling Application*. IEEE Transactions on Magnetics, 2017. **53**(5): p. 1-9.
38. Wang, X., et al., *i3DP, a robust 3D printing approach enabling genetic post-printing surface modification*. Chem Commun (Camb), 2013. **49**(86): p. 10064-6.
39. Zhang, D., et al., *Development of ultralight, super-elastic, hierarchical metallic meta-structures with i3DP technology*. Nanotechnology, 2017. **28**(45): p. 455708.
40. Espera, A.H., et al., *3D-printing and advanced manufacturing for electronics*. Progress in Additive Manufacturing, 2019. **4**(3): p. 245-267.
41. Hedges, M. and A.B. Marin. *3D Aerosol jet printing-Adding electronics functionality to RP/RM*. in *DDMC 2012 conference*. 2012.
42. Hedges, M. *3D Aerosol Jet Printing–An Emerging MID Manufacturing Process*. in *9th International Congress Molded Interconnect Devices*. 2010.
43. Hoerber, J., et al., *Approaches for Additive Manufacturing of 3D Electronic Applications*. Procedia CIRP, 2014. **17**: p. 806-811.

44. Kullmann, C., et al., *3D micro-structures by piezoelectric inkjet printing of gold nanofluids*. Journal of Micromechanics and Microengineering, 2012. **22**(5): p. 055022.
45. Ko, S.H., et al., *Metal nanoparticle direct inkjet printing for low-temperature 3D micro metal structure fabrication*. Journal of Micromechanics and Microengineering, 2010. **20**(12): p. 125010.
46. An, B.W., et al., *High-Resolution Printing of 3D Structures Using an Electrohydrodynamic Inkjet with Multiple Functional Inks*. Advanced Materials, 2015. **27**(29): p. 4322-4328.
47. Saleh, E., et al., *3D Inkjet Printing of Electronics Using UV Conversion*. Advanced Materials Technologies, 2017. **2**(10): p. 1700134-n/a.
48. McKerricher, G., M. Vaseem, and A. Shamim, *Fully inkjet-printed microwave passive electronics*. Microsystems & Nanoengineering, 2017. **3**(1): p. 16075.
49. Schirmer, N.C., et al., *On Ejecting Colloids Against Capillarity from Sub-micrometer Openings: On-Demand Dielectrophoretic Nanoprinting*. Advanced Materials, 2010. **22**(42): p. 4701-4705.
50. Ahn, B.Y., et al., *Planar and three-dimensional printing of conductive inks*. Journal of visualized experiments : JoVE, 2011(58): p. 3189.
51. Jakus, A.E., et al., *Three-Dimensional Printing of High-Content Graphene Scaffolds for Electronic and Biomedical Applications*. ACS Nano, 2015. **9**(4): p. 4636-4648.
52. Lopes, A., E. MacDonald, and R. Wicker, *Integrating stereolithography and direct print technologies for 3D structural electronics fabrication*. Rapid Prototyping Journal, 2012. **18**: p. 129-143.
53. Espalin, D., et al., *3D Printing multifunctionality: structures with electronics*. The International Journal of Advanced Manufacturing Technology, 2014. **72**(5-8): p. 963-978.
54. Macdonald, E., et al., *3D Printing for the Rapid Prototyping of Structural Electronics*. IEEE Access, 2014. **2**: p. 234-242.
55. Shin, I.J. and M.S. Park, *Direct Conductive Patterning on 3D Printed Structure Using Laser*. physica status solidi (a), 2018. **215**(1): p. 1700597.
56. Leigh, S.J., et al., *A Simple, Low-Cost Conductive Composite Material for 3D Printing of Electronic Sensors*. PLOS ONE, 2012. **7**(11): p. e49365.
57. Chizari, K., et al., *3D Printing of Highly Conductive Nanocomposites for the Functional Optimization of Liquid Sensors*. Small, 2016. **12**(44): p. 6076-6082.

58. Flowers, P.F., et al., *3D printing electronic components and circuits with conductive thermoplastic filament*. Additive Manufacturing, 2017. **18**: p. 156-163.
59. Li, J., et al., *Hybrid Additive Manufacturing Method for Selective Plating of Freeform Circuitry on 3D Printed Plastic Structure*. Advanced Materials Technologies, 2019. **4**(2): p. 1800529.
60. Kim, M.J., et al., *One-step electrodeposition of copper on conductive 3D printed objects*. Additive Manufacturing, 2019. **27**: p. 318-326.
61. Fujinaga, T. *High productivity sputtering system for seed layer of printed circuit board*. in *2014 International Conference on Electronics Packaging (ICEP)*. 2014.
62. Ishikawa, A., et al., *Selective electroless plating of 3D-printed plastic structures for three-dimensional microwave metamaterials*. Applied Physics Letters, 2017. **111**(18): p. 183102.
63. Lazarus, N., et al., *Selective Electroplating for 3D-Printed Electronics*. Advanced Materials Technologies, 2019. **4**(8): p. 1900126.
64. Wu, S.-Y., et al., *3D-printed microelectronics for integrated circuitry and passive wireless sensors*. Microsystems & Nanoengineering, 2015. **1**(1): p. 15013.
65. Cooperstein, I., M. Layani, and S. Magdassi, *3D printing of porous structures by UV-curable O/W emulsion for fabrication of conductive objects*. Journal of Materials Chemistry C, 2015. **3**(9): p. 2040-2044.
66. Patel, D.K., et al., *Highly Stretchable and UV Curable Elastomers for Digital Light Processing Based 3D Printing*. Advanced Materials, 2017. **29**(15): p. 1606000.
67. Ahn, B.Y., et al., *Omnidirectional Printing of Flexible, Stretchable, and Spanning Silver Microelectrodes*. Science, 2009. **323**(5921): p. 1590-1593.
68. Fantino, E., et al., *3D Printing of Conductive Complex Structures with In Situ Generation of Silver Nanoparticles*. Advanced Materials, 2016. **28**(19): p. 3712-3717.
69. Fantino, E., et al., *In Situ Thermal Generation of Silver Nanoparticles in 3D Printed Polymeric Structures*. Materials, 2016. **9**(7): p. 589.
70. Trunov, M.A., et al., *Effect of polymorphic phase transformations in Al₂O₃ film on oxidation kinetics of aluminum powders*. Combustion and Flame, 2005. **140**(4): p. 310-318.
71. Jeong, S., et al., *Controlling the Thickness of the Surface Oxide Layer on Cu Nanoparticles for the Fabrication of Conductive Structures by Ink-Jet Printing*. Advanced Functional Materials, 2008. **18**(5): p. 679-686.

72. Ang, T.P., T.S.A. Wee, and W.S. Chin, *Three-Dimensional Self-Assembled Monolayer (3D SAM) of n-Alkanethiols on Copper Nanoclusters*. *The Journal of Physical Chemistry B*, 2004. **108**(30): p. 11001-11010.
73. Li, J. and C.-y. Liu, *Carbon-coated copper nanoparticles: synthesis, characterization and optical properties*. *New Journal of Chemistry*, 2009. **33**(7): p. 1474-1477.
74. Pulkkinen, P., et al., *Poly(ethylene imine) and Tetraethylenepentamine as Protecting Agents for Metallic Copper Nanoparticles*. *ACS Applied Materials & Interfaces*, 2009. **1**(2): p. 519-525.
75. Li, J., J.W. Mayer, and E.G. Colgan, *Oxidation and protection in copper and copper alloy thin films*. *Journal of Applied Physics*, 1991. **70**(5): p. 2820-2827.
76. Samuel, J. and P. Edwards, *Solvent-Based Inkjet Inks*, in *The Chemistry of Inkjet Inks*. p. 141-159.
77. Chen, S.P., et al., *Inkjet Printed Conductive Tracks for Printed Electronics*. *ECS Journal of Solid State Science and Technology*, 2015. **4**(4): p. P3026-P3033.
78. Nessim, G.D., *Properties, synthesis, and growth mechanisms of carbon nanotubes with special focus on thermal chemical vapor deposition*. *Nanoscale*, 2010. **2**(8): p. 1306-1323.
79. Hu, L., D.S. Hecht, and G. Grüner, *Carbon Nanotube Thin Films: Fabrication, Properties, and Applications*. *Chemical Reviews*, 2010. **110**(10): p. 5790-5844.
80. Zhang, D., et al., *Fabrication of highly conductive graphene flexible circuits by 3D printing*. *Synthetic Metals*, 2016. **217**: p. 79-86.
81. Kamyshny, A. and S. Magdassi, *Conductive Nanomaterials for Printed Electronics*. *Small*, 2014. **10**(17): p. 3515-3535.
82. Stern, A., et al., *Conductivity Enhancement of Transparent 2D Carbon Nanotube Networks Occurs by Resistance Reduction in All Junctions*. *The Journal of Physical Chemistry C*, 2018. **122**(26): p. 14872-14876.
83. Huang, L., et al., *Graphene-based conducting inks for direct inkjet printing of flexible conductive patterns and their applications in electric circuits and chemical sensors*. *Nano Research*, 2011. **4**(7): p. 675-684.
84. Al Shboul, A., et al., *Graphene dispersions in alkanes: toward fast drying conducting inks*. *Nanoscale*, 2017. **9**(28): p. 9893-9901.
85. Parviz, D., et al., *Dispersions of Non-Covalently Functionalized Graphene with Minimal Stabilizer*. *ACS Nano*, 2012. **6**(10): p. 8857-8867.

86. Torrisi, F., et al., *Inkjet-Printed Graphene Electronics*. ACS Nano, 2012. **6**(4): p. 2992-3006.
87. Li, J., et al., *Efficient Inkjet Printing of Graphene*. Advanced Materials, 2013. **25**(29): p. 3985-3992.
88. Li, D., et al., *Printable Transparent Conductive Films for Flexible Electronics*. Advanced Materials, 2018. **30**(10): p. 1704738.
89. Cummins, G. and P.Y. Desmulliez Marc, *Inkjet printing of conductive materials: a review*. Circuit World, 2012. **38**(4): p. 193-213.
90. Galagan, Y., et al., *Photonic sintering of inkjet printed current collecting grids for organic solar cell applications*. Organic Electronics, 2013. **14**(1): p. 38-46.
91. Hösel, M. and F.C. Krebs, *Large-scale roll-to-roll photonic sintering of flexo printed silver nanoparticle electrodes*. Journal of Materials Chemistry, 2012. **22**(31): p. 15683-15688.
92. Wünsch, S., et al., *Progress of alternative sintering approaches of inkjet-printed metal inks and their application for manufacturing of flexible electronic devices*. Journal of Materials Chemistry C, 2014. **2**(48): p. 10232-10261.
93. Espalin, D., et al., *3D Printing multifunctionality: structures with electronics*. The International Journal of Advanced Manufacturing Technology, 2014. **72**(5): p. 963-978.
94. Zarek, M., et al., *3D Printing of Shape Memory Polymers for Flexible Electronic Devices*. Advanced Materials, 2016. **28**(22): p. 4449-4454.
95. Lu, B., H. Lan, and H. Liu, *Additive manufacturing frontier: 3D printing electronics*. Opto-Electronic Advances, 2018. **1**(01): p. 170004.
96. Adams, J.J., et al., *Conformal Printing of Electrically Small Antennas on Three-Dimensional Surfaces*. Advanced Materials, 2011. **23**(11): p. 1335-1340.
97. Navarrete, M., et al. *Integrated layered Manufacturing of a Novel Wireless Motion Sensor System with GPS*. 2007.
98. Sowade, E., et al., *Toward 3D-Printed Electronics: Inkjet-Printed Vertical Metal Wire Interconnects and Screen-Printed Batteries*. Advanced Engineering Materials, 2019. **21**(10): p. 1900568.
99. Li, X., et al., *Self-reinforcing graphene coatings on 3D printed elastomers for flexible radio frequency antennas and strain sensors*. Flexible and Printed Electronics, 2017. **2**(3): p. 035001.

100. Jian, J.R., et al., *High performance 3D printed electronics using electroless plated copper*. AIP Advances, 2017. **7**(3): p. 035314.
101. Ota, H., et al., *3D Printed "Earable" Smart Devices for Real-Time Detection of Core Body Temperature*. ACS Sensors, 2017. **2**(7): p. 990-997.
102. Mannoor, M.S., et al., *3D Printed Bionic Ears*. Nano Letters, 2013. **13**(6): p. 2634-2639.

Chapter 2

2 Dopamine assisted metallization process in water-soluble 3D printing resin

A new generation of initiator-integrated 3D printing, namely i3DP II, was proposed and demonstrated. This i3DP II technology dramatically simplifies the experiment procedures and eases the reaction conditions. Various metallic structures were fabricated by directly integrating a water-soluble dopamine into the water-based resin followed by a direct surface-initiated electroless plating. Ni- and Cu-coated complex structures were prepared. The proposed method avoids the tedious and time-consuming polymerization process of polydopamine. By combining the merits of 3D printing in structure design with those of catechol groups assisted surface modification, the proposed method was demonstrated as a cost-effective approach to largely extended the capability of 3D printing, and will make 3D printing technology more practical in areas of electronics, acoustic absorption, thermal insulation, catalyst supports, and others.

2.1 Introduction

As summarized in the Chapter 1, all 3D printing techniques are encountering a same manufacturing challenge: highly complex metallic parts are considerably hard to fabricate. For example, approaches of direct metal 3D printing, such as SLS or SLM, have several inherent limitations in fabricating metallic structures, due to large temperature gradients involved by the local fusion process. Thus, it is hard to manufacture objects with sub-millimeter resolution [1]. In contrast to approaches of direct metal 3D printing, indirect methods including FDM and SLA are restricted to a narrow range of applications although they can provide high customized and low-cost products.

Nowadays, the conjunction of materials together with surface modification technology inspires scientists to extend the working range of 3D printing toward more applications [2-5]. Following this thinking, bonded materials can form composites with materials properties tailored, and people can obtain even completely new materials. Metallic

objects can also be manufactured by referring to this idea. Thus, it is possible to combine the high-resolution 3D printed objects with the functionalities of metals.

The feasibility of manufacturing complex metallic structures opens a new avenue toward some emerging applications, such as volumetric electronics. Several recent studies have already demonstrated applications of electronics made by 3D printing polymers techniques, followed by electroless plating (ELP) process [6-8], which typically involves three steps: roughening, surface activation, and metal deposition. Roughening methods include the use of chemical, plasma, and laser etching [6, 9, 10], aiming to improve the adhesion of catalyst (mainly palladium) to the printed object during the surface activation step. Surface activation provides favorable sites for metal nucleation/reduction and growth in the subsequent metal deposition step. To simplify the ELP process and improve the uniformity of the coated layer, we proposed initiator-integrated 3D printing method, i3DP. By incorporating a Br-containing vinyl-terminated initiator into UV resin, 3D printed objects with functional material enable post-printing surface-initiated modification [11]. This method extends 3D printing capability to meet specific requirements for applications in electronics [12], actuator [5], metamaterial [13, 14], energy [15], and biomedical science [16], where high surface quality is required.

The existing i3DP technology is still at an early stage due to the costly initiator and nitrogen protection requirement [11]. It is therefore essential to upgrade the i3DP into a simple and cost-effective way. Recently, several surface modification approaches have been explored; and among these, dopamine is widely used as a versatile tool for in situ nucleation and growth of metal NPs [17]. Inspired by the composition of adhesive proteins in mussels, dopamine can form surface-adherent polydopamine films onto various substrates by simple dip-coating method. Polydopamine-induced second reaction can create a variety of ad-layers. Recently, Zhang et al. [2] added dopamine into printable resin through stirring and ultrasonication. The added catechol-based group acts as a seed layer to initiate the formation of polydopamine (PD), and then metallization process is applied to coat a metal layer on the 3D printed object surface. This method updates our previous i3DP technology to be a new generation, namely i3DP II technology, which dramatically simplifies the experiment procedures and eases the reaction conditions,

providing a simple solution to metallize the polymeric surface. Due to the dopamine was distributed throughout the whole printed objects, local repair can also be achieved. In comparison to the aforementioned method by Br-containing vinyl-terminated initiator, dopamine-based method is an attractive alternative because of its simple fabrication process and lower material cost. Dopamine-based coating method is depended on the formation of PD film. After immersing the objects in an aqueous alkaline solution of dopamine, spontaneous formation of PD coatings occurs on virtually all material surfaces via oxidative polymerization. The surface-adherent PD film acts as a platform for various purposes, including metallization of polymeric objects [18].

However, two concerns of the method based on dopamine-added resin need to be considered. On the one hand, the very low kinetics of the dopamine polymerization process, which usually requires 10 – 24 h to form a layer thick enough for the subsequent reaction. Besides, the limited shelf life of the dopamine aqueous solution means freshly prepared solution is necessary. During the PD formation process, basic conditions (pH 8.5) of the solution and oxygen are two critical conditions to induce dopamine polymerization. This limits the scope of possible reactions which need acid or neutral condition. On the other hand, the compatibility between water-soluble dopamine and the acrylic-based 3D printing resin makes the preparation 3D printing resin with dopamine difficult. In our previous study, a homogeneous resin with dopamine was obtained via magnetic stirring. However, due to the poor solubility of dopamine in acrylic UV resin, the aggregation of dopamine particles is unavoidable.

Aiming to address the challenges above, herein, we optimized the i3DP II by directly introducing the dopamine into the UV-curable resin, and skip the formation of polydopamine, according to the findings that although PD formation is necessary for most cases, most functionalities origin from catechol group. It is reasonable to deduce that dopamine would have a similar functionality because of the existence of catechol group.

While for the problem of solubility, water-based UV resin was selected. Thus, we can develop a customized photocurable UV resin with aqueous dopamine, with the ability of

realizing the same function of polydopamine and then endow the 3D printed objects with tunable functions, conductive and metallization as focal points. The adopted methodology follows the thinking of using aqueous media to dissolve the dopamine into water-soluble UV resin, due to dopamine has a high solubility in water. By introducing the dopamine aqueous solution into the water-based photo-curable resin for 3D printing process, the dopamine can be fully distributed in the 3D printed parts after UV curing process. The catechol-based molecules of dopamine existed on the surface work as a seed layer for the following reactions (the metallization process is demonstrated in this project due to my thesis objective), resulting in a high-quality surface functionality. As a proof of concept, various complex polymer-metal structures following the proposed method were demonstrated.

2.2 Experimental section

2.2.1 Chemicals and materials

Polyethyleneglycol diacrylate (PEGDA) and 4-acryloglmorpholine (ACMO) (Lihou company) were selected as the basis of water-based resin. 2,4,6-trimethylbenzoyldiphenyl phosphine oxide (TPO) was adopted as the photoinitiator due to its high performance in the near UV spectrum. Dopamine hydrochloride was then used to prepare dopamine solution. Silver nitrate was chosen for metallization process. 4-Methylcatechol, 2,3,4-Trihydroxybenzaldehyde, catechin hydrate, and tannic acid were used to verify the function of catechol group. All the above chemicals except other indication were purchased from Sigma-Aldrich and used without any further purification.

2.2.2 Preparation of customized 3D printing UV resin

Water-soluble UV resin base was firstly prepared by adding 0.4% TPO into PEGDA. Dopamine aqueous solution of different concentration (5 – 250 g/L) were prepared, and then various volume of dopamine solution (10 – 50 vol%) was mixed with the resin base. After complete mixing, resin base was degassed for 30 minutes in the dark which was ready for printing. Here, the UV lamp was used to cure the prepared resin to verify its printability. Specifically, 2 ml resin was poured into a dish and then cured by the UV

light for 1 min. Disk shape samples of 12 mm in radius and 4 mm in thickness were made by suitable formulations.

2.2.3 Metallization of the 3D printed structures

After cured using dopamine-integrated water-soluble UV resins with different dopamine concentration and volume percentage, the printed disk samples were placed into 0.1 mol/L silver nitrate solution to get silver coating on their surface. Then, the thickness and conductivity of the deposited silver coating were measured and calculated. By comparing the conductivity of samples, both the printability and conductivity of the corresponding formulation was considered to select for the following 3D printing process.

Commercial DLP 3D printer (PICO2, Asiga) was used in this study to print 3D objects in a layer-by-layer fashion. Specially, digital models were first designed by modeling software (SolidWorks) and then sliced into a series of images, which contained the information of each cross-section. Next, the digital model was sent to the 3D printer, where the commercial printing software reads and identifies the cross-section information. After that, the 3D printer will cure the liquid resin according to the cross-section pattern. Once one layer is cured, the building plate will move up to allow the resin refilling in the blank area, and then move down again for next layer printing. This printing process is repeated until the whole object is created. Finally, the printed object was ultrasonically rinsed for 5 min in ethanol and dried by nitrogen flow.

Dopamine-assisted metallization process is carried out by immersing the printed objects into metal salt solution. For silver deposition, the printed object was dipped into aqueous silver nitrate solution for one hour at room temperature. The object then was removed from the solution, washed with DI water, and dried with N₂.

For copper deposition, a stock solution of 50 mM ethylenediaminetetraacetic acid (EDTA), 50 mM copper (II) chloride (CuCl₂), and 0.1 M boric acid (H₃BO₃) was prepared; and using 1 N of NaOH adjusted the pH of solution to 7.0. After the dopamine-coated objects were placed in the solution for 3 hours at 37°C, 0.1 M dimethylamine-

borane (DMAB) was added to initiate the ELP of copper. After 4 hours reaction, the object was taken from the solution, and rinsed with DI water and dried with N₂.

For nickel deposition, the bath solution containing 40 g/L of Ni₂SO₄·5H₂O, 20 g/L of sodium citrate, and 10 g/L of lactic acid was prepared in ultrapure water. 1 g/L of DMAB aqueous solution was prepared separately, and the final electroless solution was prepared for a 4:1 volumetric proportion of nickel-to-reductant stocks. The dopamine-coated object was immersed into the electroless solution for 2 hours at 30°C.

2.2.4 Characterization

Cary 100 UV-visible spectrophotometer (Agilent, USA) was used to UV-spectrum test. A Nicolet 6700 spectrophotometer (Thermo Nicolet) was used to measure the Fourier transform infrared (FTIR) spectra under ATR mode. The morphology of the metallic structures was investigated by Hitachi S-4500 field-emission scanning electron microscope (SEM) at 5 kV accelerating voltage. An M 2400 Keithley Source-meter/unit (voltage range 50 V, step 1 V) was used to measure the sheet resistance using the four-probe method.

2.3 Results and discussion

2.3.1 Printability of the integrated resin and metallization process

The printability of the dopamine-added PEGDA was examined to confirm the feasibility of 3D printing process. The metal film generation relies on the catechol-groups distributed on the surface of polymeric objects. The integrated resin mainly contains photoinitiator, oligomer (PEGDA) and dopamine aqueous solution. Obviously, both the concentration and added volume of dopamine solution play a critical role in surface properties of printed architectures.

UV-visible absorbance spectra and FTIR analysis were used to investigate the UV absorption of the prepared resins and confirm the functionality of the printed samples, respectively. Figure 2-1a shows the UV-visible absorbance of the prepared resins with various dopamine concentrations (0 g/L, 50g/L, 150 g/L, and 250 g/L) and volume percentage (10 vol% and 50 vol%), and Figure 2-1b displays the spectrum of the resins

based on the same dopamine concentration with various volume percentage. With the same added volume, the absorbance decreases with the increase of the dopamine concentration; and the absorbance also declines with the increase of the volume percentage at the same concentration. According to optical spectra of all the resins, moderate absorbance in the near UV region were observed, which are feasible with our commercial 3D printer. Furthermore, the printability measurement was conducted following. In our study, 12 formulations in Figure 2-1a were prepared for the initial printability tests, and all formulations can be solidified even when the addition of dopamine solution is as high as 50 vol%. Moreover, the chemical groups of the printed sample were studied by FTIR. Figure 2-1c illustrates the FTIR spectra of samples cured by water-soluble resin (PEGDA) and dopamine-integrated water-soluble resin, respectively. The broad and strong bands in the range of 3000 – 3400 cm^{-1} was attributed to intermolecular hydrogen bonds and the peak located at 3405 cm^{-1} was due to $-\text{NH}_2$ stretching. The characteristic peaks at 1525 cm^{-1} and 1177 cm^{-1} were attributed to NH_2 scissoring vibration mode and C-C stretching vibration mode, respectively [19]. In addition, in contrast to the FTIR of polydopamine NPs from previous studies, peaks corresponding to $-\text{NH}_2$ was not present in the polydopamine spectrum, suggesting that the polymerization of the dopamine did not occur during resin preparing and UV curing process in this study [20]. From the above results, we can conclude that the dopamine has been successfully integrated into the water-soluble resin.

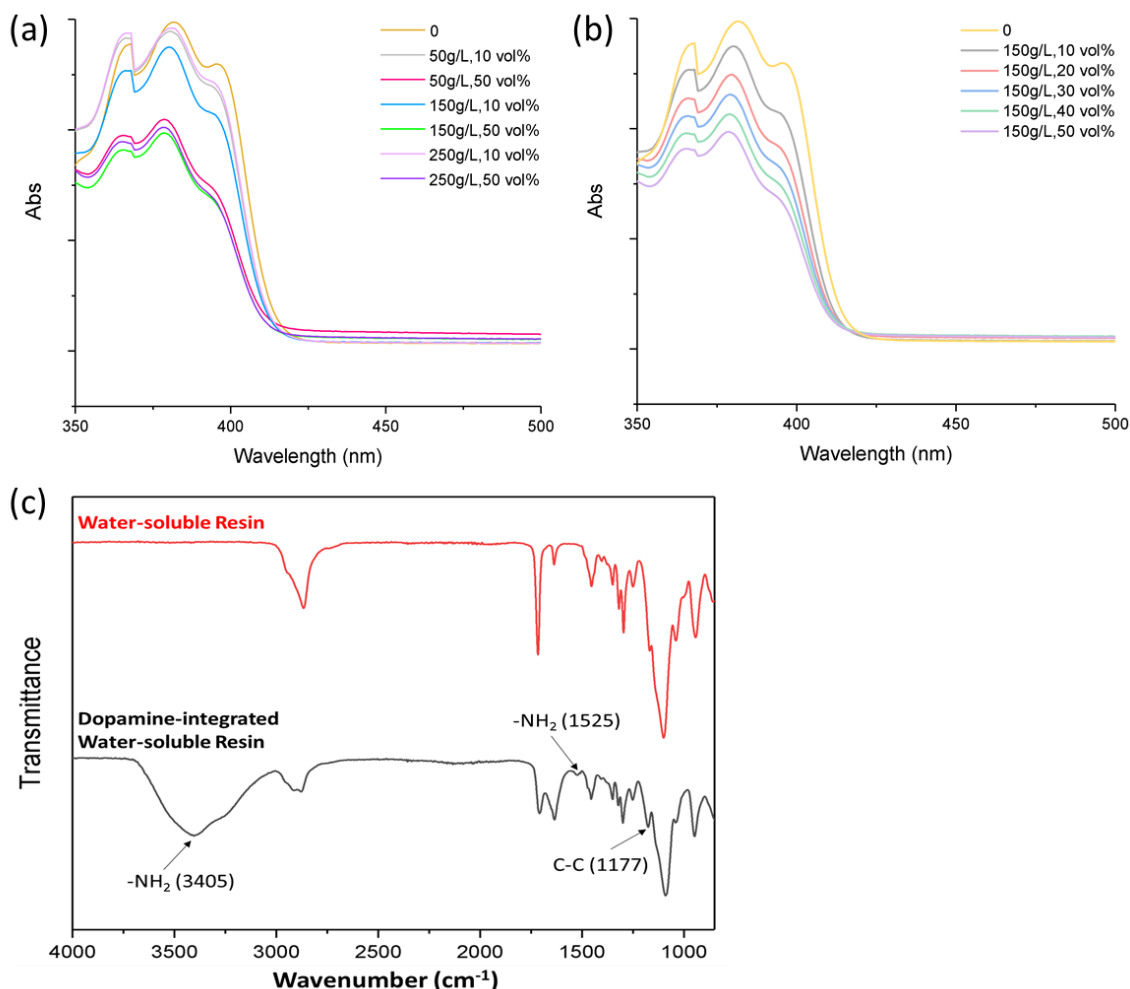


Figure 2-1: UV-visible absorbance spectra of water-soluble resins with various (a) dopamine concentration (0 – 250 g/L) and volume percentage (10 and 50 vol%), and (b) volume percentage (0 – 50 vol%) at 150 g/L aqueous dopamine solution. (c) FTIR analysis of the samples printed by dopamine-integrated 3D printing resin.

The existing of two hydroxyl groups of the catechol moiety show strong chelation affinity towards metal ions (i.e., Ag⁺ or Au³⁺), which can be directly reduced due to the redox activity of the catechol-groups. During silver deposition, the cured disk-shape samples were placed in 0.1 mol/L AgNO₃ solution for 4 h. As seen from Figure 2-2b-f, most of samples can be coated with a layer of grey-silver on the surface, which was detected as silver nanoparticles via SEM. The results prove our hypothesis that dopamine can act as reaction medium to initiate electroless deposition. However, the cured parts

with high content of dopamine solution tend to have poor mechanical performance, and cracks occurred when immersed into AgNO_3 solution (shown in Figure 2-2d(ii), e(ii) and f(ii)). In addition, through measuring the resistance of two random points on the deposited silver coating, it was found the increasing of the dopamine concentration can reduce metallic film of higher conductivity. When the concentration is lower than 50 g/L, the samples are nonconductive. It suggested that both concentration of dopamine solution and volume percentage impact the reduction process of silver ions, due to the varied density of terminate group of dopamine. Thus, formulations of three different concentrations (50 g/L, 150 g/L and 250 g/L) were chosen for the following experiments.

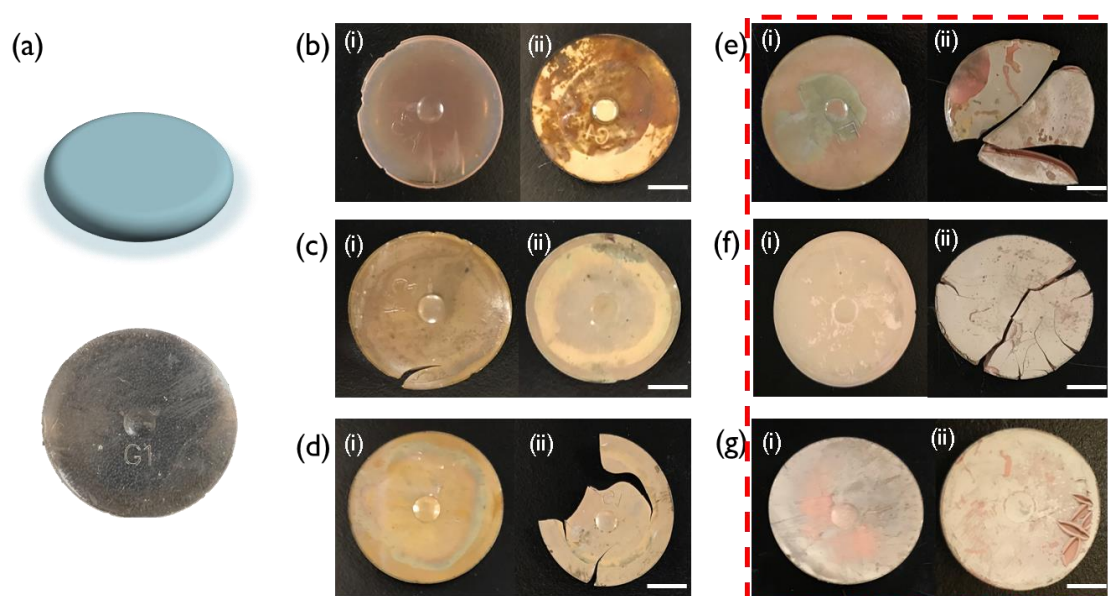


Figure 2-2: Metallization of UV-curing parts with various formulations. (a) 3D model (top) and the UV-curing object (bottom). Different concentrations of dopamine aqueous solution, such as (b) 5 g/L, (c) 10 g/L, (d) 25 g/L, (e) 50 g/L, (f) 150 g/L, and (g) 250 g/L, was used to prepare the UV resin. The cured parts were immersed into 0.1 mol/L AgNO_3 solution for 4 h. (i) and (ii) represent 10 vol% and 50 vol%, respectively. Scale bar: 10mm.

It was also worth noting that formulations with high dopamine concentration were able to deposit silver coating of comparable conductivity with that made by traditional deposition process. To contrast, the silver coating reduced by PD-assisted method is lack

of conductivity, and can only act as catalyst medium to induce another ELP process, aiming to get a conductive coating. For example, printed electronics using PD-assisted method in [21-24] required additional silver ELP process, while the samples at the concentration of 50 – 250 g/L with 50 vol% possess conductivity.

Here, the effects of the silver nitrate concentration on the coating conductivity were also studied. The formulation with 150 g/L dopamine solution and 20 vol% was used to fabricate samples. The cured samples were immersed into various AgNO_3 solution (0.1 – 0.7 mol/L) for 4 h, and no obvious difference was found between samples in conductivity (Figure 2-3). Thus, 0.1 mol/L AgNO_3 is enough for the silver deposition on the printed substrates.

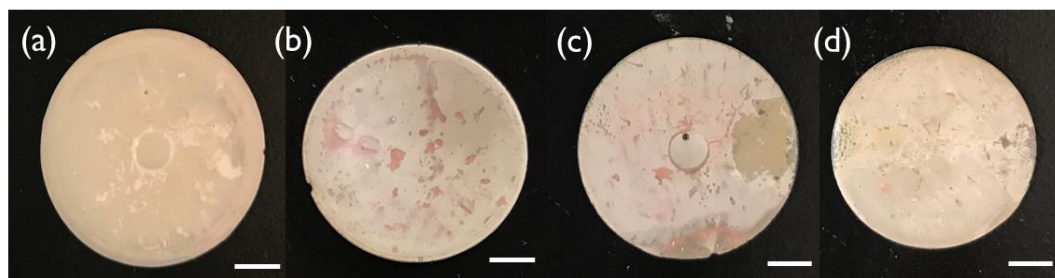


Figure 2-3: Metallic objects fabrication via silver deposition process with various AgNO_3 : (a) 0.1 mol/L, (b) 0.3 mol/L, (c) 0.5 mol/L, and (d) 0.7 mol/L. Scale bar: 10 mm.

2.3.2 Formula optimization of the integrated resin

In our study, the increasing amount of dopamine solution in the resin enhanced the silver reduction, while more dopamine solution mixed in the resin usually resulted in poorer mechanical performance. It is therefore critical to optimize the amount of dopamine in order to balance the reduction function and the mechanical property. Thus, formulations of three different concentrations (50 g/L, 150 g/L and 250 g/L) were chosen for the following experiments to optimize the formulations.

According to the initial experimental results, five amounts of dopamine solution (10 to 50 vol%, 10 vol% as interval) were mixed with PEDGA-based resin, and dopamine solution of three different concentrations (50 g/L, 150 g/L, and 250 g/L) were used. The resultant

dopamine-added resin was photocured to disk shape samples which were deposited with a layer of silver coating following the protocol mentioned above. All the silver treated samples are shown in Figure 2-4 and the samples using formulation with 150 g/L dopamine solution (20 – 50 vol%) had a better conductivity, which were measured as 1 - 4 Ω /cm. For the sample prepared by 50 g/L dopamine solution, when lower fraction of dopamine solution was mixed (< 20 vol%), the sample can only partially get metallized, while a complete silver film can form on the sample when higher v/v percentage of dopamine solution was involved. In addition, when the dopamine solution concentration was larger than 150 g/L, the further increasing of the dopamine concentration will decrease the metal reducibility, and cannot get an entire silver coating on the sample. Folded structures were detected on the sample (250 g/L and 50 vol%), and cause a poor adhesion to the Ag^+ ions. The purple dash box in Figure 2-4 shows the broken samples which were prepared by using 50 vol% dopamine solution after 4 h AgNO_3 treatment, indicating the 50 vol% dopamine solution is not feasible with 3D printing process.







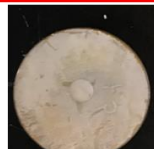


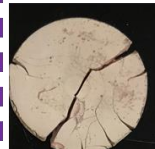
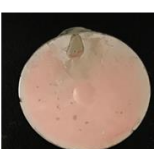




Dopamine Concentration (g/L)	Percent % (v/v)				
	10 vol%	20 vol%	30 vol%	40 vol%	50 vol%
50					
150					
250					

Figure 2-4: Metallic samples with various dopamine solution concentrations (50 g/L, 150 g/L, and 250 g/L) and volume/volume percentage (10 vol%, 20 vol%, 30 vol%, 40 vol%, and 50 vol%).

Layer thickness and sheet resistance of three formulations with different volume percentage (20 vol%, 30 vol%, and 40 vol%) were measured and calculated, respectively. The metallic sample with 150 g/L and 50 vol% was cleared out due to its poor mechanical property. The SEM images of each sample's cross-section were shown in Figure 2-5, illustrating the compactness and thickness of the silver films. After 12 h immersion, the silver thickness is about 13 μm . To satisfy the practical applications, thick and highly conductive film is preferred. The samples prepared by dopamine-added resin have acceptable sheet resistances, which can reach 0.1246 Ω/sq (Figure 2-5d). The conductivity for 20 vol% is 0.276 Ω/sq , inferring the conductivity is 41.9% of the corresponding bulk silver, which can meet the requirement for most practical applications. Considering the conductivity and mechanical performance, the integrated resin with 150 g/L and 20 vol% is the best choice for 3D printed electronics.

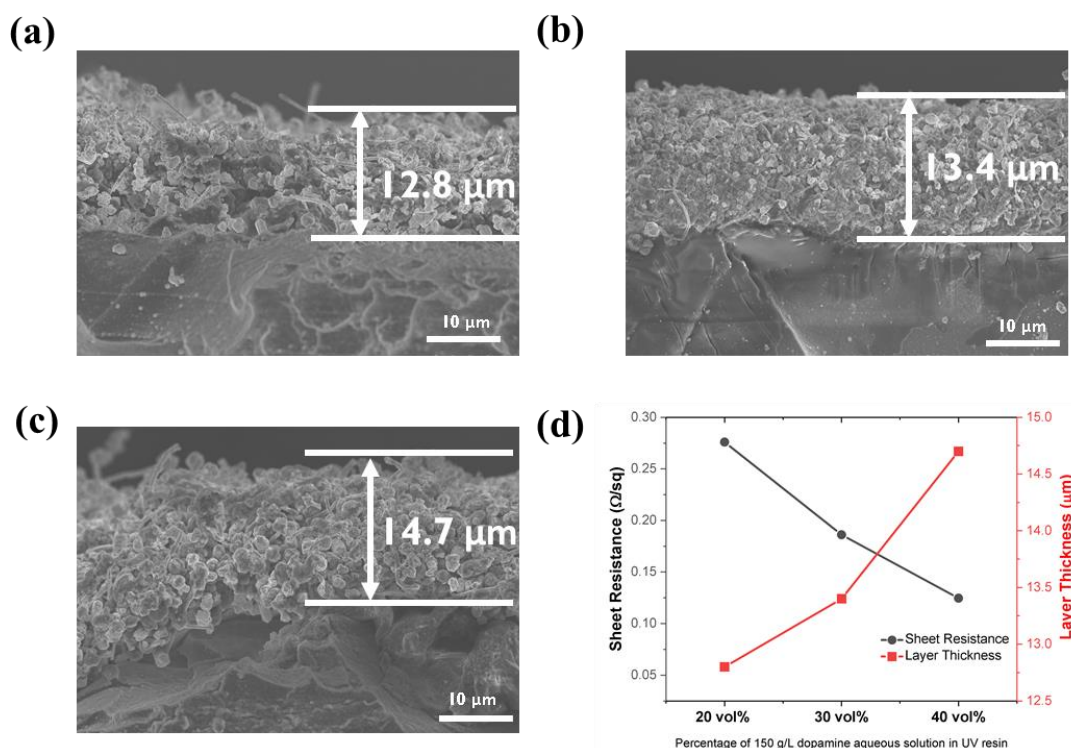


Figure 2-5: Thickness of coated silver film with various dopamine concentration: (a) 20 vol%, (b) 30 vol%, and (c) 40 vol%. (d) Sheet resistance and layer thickness obtained at the various dopamine concentration.

2.3.3 Surface morphology of metallic parts

The influence of ELP time on the deposited silver film was investigated taking the cured samples using resin with 20 vol% 150 g/L dopamine solution as the research object (Figure 2-6). The silver deposition reaction is fast: at first 5 min, above 50% area was covered by the silver film, and a complete film was formed after 1 h immersion in AgNO_3 solution. At early stage, the deposited silver structure was worm-like elongated interconnected clusters (Figure 2-6a-c). Then, the silver further grew, causing a rougher layer, and silver nanowire emerged (Figure 2-6d). With the reaction time increased, Figure 2-6f shows the random orientation of the silver nanowire over the whole film, forming an interconnected network with stacked micro-flakes. The previous reports have proved that silver nanowire is the desired morphology for efficient electron transport due to its high aspect ratio of silver nanowires and low number of inter-nanoparticle contacts [25, 26].

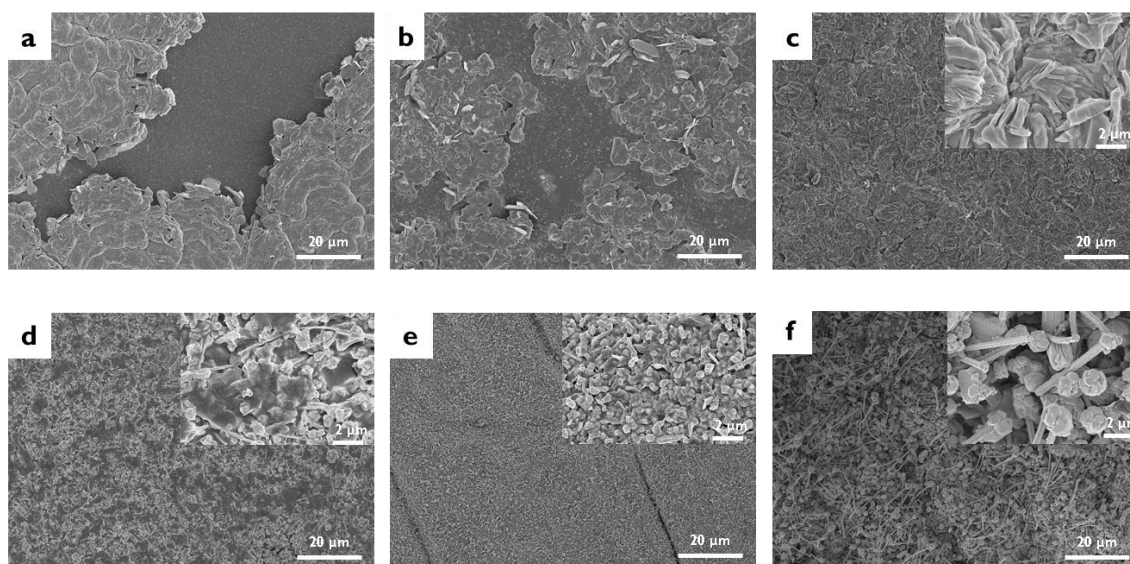


Figure 2-6: FE-SEM images of the surface with various ELP time: (a) 5 min, (b) 15 min, (c) 30 min, (d) 1 h, (e) 4 h and (f) 12 h. Inset is the enlarged picture.

2.3.4 3D printing of complex metallic structures

As the printability of the liquid resin and metal bonding affinity of the dopamine-added resin have been proved, the optimized resin was then applied to DLP 3D printer to print complex 3D structures. Taking advantage of the digital design, 3D printed complex

architectures were printed and metallic coating was obtained after ELP (Figure 2-7). The layer thickness was set as 50 μm during 3D printing process and printed objects with acceptable resolution can be obtained. The printed objects confirmed again that the addition of 20 vol% dopamine aqueous solution affect minimally the 3D printing process. Moreover, the dopamine-integrated UV resin is also applicable to deposit other metal coatings such as Ni (Figure 2-7a) and Cu (Figure 2-7b). The adoption of a variety of metals coating onto 3D printed objects provides several advantages for practical applications. Take Cu for example, it possesses a bulk resistivity ($1.7 \times 10^{-8} \Omega \text{ m}$) comparable to Ag ($1.6 \times 10^{-8} \Omega \text{ m}$), but copper is significantly cheaper, making it a good alternative to electronics. During ELP, the oxidation of copper is dramatically inhibited. Herein, dopamine immobilized on the surface acts as an ELP catalyst to initiate metal reduction and growth. Without tedious process and expensive catalyst, our approach provides a simple and low-cost way to fabricate Cu-polymer architectures.

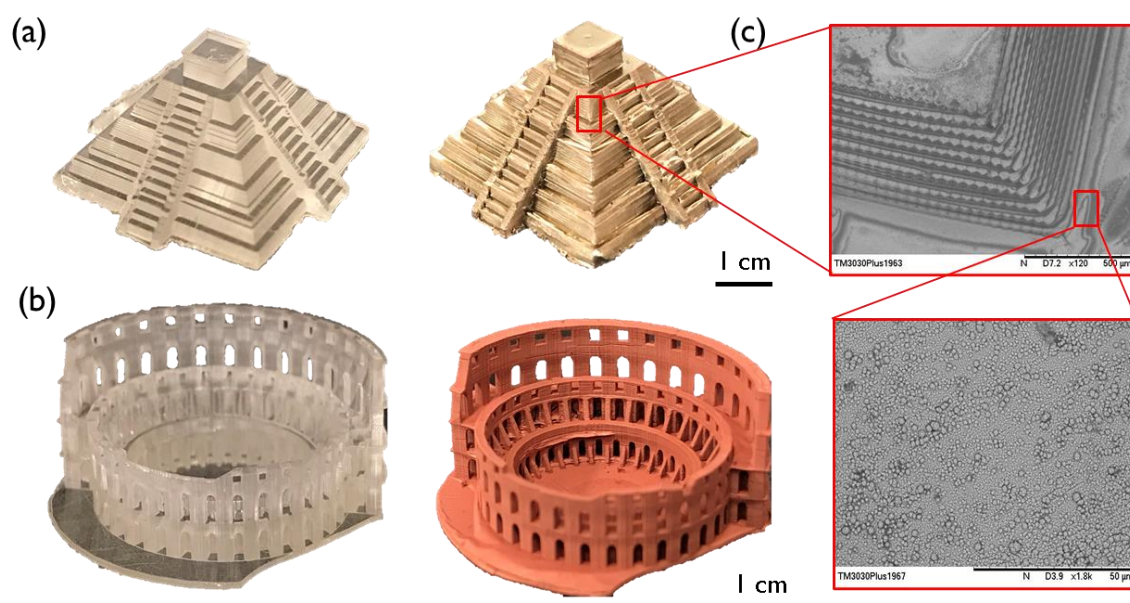


Figure 2-7: Complex metallic architectures printed using dopamine-integrated UV resin. (a) Polymeric and nickel-coated colosseum. (b) Polymeric and copper-coated colosseum. (c) Nickel-coated colosseum morphology in Z direction surface and X/Y direction surface.

2.3.5 The applicability of other phenol/polyphenol and water-soluble resin

Besides dopamine, the use of other structurally related to catechol group, such as plant phenols and polyphenols (collectively referred to as '(poly)phenols'), as precursors for metal bonding affinity was recently reported. Hypothesizing that catechol group alone facilitates the initial nucleation and growth of the silver film, (poly)phenols should be applicable with our method.

We chose four different (poly)phenols: 4-Methylcatechol, 2,3,4-Trihydroxybenzaldehyde, catechin hydrate, and tannic acid. Similar to the preparation process of dopamine-integrated UV resin, four types of (poly)phenols were dissolved in water (150 g/L), and then 20 vol% aqueous solution were added into PEGDA, separately. 2 ml resin was filled in a disk shape container, following by the UV exposure for 1 min. As shown in Figure 2-8a-d, the adding of the alternatives does not affect the printability. After silver nitrate treatment for 4 h, the color change for the four cured samples suggests that in situ generation of silver NPs occurs on the substrate surfaces. Thus, the reduction of silver by catechol group is proved. However, the treated samples are nonconductive probably because of insufficient silver deposition. In other words, not only catechol group, but the amine groups in dopamine also assist the metal deposition process. We can conclude that the coexistence of catechol and amine groups is crucial for metallization of polymeric structures.

In addition, a second type of UV resin (ACMO) was also used to verify the applicability of our strategy. As PEGDA, ACMO is also dissolvable in aqueous solution. After UV curing, all the liquid resin with (poly)phenols can be solidified, but not all the samples can keep the shape due to poor printability and mechanical performance. Figure 2-8e(i-iii) show obvious fold morphology and deformation after the samples were cleaned by ethanol. The additional (poly)phenols have different effects in UV curing process, and this influence may be caused by the side chain of the (poly)phenols. Compared with the samples shown in Figure 2-8a-d, dopamine-integrated PEGDA resin has a better printability.

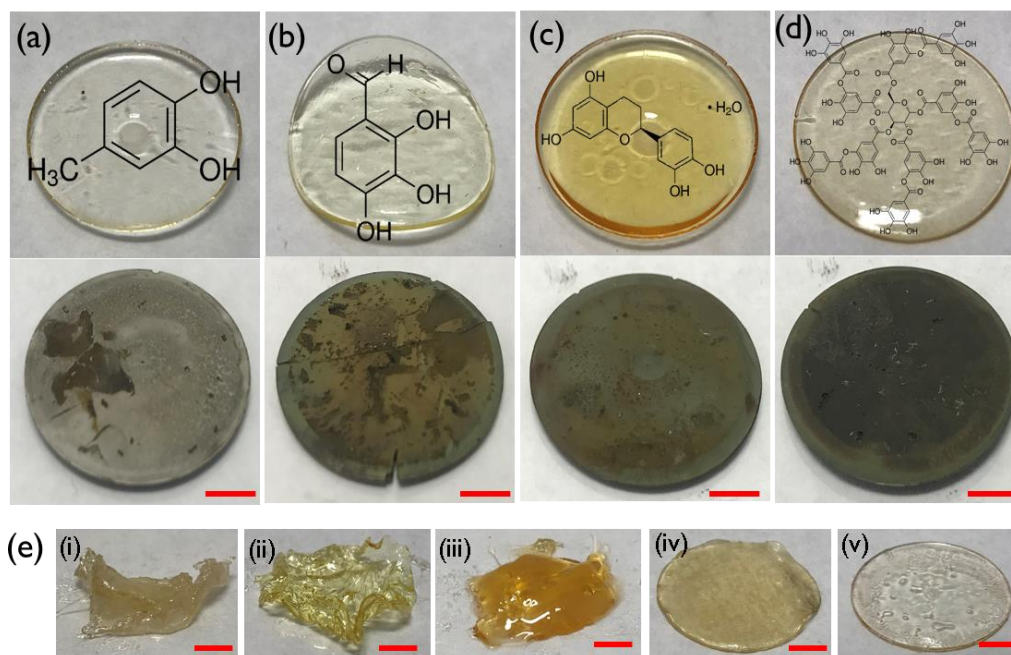


Figure 2-8: (a-d) The UV cured samples without (top) and with (bottom) silver nitrate treatment. PEGDA mixing with 20 vol% (a) 4-Methylcatechol, (b) 2,3,4-Trihydroxybenzaldehyde, (c) catechin hydrate, and (d) tannic acid, respectively. (e) The UV cured samples using ACMO with five (poly)phenols: (i) 4-Methylcatechol, (ii) 2,3,4-Trihydroxybenzaldehyde, (iii) catechin hydrate, (iv) tannic acid, and (v) dopamine. Scar bar: 5mm.

2.4 Conclusions

In this study, we developed a simple yet robust dopamine-added UV-curable resin for 3D printing. Water-soluble PEGDA serves as oligomer in UV resin due to its compatibility with dopamine aqueous solution. After printing, the dopamine is distributed throughout the 3D printed objects. Due to the chemical versatility of catechol group from dopamine, a surface with a strong metal bonding affinity is created, and silver deposition can be achieved via one-step dipping. In contrast to the conventional metallization approaches, such as the ones need to deposit precious metal as catalyst, our developed material provides a low-cost and green alternative solution for metallization.

Moreover, relying on the homogeneous distribution of dopamine in UV resin, cross-linking network can act as a platform to immobilize dopamine molecules. A class of

metal materials, such as Ni and Cu, can also be deposited on the 3D architectures directly through dopamine molecules. Herein, the amine groups can also assist the metal deposition process, resulting in a layer of conductive metal coating of high adhesion. More significantly, all these metal films can regrow on the surface at any time, extending the lifespan of our 3D printed electronics. In summary, dopamine-integrated UV resin couples the advantages of the 3D printing in complex geometries fabrication with the versatility of the dopamine, which extends the capability of 3D printing as a universal and cost-effective method in electronics fabrication.

References

1. Duda, T. and L.V. Raghavan, *3D Metal Printing Technology*. IFAC-PapersOnLine, 2016. **49**(29): p. 103-110.
2. Zhang, D., et al., *Introducing Bioinspired Initiator into Resins for In Situ Repairing of 3D-Printed Metallic Structures*. ACS Applied Materials & Interfaces, 2020. **12**(43): p. 49073-49079.
3. Zhang, D., et al., *3D-printed highly porous and reusable chitosan monoliths for Cu(II) removal*. Journal of Materials Science, 2019. **54**(8): p. 6728-6741.
4. Dongxing, Z., et al., *Development of ultralight, super-elastic, hierarchical metallic meta-structures with i3DP technology*. Nanotechnology, 2017. **28**(45): p. 455708.
5. Zhang, D., et al., *Initiator-Integrated 3-D Printing of Magnetic Object for Remote Controlling Application*. IEEE Transactions on Magnetics, 2017. **53**(5): p. 1-9.
6. Ishikawa, A., et al., *Selective electroless plating of 3D-printed plastic structures for three-dimensional microwave metamaterials*. Applied Physics Letters, 2017. **111**(18): p. 183102.
7. Jian, J.R., et al., *High performance 3D printed electronics using electroless plated copper*. AIP Advances, 2017. **7**(3): p. 035314.
8. Konda, A., et al., *Soft Microreactors for the Deposition of Conductive Metallic Traces on Planar, Embossed, and Curved Surfaces*. Advanced Functional Materials, 2018. **28**(40): p. 1803020.
9. Charbonnier, M., et al., *Surface plasma functionalization of polycarbonate: Application to electroless nickel and copper plating*. Journal of Applied Electrochemistry, 2001. **31**(1): p. 57-63.
10. Zhang, J., et al., *Fabricating Metallic Circuit Patterns on Polymer Substrates through Laser and Selective Metallization*. ACS Applied Materials & Interfaces, 2016. **8**(49): p. 33999-34007.
11. Wang, X., et al., *i3DP, a robust 3D printing approach enabling genetic post-printing surface modification*. Chemical Communications, 2013. **49**(86): p. 10064-10066.
12. Wang, X., et al., *Initiator-Integrated 3D Printing Enables the Formation of Complex Metallic Architectures*. ACS Applied Materials & Interfaces, 2014. **6**(4): p. 2583-2587.

13. Zhang, D., et al., *Hierarchical metal/polymer metamaterials of tunable negative Poisson's ratio fabricated by initiator-integrated 3D printing (i3DP)*. *Nanotechnology*, 2018. **29**(50): p. 505704.
14. Cai, X., et al., *Water based fluidic radio frequency metamaterials*. *Journal of Applied Physics*, 2017. **122**(18): p. 184101.
15. Bian, B., et al., *Application of 3D Printed Porous Copper Anode in Microbial Fuel Cells*. *Frontiers in Energy Research*, 2018. **6**(50).
16. Guo, Q., et al., *"Paintable" 3D printed structures via a post-ATRP process with antimicrobial function for biomedical applications*. *Journal of Materials Chemistry B*, 2013. **1**(48): p. 6644-6649.
17. Lee, H., et al., *Mussel-Inspired Surface Chemistry for Multifunctional Coatings*. *Science*, 2007. **318**(5849): p. 426-430.
18. Kang, S.M., et al., *Simultaneous Reduction and Surface Functionalization of Graphene Oxide by Mussel-Inspired Chemistry*. *Advanced Functional Materials*, 2011. **21**(1): p. 108-112.
19. Ho, C.-C. and S.-J. Ding, *The pH-controlled nanoparticles size of polydopamine for anti-cancer drug delivery*. *Journal of Materials Science: Materials in Medicine*, 2013. **24**(10): p. 2381-2390.
20. Dreyer, D.R., et al., *Elucidating the Structure of Poly(dopamine)*. *Langmuir*, 2012. **28**(15): p. 6428-6435.
21. Zhang, F.-T., et al., *Electroless Deposition Metals on Poly(dimethylsiloxane) with Strong Adhesion As Flexible and Stretchable Conductive Materials*. *ACS Applied Materials & Interfaces*, 2018. **10**(2): p. 2075-2082.
22. Zhao, L., D. Chen, and W. Hu, *Patterning of Metal Films on Arbitrary Substrates by Using Polydopamine as a UV-Sensitive Catalytic Layer for Electroless Deposition*. *Langmuir*, 2016. **32**(21): p. 5285-5290.
23. Mao, Y., et al., *Well-defined silver conductive pattern fabricated on polyester fabric by screen printing a dopamine surface modifier followed by electroless plating*. *Soft Matter*, 2018. **14**(7): p. 1260-1269.
24. Ma, S., et al., *Fabrication of highly electrically conducting fine patterns via substrate-independent inkjet printing of mussel-inspired organic nano-material*. *Journal of Materials Chemistry C*, 2014. **2**(20): p. 3885-3889.
25. Yu, Y.-H., et al., *Electrical, morphological, and electromagnetic interference shielding properties of silver nanowires and nanoparticles conductive composites*. *Materials Chemistry and Physics*, 2012. **136**(2): p. 334-340.

26. Stewart, I.E., M.J. Kim, and B.J. Wiley, *Effect of Morphology on the Electrical Resistivity of Silver Nanostructure Films*. ACS Applied Materials & Interfaces, 2017. **9**(2): p. 1870-1876.

Chapter 3

3 A modified-dopamine customized UV resin for electroless metallization in 3D printing

To further broaden the scope of applications enabled by i3DP II, lipid-soluble dopamine methyl acrylamide (DMA) was synthesized in this chapter to comply with the commonly used acrylic-based photo-curable resin. Since DMA is also a kind of polyphenol matters similar to dopamine, it contains catechol groups and enables the printed object redox active, allowing metal ions reduction. After DMA was introduced into the acrylic-based resin for photopolymerization-based 3D printing, complex metallic structures can be manufactured through DMA-assisted metal ELP process. Moreover, DMA embedded inside the object has a potential function of re-triggering the ELP process to form a new layer of metal coating. This characteristic allows repeating the growing process of the metal layers and realizing an in situ repairing of the damaged area. Overall, the proposed method is not only presented as a facile and effective approach to fabricate complex metallic structures of various functionalities, but also presented as a feasible solution for the long-term challenge of repairing nonstandard or unavailable parts.

3.1 Introduction

Chapter 2 demonstrated the usage of dopamine for 3D printing metallic structures. Water-based photo-curable resin was developed to comply the water-solubility of dopamine. Nevertheless, most 3D printing photopolymer is acrylic resin and only a few types of water-soluble resin are available in the market; the applicability of the method which introduces dopamine into water-soluble oligomer is significantly limited in research and academic field. In this chapter, to further broaden the scope of applications, commonly used acrylic-based photo-curable resin was selected as the resin base. However, one problem is the dopamine is water-soluble and can rarely be dissolved in acrylic oligomers/monomers. That means, to utilize the function of dopamine, necessary modification should be done to increase its solubility in acrylic base. A practical solution to address the above problem is improving the hydrophobic nature of dopamine by acylation, which could be achieved by chemical synthesis [1, 2].

To integrate dopamine with most types of 3D printing resin, we improve the solubility of the dopamine in acrylic resin through acylation. The introducing of methacrylate group changes the hydrophilic nature of dopamine, making it compatible with most used acrylic-based UV resin. DMA, which is also a kind of polyphenol matters similar to dopamine, was synthesized by modifying the dopamine. DMA contains catechol groups and enables the printed object redox active, allowing silver ions reduction. The formation of thin silver film catalyzes ELP to form robust metal layers (such as Ag, Cu and Ni). The proposed method schematically provides a universal solution to combine the functionality of catechol groups from dopamine with the merits of 3D printing techniques. Moreover, as the synthetic dopamine is distributed throughout the whole 3D printed parts, locally repairing of the induced metal layer is available.

3.2 Experimental section

3.2.1 Chemicals and materials

Tetrafunctional oligoether acrylate, SR494, was chosen to verify the solubility of DMA, which was bought from Startomer Company. Four different types of commercial 3D printing photopolymer were used to mix with DMA. They are VeroWhite from Stratasys Company, Formi Clear resin from Formi Company, eResin-PLA Bio-Photopolymer (red) from eSun Company, and BV-002 (blue) from MiiCraft Company. Dopamine hydrochloride and silver nitrate were purchased from Sigma-Aldrich and used without any further purification.

3.2.2 Synthesis of dopamine methyl acrylamide

DMA was synthesized according to Figure 3-1a. A solution was prepared by dissolving NaHCO₃ (8.5 g) and Na₂B₄O₇(H₂O)₁₀ (4.4 g) in 100 mL of water. After being degassed by purging with nitrogen, 5.0 g of dopamine hydrochloride was added to the solution. The reaction was started by the addition of 26 mL of THF containing 4.5 mL of methacrylate anhydride, after the pH of the solution was adjusted to > 8.0. The reaction was kept under a N₂ at room temperature and stopped after 12 h. The pH of the reaction solution was adjusted to <2 with 6 M HCl and extracted four times with ethyl acetate. The organic phase was dried over anhydrous MgSO₄ and condensed by rotary

evaporation. Finally, hexane was added to the residual solution and stored overnight at room temperature for complete precipitation of the product. A light gray powder was obtained after filtration and drying at 60 °C overnight in a vacuum (Figure 3-1b). To investigate the solubility of DMA in acrylic resins, four different resins were chosen to dissolve DMA. From Figure 3-1c, the prepared resins with 5 wt% DMA can be obtained, indicating that modified-dopamine has an improved solubility in acrylic resins.

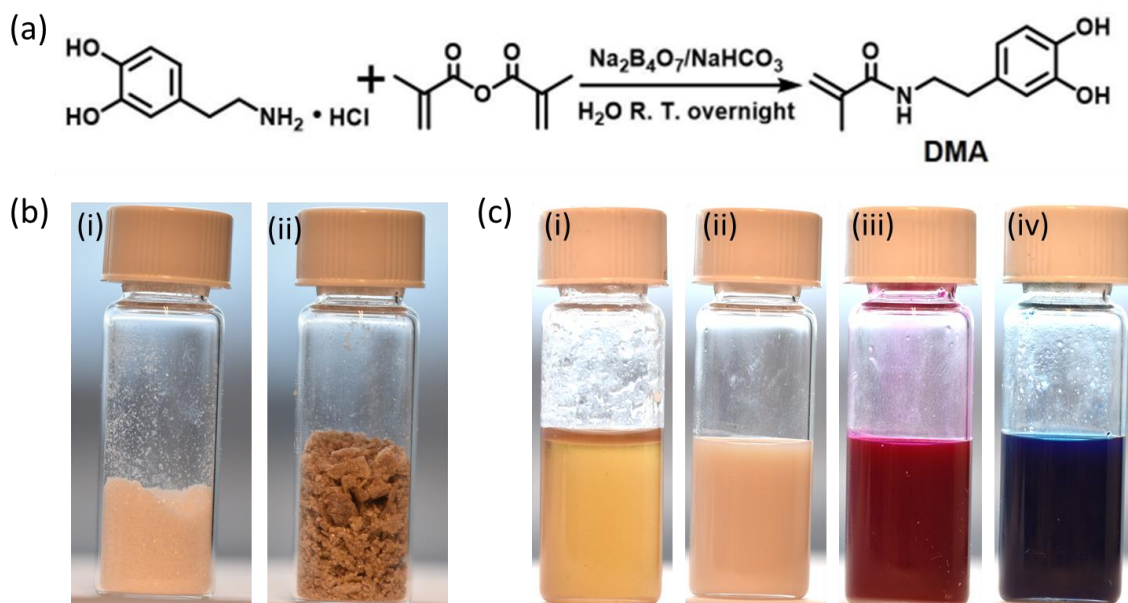


Figure 3-1: (a) The synthesis of DMA. (b) (i) Dopamine powder (white) and (ii) DMA powder (gray). Homogeneous DMA-integrated UV resins are prepared with: (i) VeroWhite, (ii) Formi Clear, (iii) sResin-PLA, and (iv) BV-002.

3.2.3 Preparation of customized 3D printing material

The customized 3D printing photopolymer was prepared by adding different amount of DMA. After mixing well, degassing of the resin base was conducted for 30 minutes in the dark. Then, the resultant resin was ready for printing: 0.5 ml resin was poured into a regular hexagon mold and an UV lamp (36 W) was used to verify its printability.

3.2.4 Metallization of the 3D printed structures

Commercial DLP 3D printer (PICO2, Asiga) was used to conduct 3D printing process. At first, the exposure time for single layer was measured, which is an important parameter to

ensure a successful 3D printing process. In our study, a 30 x 40 mm film of 50 μm in thickness was used to measure the minimum exposure time for one single layer. Digital models can be designed by SolidWorks and sliced into a series of images. During 3D printing process, the building plate would move up to allow the resin refilling in the blank area after printing one layer, and then move down again for next layer printing. This printing process was repeated until the whole object was created. The printed object was ultrasonically rinsed for 5 min in ethanol and dried by nitrogen flow. DMA-assisted metallization process is carried out in metal salt solution, which is same as the process of PD electroless plating.

For silver deposition, the printed object was first dipped into 0.1 mol/L aqueous silver nitrate solution for 1 hour at room temperature to grab Ag^+ ions as catalyst for the following ELP process. The object was then taken from the solution, washed with DI water, and dried with N_2 . To obtain a dense silver layer, the as-prepared Ag activated polymeric object was immersed into ELP solution with a bath ratio 1:50 containing freshly prepared solution A and solution B. Solution A consists of 40 g/L AgNO_3 , 40 ml/L ammonia and 0.06 mol/L ethylenediamine. Solution B contains 40 g/L glucose, 2.5 g/L potassium sodium tartrate tetrahydrate, 40 ml/L ethyl alcohol and 0.075 g/L polyethylene glycol.

The electroless copper plating process was performed in two steps: (i) grabbing silver seeds on the surface of the 3D printed objects and (ii) deposition of copper coating. The silver coating can be easily observed when the object was taken from the silver nitrate solution. Then, the Ag^+ -loaded sample was immersed into the ELP solution which is made of 1:1 mixture of freshly prepared solution A and solution B. Solution A consists of 15 g/L $\text{CuSO}_4 \cdot 5\text{H}_2\text{O}$, 15 g/L $\text{K}_4\text{Fe}(\text{CN})_6$, 0.01 g/L $\text{K}_4(\text{CN})_6 \cdot 3\text{H}_2\text{O}$, 15 g/L NaOH. Solution B consists of 9.5 mg/L HCHO in water. Similar to Cu, the ELP of Ni was conducted by immersing the sample with silver NPs into plating solution, which contains 20 g/L $\text{Ni}_2\text{SO}_4 \cdot 5\text{H}_2\text{O}$, 33 g/L sodium citrate, 14 g/L sodium hypophosphite, and 3 g/L DMAB in water. The bath pH should be adjusted to 10.

3.2.5 In situ repairing of metallic structures

Silver nitrate solution was applied to the damaged area. After 1 h, the object was cleaned by DI water. Ag/Cu/Ni plating bath prepared as above was used for metal deposition on the target area. More details are described in next section.

3.2.6 Characterization

The morphology of the metallic structures was investigated by Hitachi S-4500 field-emission scanning electron microscope at 5 kV accelerating voltage. An M 2400 Keithley Source-meter/unit (voltage range 50 V, step 1 V) was used to measure the sheet resistance using the four-probe method. Fourier transform infrared spectroscopy (FTIR) was carried out to identify the chemical structures. Cary 100 UV-visible spectrophotometer (Agilent, USA) was used to UV-spectrum test. AFM experiments were carried out with a Dimension V AFM equipped with Nanoscope controller V (Veeco, Inc.). A silicon nitride cantilever with a nominal spring constant of 40 N/m and tip radius of around 10 nm was used. The spring constant of the cantilever was also calibrated by the thermal tune method [3], which was 38.5 N/m. The sample was placed on the holder under the AFM cantilever tip, which can be observed together through the camera. The cantilever tip can be positioned at any site of interest on the sample using Nanoscope controller software (Nanoscope 7.30, Veeco).

3.3 Results and discussion

3.3.1 DMA-integrated 3D printing UV resin

The key characteristic of DMA is its solubility in acrylate-based resin. To investigate the solubility of DMA in UV resin, SR494 – the mostly used base in acrylic-based resin- was selected as the solvent to verify. The solubility of dopamine and modified-dopamine (DMA) was measured and compared. According to the experimental results, the solubility of dopamine in SR494 is 0.25 g/100g, while the solubility of DMA is 6 g/100g, suggesting a significantly improvement of solubility in the acrylic resin. Based on the positive results, DMA was introduced to four mostly commercial photopolymers (VeroWhite, Formi Clear, eResin-PLA and BV-002), aiming to broaden the applications.

In our study, 1 wt%, 3 wt%, and 5 wt% DMA was added into the four kinds of UV photopolymer, respectively. Since all the four kinds of commercial photopolymer have similar monomer base to SR494, 5 wt% DMA can be dissolved completely in all these 3D printing materials. DMA-added resin did not have the precipitation phenomenon which existed when directly using dopamine and kept homogeneously even after long time storing. We stored the prepared resins in tightly sealed opaque containers and allowed them to rest for 24 h. No aggregation was observed. Since the increase of solubility in lipid resin ensures more catechol groups incorporated with UV resin material, the 3D printed objects allow more effective surface modification.

FTIR analysis was conducted to verify the existence of DMA on the surface of 3D printed object. In Figure 3-2, the original 3D printing material presents a typical spectrum of acrylate-based UV resin, with signals of C=O and C-O appearing at 1704 and 1210 cm^{-1} , respectively. For DMA-integrated resin, signal of N-H (3310-3350 cm^{-1}) shows up, indicating the existence of amine group from DMA.

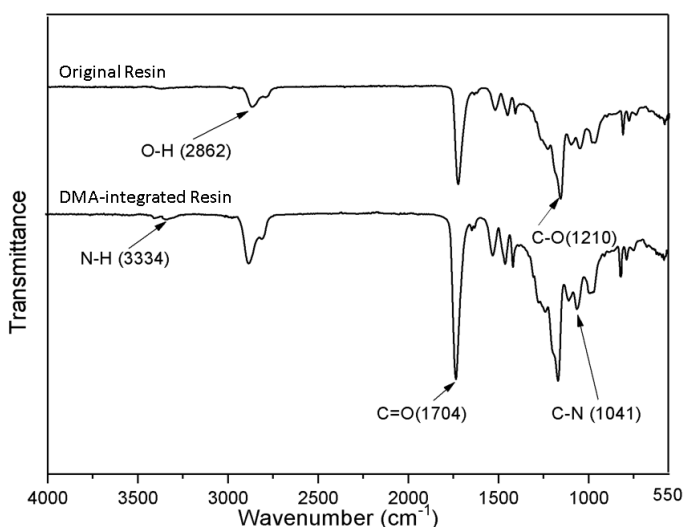


Figure 3-2: FTIR signals of original resin and DMA-integrated resin.

3.3.2 Printability of the DMA-integrated resin

The printability of DMA-added resin was investigated to guarantee its application in 3D printing. For each formulation, 0.5 ml as-prepared resin was filled in a mold, and then a

UV lamp (36W) was used to cure the resin. From Figure 3-3, all formulations were able to be cured and solidified. The rough surface was caused by the limited UV penetration depth. Due to the thickness of the samples, only small amount of UV light can reach the bottom, causing inadequate energy to cure the bottom surface.

Since catechol group has the properties of in situ reduction and chelating metal ions, the immersion of the above printed object into the AgNO_3 solution would lead to the reduction of Ag^+ on the surface. To verify this hypothesis, all cured samples were immersed into silver nitrate solution for 4 h. Compare with as-cured samples, complete silver films were formed on some Ag^+ -samples, especially for high content of DMA, while the samples without DMA do not obvious change after Ag^+ treatment (Figure 3-3). Particularly, all resins with 5 wt% DMA was successfully coated with a silver layer, suggesting that 5 wt% DMA can play its best in metal reduction.

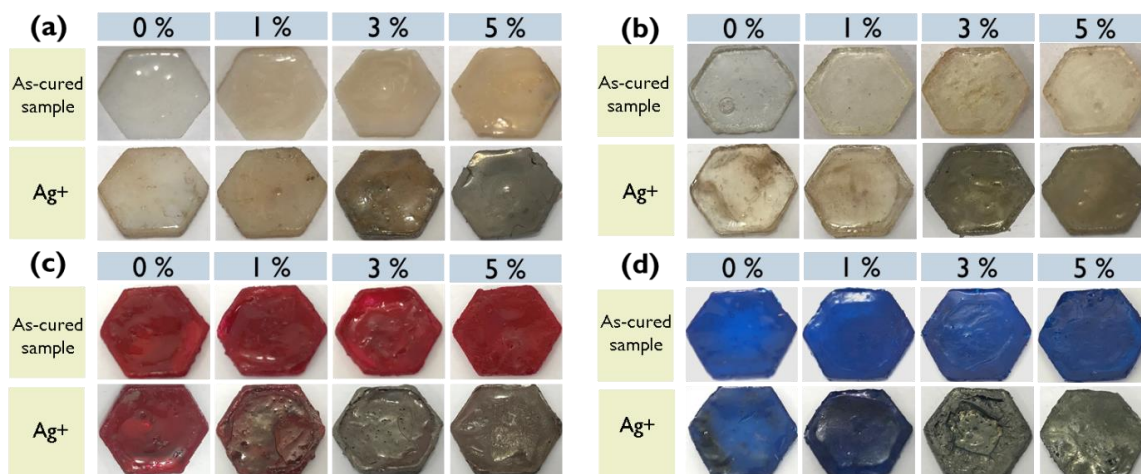


Figure 3-3: The as-cured samples (top) and the samples after silver nitrate treatment (bottom) with different weight percent (from left to right: 0 wt%, 1 wt%, 3 wt%, and 5wt%). The 3D printing material are (a) VeroWhite, (b) Formi Clear, (c) sResin-PLA, and (d) BV-002.

3.3.3 UV-visible spectrum of DMA-integrated resin

To investigate the influence of DMA on the photopolymerization process, UV absorption of the DMA-added resin was detected via UV-visible spectrum. In our study, we selected

Formi Clear resin as resin base for the following experiments. In Figure 3-4, the UV-vis absorbance of the prepared resins with different concentrations of DMA (0 -5 wt%) was displayed. The absorbance increases with the increase of the concentrations of DMA and all resins had maximum absorption wavelength in range of 350 nm to 410 nm. Since the wavelength of the light source used in the commercial 3D printer (Asiga DLP 3D) is 405 nm, DMA-added resin is feasible to work with the printer.

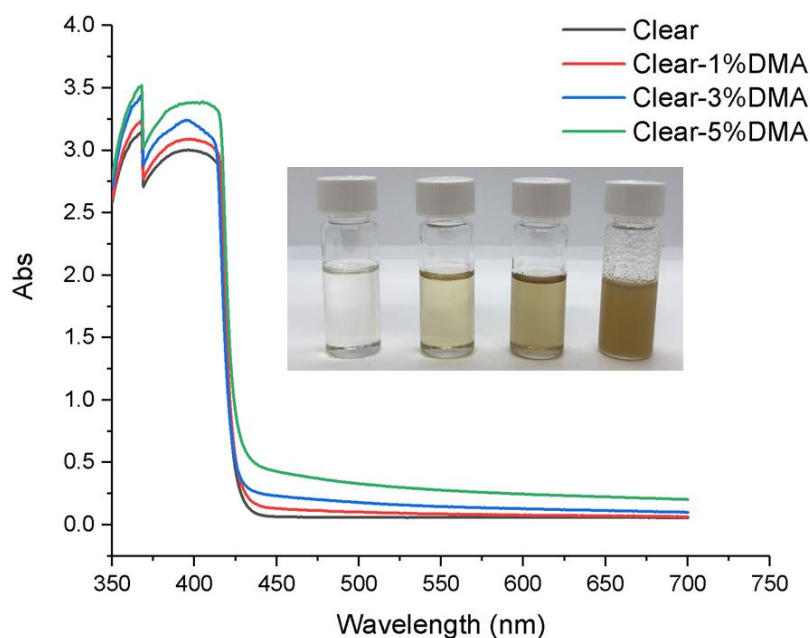


Figure 3-4: UV-vis absorbance spectra of DMA-integrated resins with various concentrations (0 – 5 wt%). The inset shows optical image for different concentrations of DMA in UV resins.

3.3.4 Effect of DMA on exposure time during 3D printing

As exposure time is a key printing parameter during 3D printing process, exposure time of 1 s to 1.4 s was conducted on the resin of single layer (50 μ m). The relationship between exposure time and DMA concentration was plotted in Figure 3-5. Since the color of the resin changes from clear to brown with the increase of DMA amount, longer exposure time was required for the resin of higher DMA concentration. The exposure time – DMA concentration helped to adjust the parameters of the following 3D printing process.

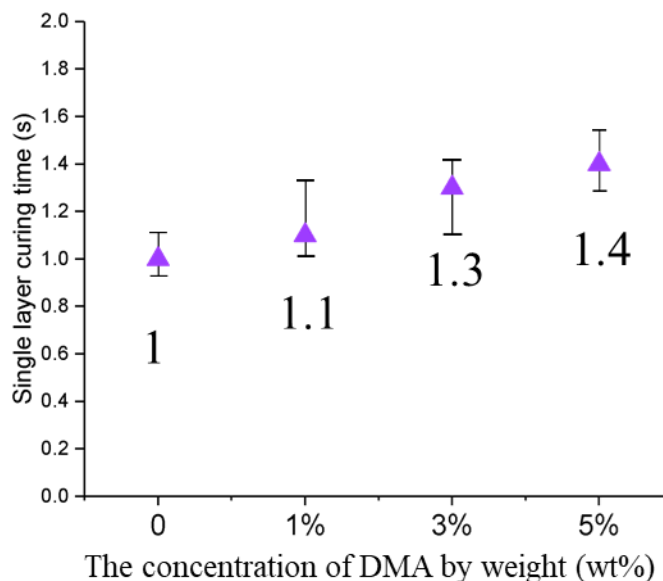


Figure 3-5: The exposure time for single layer of various DMA concentrations.

3.3.5 Confirmation of DMA distributed on the surface

The existence of DMA on the surface was confirmed through comparing the change of hydrophilicity and surface detach force before and after the addition of DMA. We also analyzed the effect of DMA on the hydrophilicity of objects printed by DMA-added resin. Because hydroxy radical from catechol group is the hydrophilic, it is deduced that larger DMA concentration will result in higher hydrophilicity of 3D printed parts. However, contradictory phenomenon was found that the object made of higher DMA concentration had a bigger contact angle on the surface, meaning a lower hydrophilicity (seen in Figure 3-6). One reason explains the phenomenon is, the addition of DMA lead to a rougher surface, and the micro-nano structures on the surface will increase the surface energy. This was supported by the surface morphology obtained through AFM detecting. The surface roughness increased from $\sim 2.5 \mu\text{m}$ to $\sim 4.5 \mu\text{m}$ after 5 wt% DMA was added (insets of Figure 3-7). It is worth noting that, the hydrophilicity change is small, and the contact angle kept in range of 58° to 68° . Thus, the increasing of hydrophilicity caused by DMA will not affect the following ELP process. In contrast to PD, the deposition of PD film can introduce plenty of hydrophilic groups such as hydroxy and amino, so as to enhance the hydrophilicity of the substrates. The PD film thickness is around 40 nm with

a rough morphology at the molecular level [4-7]. The water contact angel of PD coated substrates can fall within a range of 37 -90° after PD coating [8].

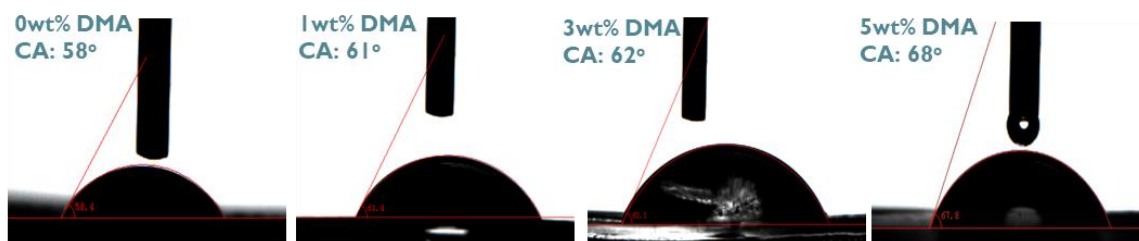


Figure 3-6: Water contact angel of printed substrates cured by different DMA concentration resins.

Since the cross-linking network of DMA-added resin contains DMA molecules, the DMA-sample has a softer and more adhesive surface when compared to those of none-DMA sample. Change of detach force was also measured on the objects printed using DMA-added resin and pure resin, aiming to prove the existence of DMA on the object surface. According to Figure 3-7a, the surface of none-DMA sample had a less detach force, which was 0.25 ± 0.05 nN. For the 5 wt% DMA-added sample, the detach force increased to 0.70 ± 0.05 nN. Higher detach force implies a softer surface, which further proves the existence of DMA molecules distribute on the surface of printed object.

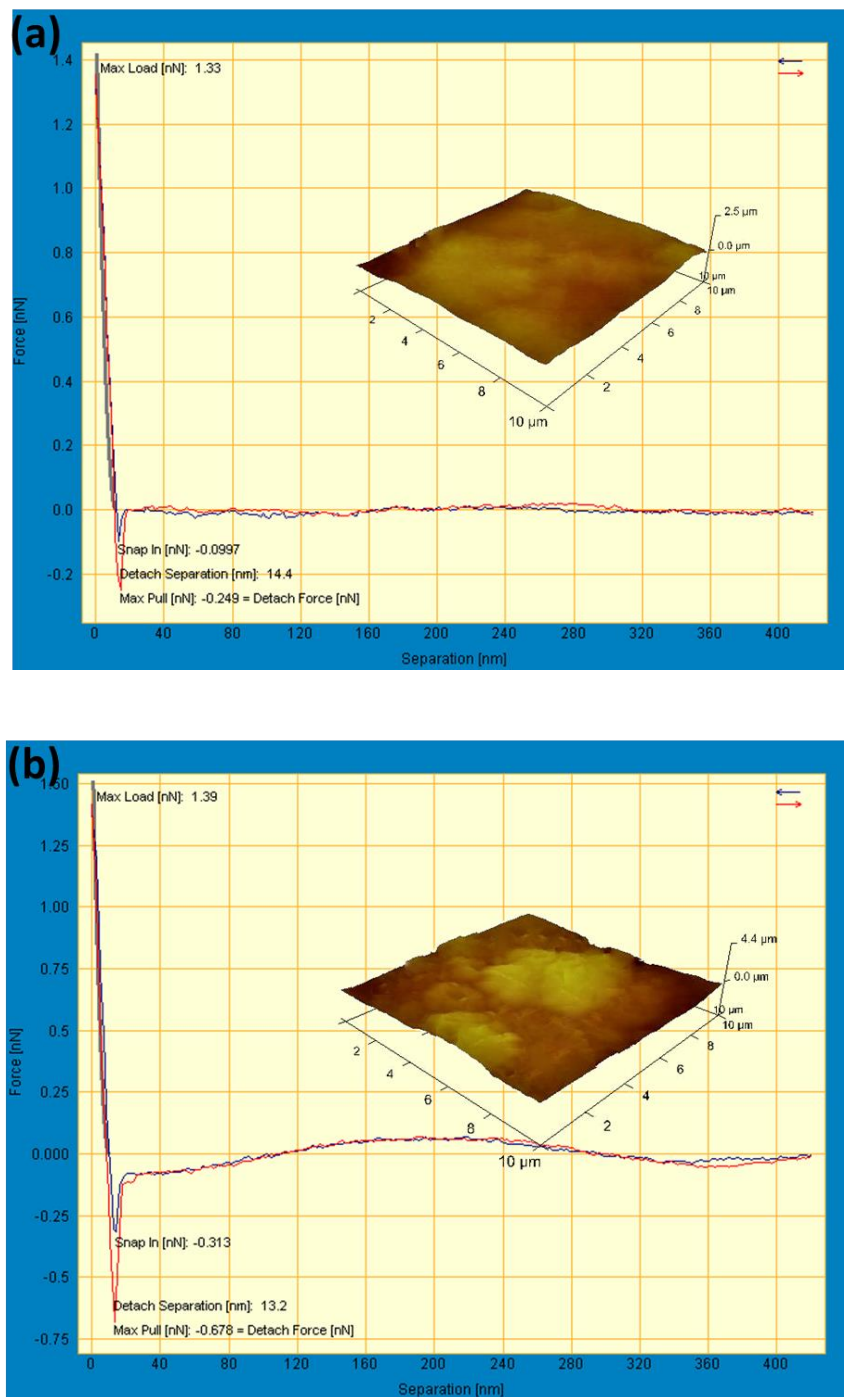


Figure 3-7: Adhesion forces of (a) none-DMA-added sample and (b) 5 wt% DMA-added sample. Insets are the surface morphology from AFM scanning.

3.3.6 3D printing of complex metallic structures

Stereolithography-based 3D printing technology provides a high flexibility to fabricate complex structures with high resolution. In our study, complex structures (lattice heart and rabbit-shape structures) were demonstrated using modified resin with 5 wt% DMA added (Figure 3-8). The printed polymeric lattice structures had good surface quality and high-quality details, indicating again that the addition of DMA had a negligible influence on the printing ability of high-resolution fabrication. Copper and nickel coating were deposited on the printed structure surface. The metallization process was conducted by simply dipping in the AgNO_3 solution first for growing catalyst and the subsequent Cu or Ni deposition process in ELP bath. All these processes do not require expensive equipment and chemicals. The metal-binding ability of catechol groups present in the DMA was especially exploited to form continuous and compacted metal coatings based on various types of UV resin by ELP without traditional process, for example the tedious and environment unfriendly activation treatment. Additionally, multiple classes of metals deposition on the printed structures can expand the applications. For example, the coated Ni layer can enable remote control of a lightweight and complex device, providing a promising application for medical robots.

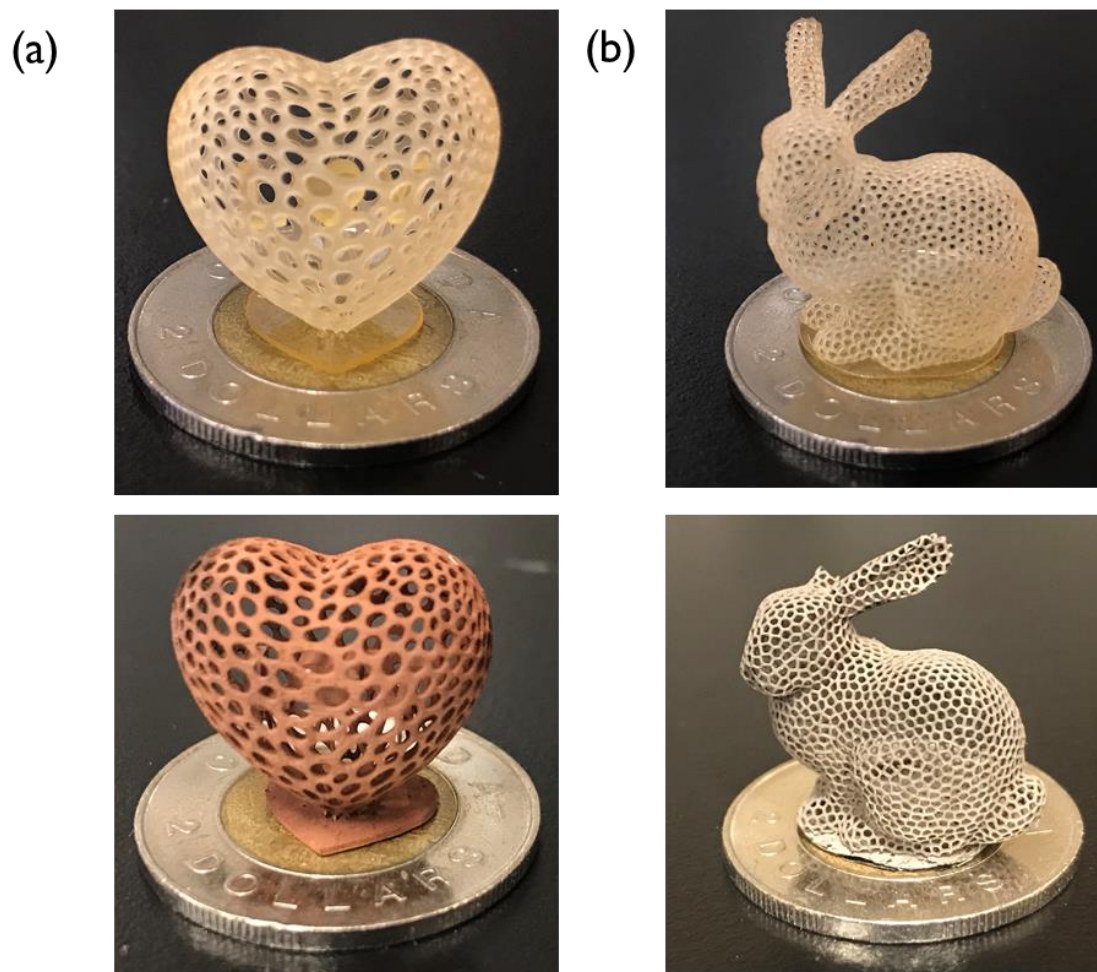


Figure 3-8: Complex 3D printing structures and their metallic structures after ELP. (a) Cu-lattice heart and (b) Ni-lattice rabbit.

The effect of the DMA concentration on Cu deposition, as an example, was investigated. Immediately after the as-printed objects immersing into AgNO_3 solution, silver seeds were successfully produced on the substrate of the printed objects. Then the silver layer acts as a reaction layer to immobilize and reduce the copper ions, and copper particles started to grow on the surface. For Formi Clear resin, silver film can be formed at the DMA concentration of 3 wt% and 5 wt% in 0.1 mol/L silver nitrate solution. The Ag^+ -loading substrates were then immersed into copper ELP baths. After 12 h, Cu film was coated on both samples. From Figure 3-9, copper NPs congregated in flake-shape were observed. For UV resin with 3 wt% DMA some small defects showed up on the substrate, while the Cu NPs are denser on the substrate by UV resin with 5 wt% DMA.

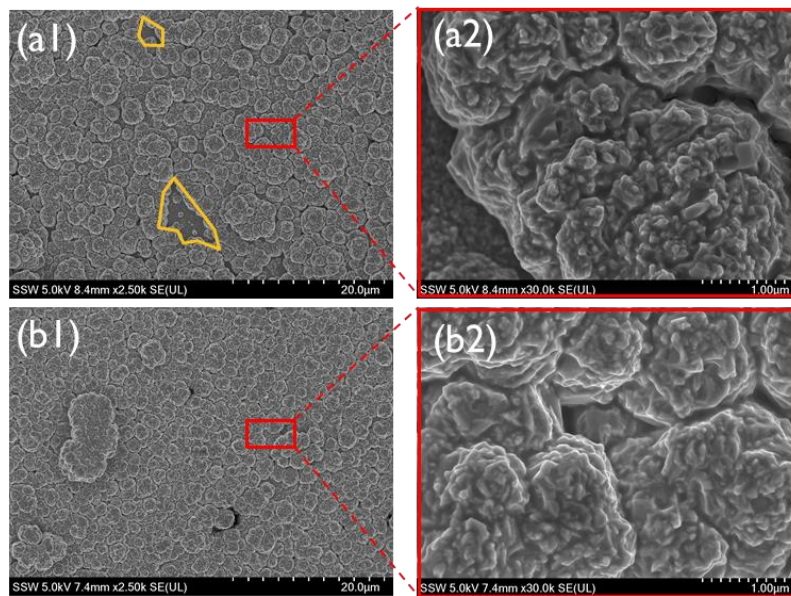


Figure 3-9: Surface morphology for Cu coated substrates printed by UV resin with (a) 3 wt% and (b) 5 wt% DMA.

Copper NPs deposition processes recorded along with ELP time was analyzed via SEM. It was found the Cu deposition process was slow. Even after 6 h, over 50% area had not been covered by the metal layer (Figure 3-10a). With increase of reaction time, Cu NPs continued to aggerate and a dense copper layer was finally obtained after 12h (Figure 3-10d). The metal thickness was 2.21 μm and the sheet resistance was 0.321 Ω/sq after 12 h deposition of (Figure 3-10h).

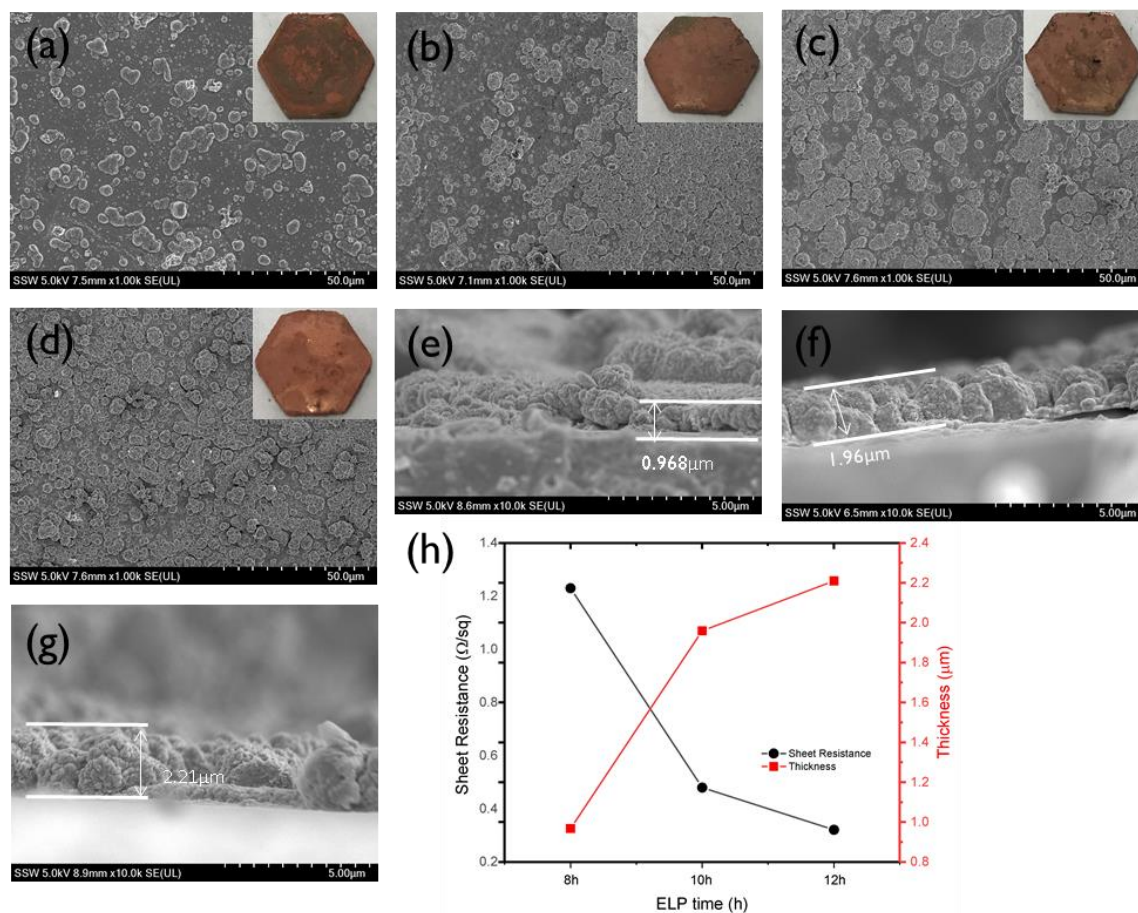


Figure 3-10: SEM used to record the growth of copper particles on the 3D printed object with various ELP time: (a) 6 h, (b) 8 h, (c) 10 h, and (d) 12 h. The inset shows images of the Cu-coated object. (e-g) displays the thickness of the copper film with various reaction time: (e) 8 h, (f) 10 h, and (g) 12 h. (h) Sheet resistance and layer thickness of the deposited on the substrates with different ELP time.

3.3.7 In situ repairing of metallic structures

Benefitting from the high lipid-solubility of DMA, the functional catechol groups distributed throughout the 3D printed objects, thus, newly exposed area after peeling off the metal coating also existed catechol groups which are ready to repeat the ELP process. Figure 3-11 illustrates the in-situ repairing process. Herein, a simple circuit was set up, and a 3D printed bar coated with a copper layer was used to connect battery and LED. At first, the original conductive bar can light up the blue LED. Then a circular incision was

made to disconnect the circuit and LED was turned off. Due to the existence of the catechol groups on the damaged area, the conductivity can be re-gained through successively immersing the damaged bar into AgNO_3 and copper ELP solution. To verify the stability of this approach, we repeated this in-situ process 10 times. NO. 1-10 shown in Figure 3-11 was inferred to 10 different scraped areas for experiment. Finally, all of the 10 repairing experiments were successful, and the damaged area can be recovered by generating a new layer of copper coating, and then connected the battery and LED again (Figure 3-11b).

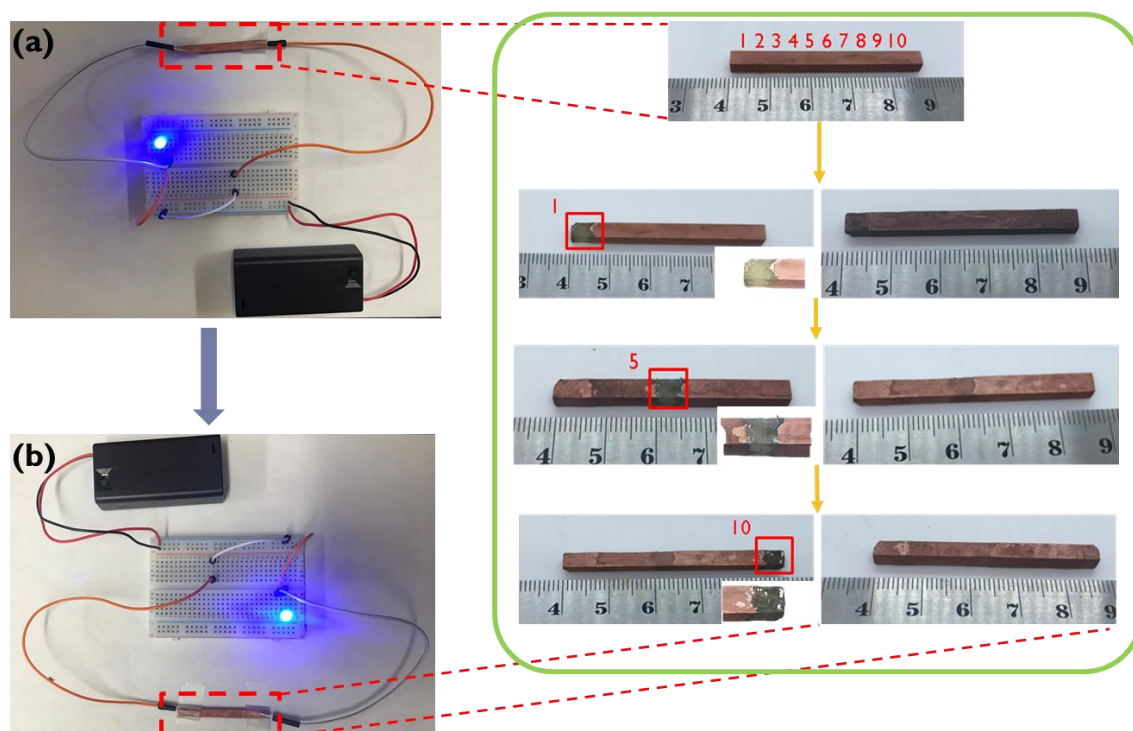


Figure 3-11: In situ repairing of the conductive copper film. (a) Cu-coated bar was used to light LED. (b) After 10 times repairing, the bar can still light LED. The green box shows the 1st, 5th, and 10th repairing experiment as examples. 1-10 indicates the different damaged area.

In our study, the whole bar was placed into the baths. Thus, the conductivity tends to be improved with the increasing of repairing experiments (Figure 3-12). Not only the damaged area got copper particles deposited, but also the rest copper covered area will be deposited new copper particles. With deposition of more metal particles, the conductivity

of the bar increased. Since this repairing method is not practical and cost-effective, for small area cracks, the ELP solution can be applied directly onto the target area by a brush-type tool.

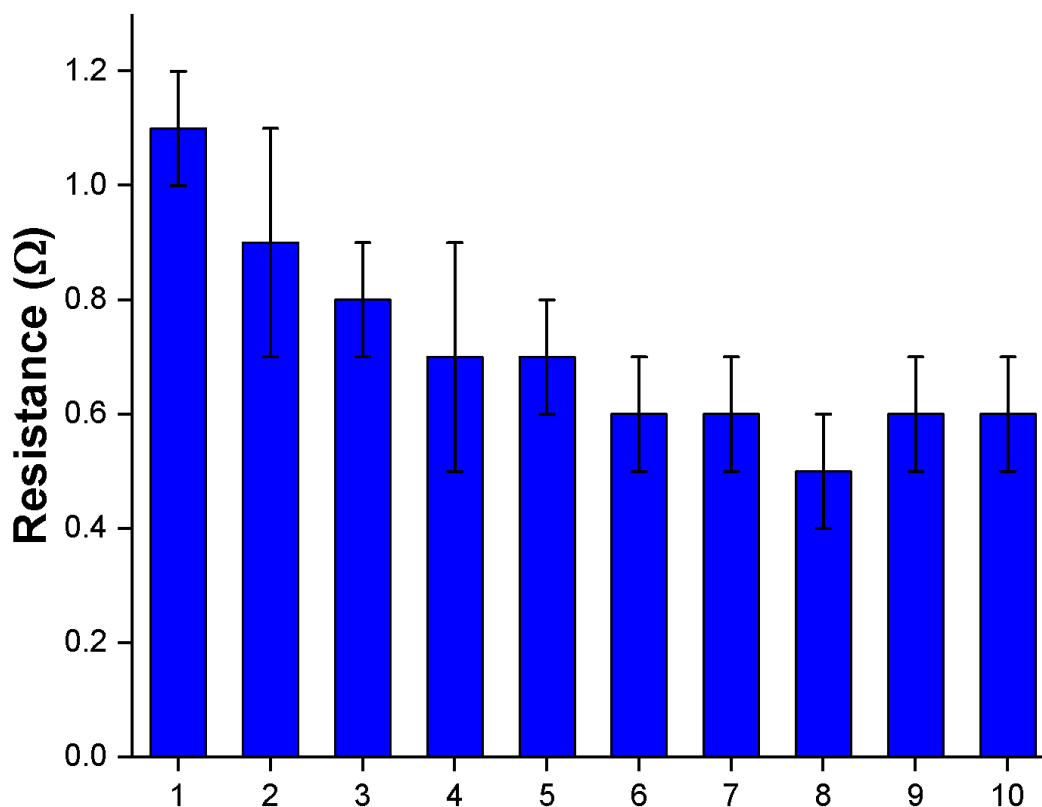


Figure 3-12: Resistance of the Cu-coated bar after different times of in situ repairing.

3.4 Conclusions

In this study, a facile and effective DMA was synthesized and integrated into the acrylic UV resins. In comparison with the method of simply blending dopamine with UV resin in chapter 2, the developed dopamine (DMA) has a higher solubility in commonly used acrylic-based 3D printing materials. Thus, the resultant DMA is compatible with most commercially available 3D printing resins. Due to the high metal-binding ability of catechol groups existing in DMA, the as-printing structure can act as a good substrate to immobilize all the catechol groups to initial multiple metals deposition (such as Ag, Cu, and Ni). The 3D printed structures using DMA-added UV resin works for metal

deposition without additional surface modification. Moreover, because DMA distributes throughout the 3D printed objects, the catechol groups can be reused when the deposited metal coating was peel off. It enables in situ repairing of the damaged metal coating. This characteristic can not only prolong the lifespan of the functional structures, but also address the long-term challenge of repairing the nonstandard 3D printing parts.

References

1. Liu, L., C. Jin, and Y. Zhang, *Lipophilic phenolic compounds (Lipo-PCs): emerging antioxidants applied in lipid systems*. RSC Advances, 2014. **4**(6): p. 2879-2891.
2. Lee, H., B.P. Lee, and P.B. Messersmith, *A reversible wet/dry adhesive inspired by mussels and geckos*. Nature, 2007. **448**(7151): p. 338-341.
3. Hutter, J. and J. Bechhoefer, *Calibration of atomic force microscope tips*. Review of Scientific Instruments, 1993. **64**: p. 1868.
4. Ponzio, F., et al., *Polydopamine Films from the Forgotten Air/Water Interface*. The Journal of Physical Chemistry Letters, 2014. **5**(19): p. 3436-3440.
5. Ball, V., *Polydopamine Nanomaterials: Recent Advances in Synthesis Methods and Applications*. Frontiers in Bioengineering and Biotechnology, 2018. **6**(109).
6. Hong, S., et al., *Poly(norepinephrine): Ultrasooth Material-Independent Surface Chemistry and Nanodepot for Nitric Oxide*. Angewandte Chemie International Edition, 2013. **52**(35): p. 9187-9191.
7. Ball, V., et al., *Kinetics of polydopamine film deposition as a function of pH and dopamine concentration: Insights in the polydopamine deposition mechanism*. Journal of Colloid and Interface Science, 2012. **386**(1): p. 366-372.
8. Liu, Y., K. Ai, and L. Lu, *Polydopamine and Its Derivative Materials: Synthesis and Promising Applications in Energy, Environmental, and Biomedical Fields*. Chemical Reviews, 2014. **114**(9): p. 5057-5115.

Chapter 4

4 Metallization and functionalization of 3D printed polymers assisted with polyphenols

The 3D printing of complex structures by polymeric materials will continue to be one of the most popular methods in the 3D printing industry. For real-world applications, it is believed that 3D printed structures with functional groups is a highly desirable to largely extend the applications of 3D printing, preferably with a cost-effective method. It is ideal to use one single 3D printing material to meet multiple requirements for different applications. Thus, in this chapter, we further extended the capacity of i3DP II by optimizing the added seed components to comply more applications of not only initiating the metallization process but also introducing other functions for better serving the practical scenarios.

In this chapter, we followed the same thinking of i3DP II with Chapter 2 and Chapter 3, and identified polyphenol as precursors for material engineering and surface functionalization. Polyphenolic compounds are a group of natural molecules derived from plants, which are especially attractive for the concept of circular economy. In addition, polyphenols have shown great potential to serve as building blocks for making various functional materials. In Chapter 4, polyphenol-enabled surface functionalization was demonstrated with focusing on 3D printed electronics application.

4.1 Introduction

Polyphenols are a large family of organic compounds with phenol units, which are abundant in natural plants and fruits. Therefore, it can also exist in the byproducts in agricultural industry. Thanks to their rich derivatives, polyphenols have been used for forming a variety of applications. One interest to this research is the strong solid-liquid interfacial activity and their capability of developing functional coatings of polyphenols, which can be useful for surface modification by integrating into 3D printing resin as a precursor or seed component.

In the previous study from our group, we introduced i3DP strategy to make 3D printed structures possible for various desired surface modification exhibiting varied surface properties. However, it will need a complex SI-ATRP to introduce various functions groups onto the printed parts. In the last two chapters, we upgraded the i3DP to a new generation (i3DP II) step by step through optimizing the initiator. Dopamine and its modification, DMA, have been employed to incorporate with 3D printing resins. Through the formation of polydopamine via auto-oxidation process, the printed objects allow for the formation of metal coating with a facial postprocess procedure. To introduce dopamine-based initiators into 3D printing resins, strategies were developed to form two categories of customized 3D printing resins, one is water-soluble UV resin incorporating with dopamine aqueous solution, the other is incorporating a modified dopamine into regular UV resin by improving the hydrophobic nature of dopamine. Due to some intrinsic limitation, there are certain drawbacks for the applications. For example, there are lacking water-soluble oligomer available in the market due to their poor mechanical properties and high shrinkage as 3D printing materials; it is quite costly and time-consuming for improving the solubility of modified-dopamine in regular UV resin via additional chemical synthesis processes. However, both studies have achieved considerable success which showed that catechol group from dopamine enables the creation of functional surface on the printed structures for the secondary reactions. These are typical bio-inspired approaches for surface modification application and the discovery is consistent with other bio-inspired studies. From the study of mussel adhesive proteins, 3,4-dihydroxy-L-phenylalanine (DOPA), which also has the side chain of catechol, functioning as adhesive molecules are found abundant near plague-substrate interface. The interfacial activity and the binding capability are essential for dopamine to function as a building block for surface modification.

Thanks to the structural resemblance to dopamine, plant polyphenols possessing a remarkable abundance of catechol and gallol functional groups are expected to be promising alternatives to dopamine. Despite rapidly growing interest in the polydopamine coatings, only a small number of studies focus on other classes of phenolic biomolecules. Noting previous success with plant polyphenols, the aromatic vicinal diol, i.e. catechol, was proven as a common structural feature of multifunctional coating

precursors. Especially, a number of plant-derived polyphenols were used as precursors for multifunctional coating. These studies include tannic acid (TA), epigallocatechin (EGCG), morin, and hydroxyhydroquinone (HHQ) used to form functional film [1]. As mentioned, the functional groups were same with those in the previous two chapters. Thus, polyphenols have with strong solid-liquid interfacial properties are capable of cross-linking and binding, both of which are attractive to be integrated into polymerization-based 3D printing.

Polyphenols have several thousand different derivatives, like pyrogallol (PG), epicatechin gallate (ECG), TA and etc. While they all share a common amphiphatic behaviour, because the hydroxyl groups are hydrophilic, and the aromatic rings are hydrophobic. Thus, they are expected to be soluble in multiple solvent including water. In this study, we have screened out several polyphenols which have a good solubility in UV resins via simulation and experiments. Since water soluble resins are not widely used, the integration of polyphenols into regular acrylic UV resin to explore their functionalization capability can better serve the application. The catechol-integrated UV resin preparation method provides the advantages of a robust one-step surface functionalization with simple mixing, mild reaction condition, and compatible with various types of UV resin. More importantly, the functionalized layer on the printed surface could act as a versatile platform for secondary reactions via a simple dipping method. A series of experiments were conducted to verify the functionalities of the 3D printed structures.

4.2 Experimental section

4.2.1 Chemicals and materials

The solubility of 12 kinds of polyphenols were studied. They include pyrogallol (PG), catechol (CtI), caffeic acid (CA), TA, HHQ, 4-Methylcatechol, epigallocatechin (EGC), Ethyl 3,4-dihydroxybenzoate, 2,3,4-Trihydroxybenzaldehyde, myricetin, and Baicalein. Since dopamine also phenol group, it is treated as a control in this study. The solubility in ethoxylated pentaerythritol tetraacrylate (SR494, from Sartomer Americas) is also studied for screening purpose.

Four commercial 3D printing UV resins were adopted to verify the solubility of PG and Ctl, including VeroWhite from Stratasys Company, Formi Clear resin from Formi Company, eResin-PLA Bio-Photopolymer (red) from eSun Company, and BV-002 (blue) from MiiCraft Company. Moreover, we prepared water-soluble UV resin and epoxy UV resin.

Regarding the multifunctional 3D printed electronics, flexible resin used for actuator and flexible electronics fabrication was purchased from Times80s Company. Heat-resisting electronics was printed by High Temp from Formi Company. ACOMO resin was used to prepare UV resin for water-soluble structures printing.

N-(2-aminoethyl)-1,2-ethylenediamine (diethylenetriamine, DETA) and octadecanethiol (Oct) were used for surface hydrophilization and hydrophobization, respectively, which were purchased from Sigma Aldrich.

4.2.2 Solubility test

The solubility of polyphenols in a typical monomer SR494 was studied as the basis for evaluating the solubility in UV curable resin. SR494 is a fast curing tetrafunctional monomer for use in UV polymerization, which is a classic and widely used acrylic-based monomer, which could help with screening lipophilic polyphenols. The surface tension of SR494 is 37.9 dynes/cm, and the viscosity of which is 45 cPs @ 25°. Total 12 polyphenols were chosen for measuring solubility experimentally. In specific, 0.25 wt% of polyphenol compound was added into 10 g SR494 stepwise. The mixture was stirred thoroughly on a tube vortexer for 3 minutes at least twice until no further dissolving is observed. If there was an aggregate, ultrasonic bath will be applied to ensure better dispersion. Then the mixed solution will be left on a shake over night. After 24 hours, the precipitation was observed to evaluate the solubility. The amount of weight was recorded once the compound is no longer dissolve.

4.2.3 Metallization

Polyphenol in the printed sample was used to reduce Ag^+ ions to silver nanoparticles (AgNPs) on the sample surface [2]. Since polyphenol can absorb metal ions on the

surface, and the polyphenol on the sample was not dissolving into the solution, all the reduced silver was on the sample surface.

For silver deposition, the printed object was first immersed into 0.1 mol/L aqueous silver nitrate solution for 1 hour at room temperature. The sample was then taken out from the solution, further washed by DI water, and dried by N₂. A thin layer of silver nanoparticle can be observed on the surface, which will serve as the catalyst for ELP process.

To obtain a dense silver layer, the as-prepared Ag activated polymeric object was then immersed into a silver ELP solution, which was prepared with a bath ratio 1:50 containing freshly prepared solution A and solution B. Solution A consists of 40 g/L AgNO₃, 40 ml/L ammonia and 0.06 mol/L ethylenediamine. Solution B contains 40 g/L glucose, 2.5 g/L potassium sodium tartrate tetrahydrate, 40 ml/L ethyl alcohol and 0.075 g/L polyethylene glycol.

The electroless copper plating process was performed with the reduced silver as a catalyst. The silver coating can be easily observed when the object was taken from the silver nitrate solution. Before drying, the Ag⁺ loaded sample was immersed into the copper ELP solution, which is made of 1:1 mixture of freshly prepared solution A and solution B. Solution A consists of 15 g/L CuSO₄·5H₂O, 15 g/L K₄Fe(CN)₆, 0.01 g/L K₄(CN)₆·3H₂O, 15 g/L NaOH. Solution B consists of 9.5 mg/L HCHO in water.

Similar to Cu, the ELP of Ni was conducted by immersing the sample with AgNPs into plating solution, which contains 20 g/L Ni₂SO₄·5H₂O, 33 g/L sodium citrate, 14 g/L sodium hypophosphite, and 3 g/L DMAB in water. The bath pH should be adjusted to 10.

4.2.4 Demonstration of a dual metal actuator

Instead of coating the surface with one metal, the strip was coated with nickel and copper into separated layers. The sample was placed into an oven to study the heat triggered actuation process. The temperature of the oven was set to 80 °C, 100 °C, 120 °C, and 140 °C. A camera recording was carried out to observe the procedure of the displacement at different temperatures. To make sure sufficient deformation of the strip, images were

taken at each temperature once steady state conditions had been achieved. Measurements were repeated four times to confirm the performance.

4.2.5 Adsorption measurement for water purification

The adsorption tests were carried out in a temperature-controlled water bath shaker using an agitation speed of 100 rpm. Methylene blue (MB) was used as organic contaminants to evaluate the water purification performance of the printed sample using PG-integrated resin. First, a series of aqueous solutions containing different contaminants were prepared. Second, the printed sample was placed into 100 mL of each solution and shaken in a rotary shaker for 12 h to reach the adsorption equilibrium. At fixed time intervals, the concentrations of the measurement samples were analyzed. The apparent concentrations of MB were measured using a UV-vis spectrometer (Cary 100 Bio UV-vis spectrophotometer) and calculated by absorbance at 664 nm.

4.2.6 Surface hydrophilization, hydrophobization and oil-water separation

Surface hydrophilization. DETA was dissolved into DI water with different concentrations (50 – 250 mg/ml). The printed samples were immersed into each concentration for 6 h at room temperature. After that the samples were washed three times and dried by N₂ gas. Also, a printed sample was also immersed into water for 6 h as a reference sample.

Surface hydrophobization. All printed samples were immersed in a 0.1 mol/L silver nitrate solution for 36 h. The Ag-loading samples were further rinsed with D.I. water and dried in an oven at 60°. To further enhance the micro/nano hierarchical roughness of the substrates, the samples were soaked into an ethanolic solution of octadecanethiol (1:100 v/v) to react for 0-36 h. The samples prepared with different AgNO₃ treating time and octadecanethiol reaction time were labeled as as-printed, 36hAg, 36hAg/12hOct, 36hAg/24hOct, and 36hAg/36hOct, respectively.

Oil-water separation. Oil phase (n-octane, hexane and toluene) and water phase were mixed at the ration of 1:50 (v/v). The emulsions were obtained after sonication for 12h.

The 3D printed mesh was fixed between two quartz tubes, and the prepared emulsion was poured onto the surface of the printed mesh. Then, the oil contents were quantitatively measured by the oil content analyzer before and after separation process.

4.3 Results and discussion

4.3.1 Lipophilic polyphenols screening

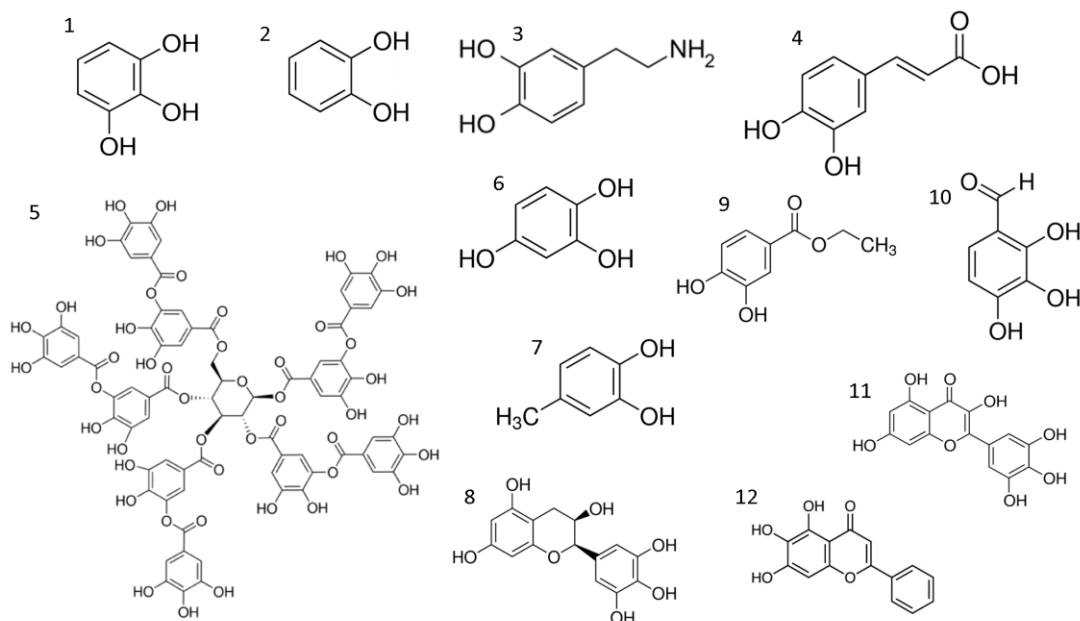


Figure 4-1: Chemical structures of (poly)phenols studied in our study. The name and plant source of all compounds can be found in Table 2.

Polyphenols are serving as the building blocks for the following preparation of functional materials. We first identified 12 representative polyphenols for the primary experiments. Based on initial screening results shown in

Table 2, four phenols (PG, Ctl, 4-Methylcatechol, Ethyl 3,4-dihydroxybenzoate) were found to exhibit a favourable solubility in SR494. These polyphenols are considered to be lipophilic polyphenols to have higher lipid solubility. To further confirm the solubility of polyphenols in 3D printing resin, the solubilities of selected four phenols were investigated in an acrylic resin and the corresponding results are consistent with the

results of SR494. Finally, these four phenols were mixed with Formi Clear resin for the following experiments.

Table 2: Summary of (poly)phenol used in our experiments, including their plant sources and solubility in SR494.

Number	(Poly)phenol ^a	Plant Source ^b	Solubility in SR494 (g/100g)
1	PG	Eurasian watermilfoil	50
2	Ctl	Argan	90
3	Dopamine	None	0.5
4	CA	Argan	1
5	TA	Oak	0.25
6	HHQ	None	1
7	4-Methylcatechol	Picea	75
8	EGC	Green tea	0.25
9	Ethyl 3,4-dihydroxybenzoate	Olives	55
10	2,3,4-Trihydroxybenzaldehyde	None	2
11	Myricetin	Tomato	0.5
12	Baicalein	Plantago	0.75

^a See Figure 1 for structures. ^b Not intended to list all known natural sources.

4.3.2 Silver reduction with the polyphenol modified resin

Thanks to the reducing property of polyphenols, the polyphenol integrated 3D printing resin is introduced with the ability of metallization in this study. AgNO₃ solution was used to treat the photopolymerized samples to investigate the reduction performance. From the experiments, limited silver was deposited on the samples by UV resin with 4-Methylcatechol and Ethyl 3,4-dihydroxybenzoate. Therefore, only PG and Ctl are suitable to be integrated into 3D printing UV resins for functionalization purpose.

In this study, PG was used as an example for the following experiments. First, PG was introduced into various types of 3D printing materials, including water-soluble, acrylic,

and epoxy UV resins. According to Figure 4-2, various prepared UV resins were homogeneous without sediment, suggesting that PG has a good compatibility with the existing 3D printing materials.

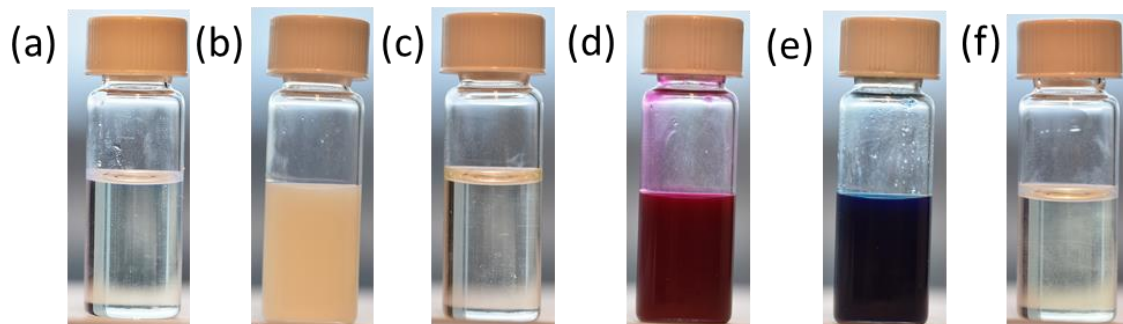


Figure 4-2: PG-integrated UV resins: (a) water-soluble resin, (b) VeroWhite resin, (c) Formi Clear resin, (d) sResin-PLA resin, (e) BV-002, and (f) epoxy resin.

As shown in Figure 4-3, PG with a content up to 5 wt% was dissolved well in the four commercial 3D printing materials and the addition of PG did not affect the printability of original resins. In addition, the presence and redox-active nature of catechol groups on the surface of the cured samples were indicated by silver staining. Immersing the samples with PG into silver nitrate solution, the surface was darkened due to the formation of silver particles through a redox couple between silver ions and catechol groups [3]. Here, 1 wt% PG is sufficient for silver deposition on the surface, implying the high efficiency of silver reduction reaction of PG. Also, Ctl was added into Formi Clear to verify its functionality. From Figure 4-3e, Ctl-integrated UV resin can be used to fabricate 3D structures with multifunctional surface as PG-integrated UV resin. Therefore, PG and Ctl show great potential to be a universal additive to make multifunctional surface of the 3D printed objects.

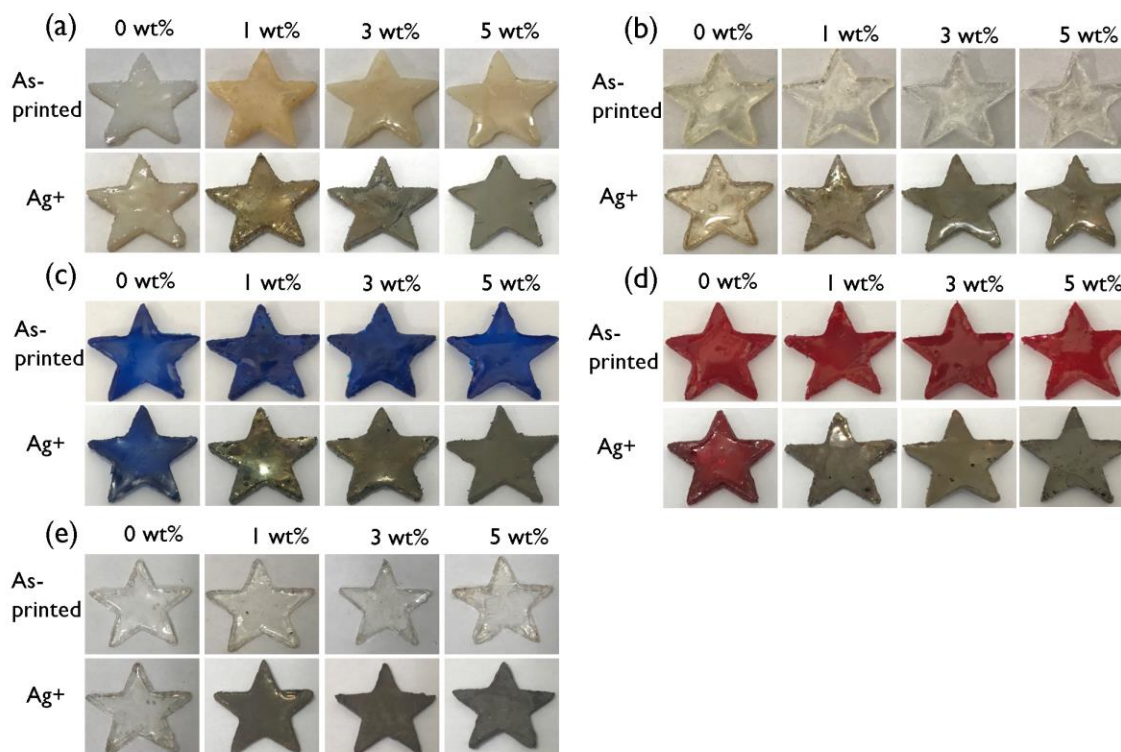


Figure 4-3: Digital images of as-cured and AgNO_3 -treated samples demonstrating versatility of catechol group. Different concentrations of PG (0 - 5 wt%) were added into the (a) VeroWhite, (b) Formi Clear, (c) BV-002, and (d) sResin-PLA, respectively. (e) Different concentrations of Ctl (0-5 wt%) were added into Formi Clear resin.

The effect of the AgNO_3 concentration was also investigated. There is no evident change of the silver deposition with various AgNO_3 concentration. Regardless of the PG content, all the samples were coated with a thin layer of silver (Figure 4-4), indicating the success reduction of Ag^+ ions..

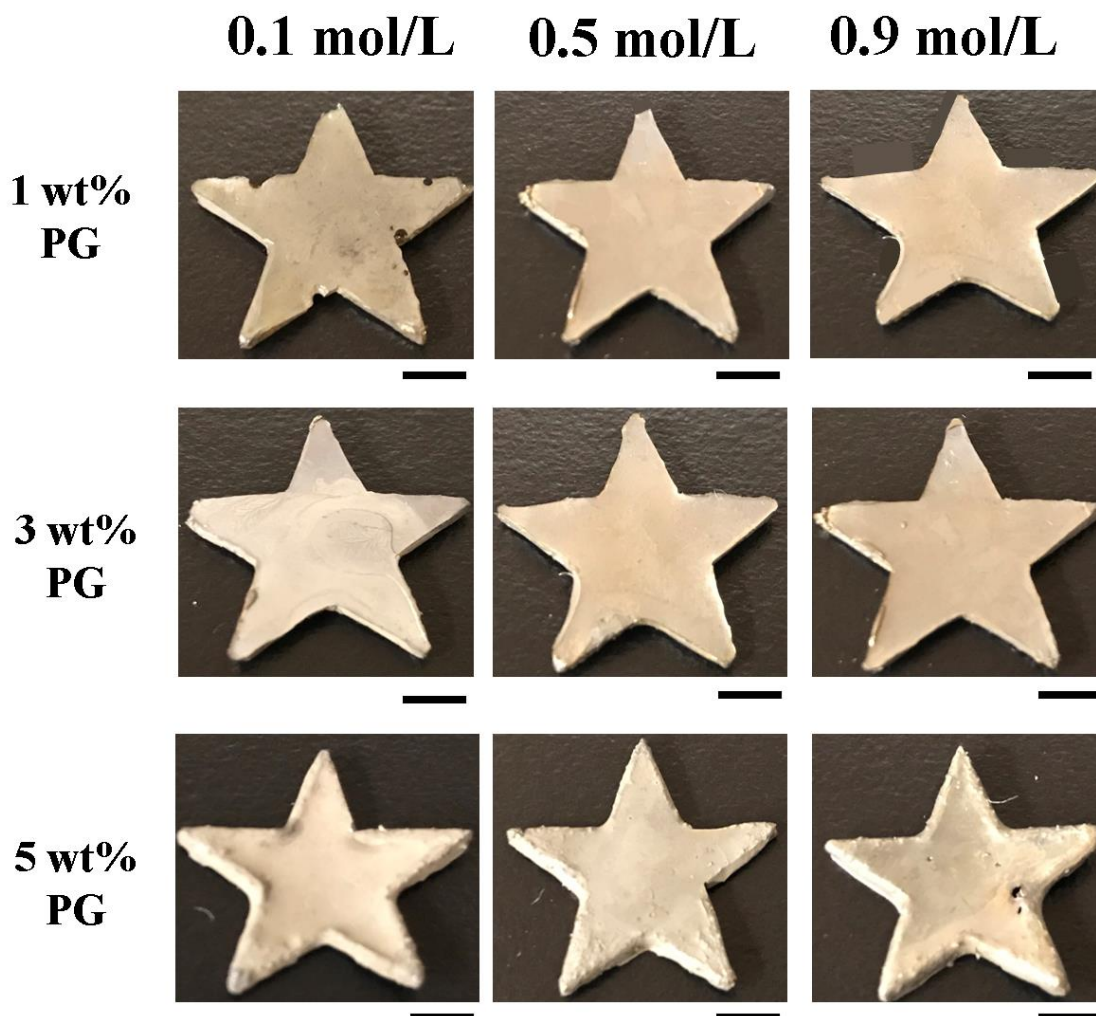


Figure 4-4: The effects of the concentration of AgNO_3 solution. UV-cured samples with 1 – 5 wt% PG were immersed into 0.1 – 0.9 mol/L AgNO_3 solution, separately.

Scar bar is 5mm.

4.3.3 Characterization of the PG-integrated resin

In this study, we used Formi Clear resin as an example for following experiments. 50 mL of Formi Clear resin was mixed with different concentrations of PG for testing their printability on an Asiga 3D printer. Firstly, the UV-vis absorbances of UV resin with different concentrations of PG were measured. As illustrated in Figure 4-5, all samples have a strong absorption peak at the range of from 350 nm to 410 nm for UV based photopolymerization. Although the printability is not influenced by the addition of PG,

the exposure times of printing a single layer (50 μm) were different. Results shown in Figure 4-6 indicate that the addition of PG will increasingly affect the photopolymerization time. 5 wt% PG requires 2.2s to cure one layer while 1s is enough for original resin. In our experiments, when the amount of PG reaches 8 wt%, it is very hard to photopolymerize a complete film under UV exposure.

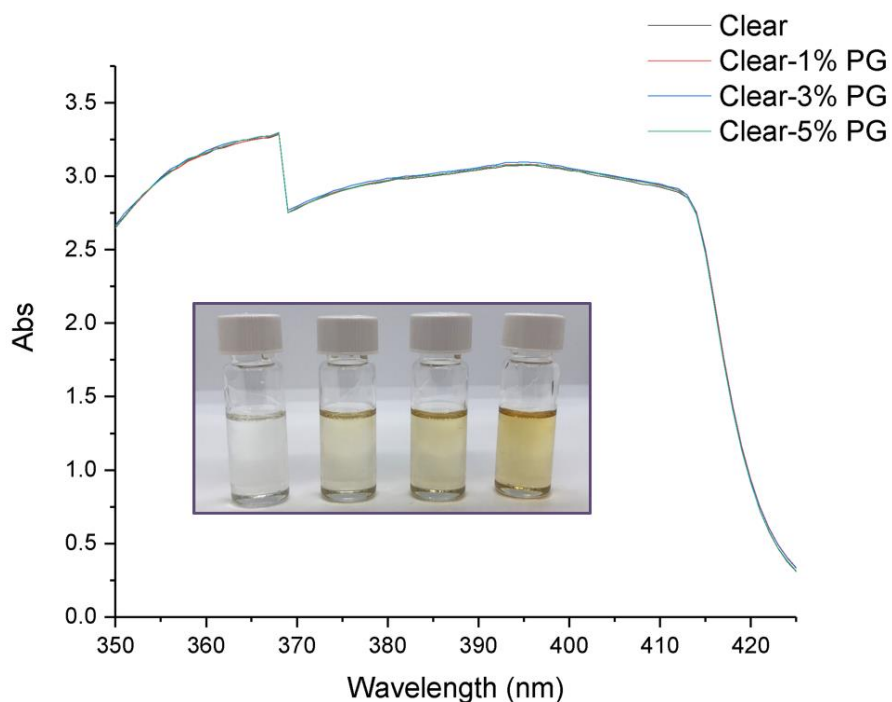


Figure 4-5: UV-vis absorbance spectra of PG-integrated resins with various concentrations (0 – 5 wt%). The inset shows optical image for different concentrations of PG in Formi clear resin.

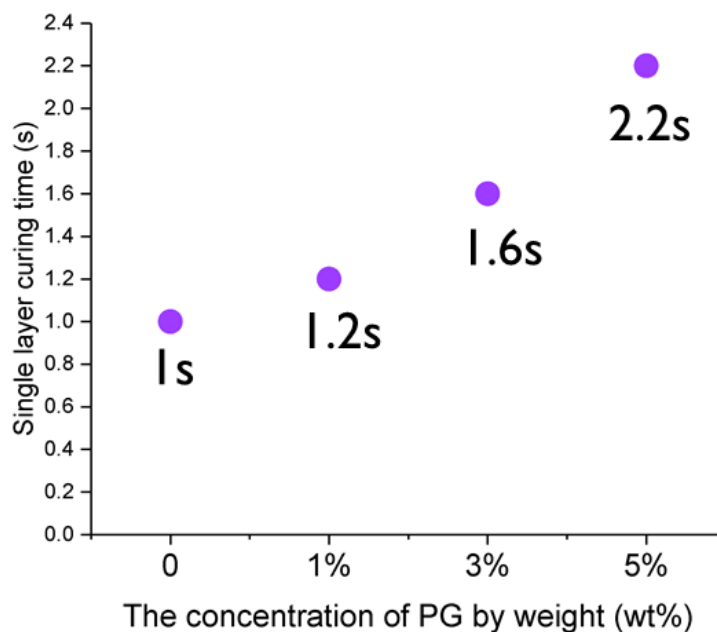


Figure 4-6: The single layer exposure time of various PG concentrations in Formi clear resin.

In general, the existence of the hydroxy group is expected to enhance the hydrophilicity of the surface. However, contradictory phenomenon was found that the object made of higher DMA concentration had a slightly bigger contact angle on the surface, meaning a lower hydrophilicity (seen in Figure 4-7). One reason explains the phenomenon is, the addition of DMA lead to a rougher surface, and the micro-nano structures on the surface will increase the surface energy. It is worth noting that, the hydrophilicity change is small, and the contact angle kept in range of 58° to 68° . Thus, the increasing of hydrophilicity caused by DMA will not affect the following ELP process.

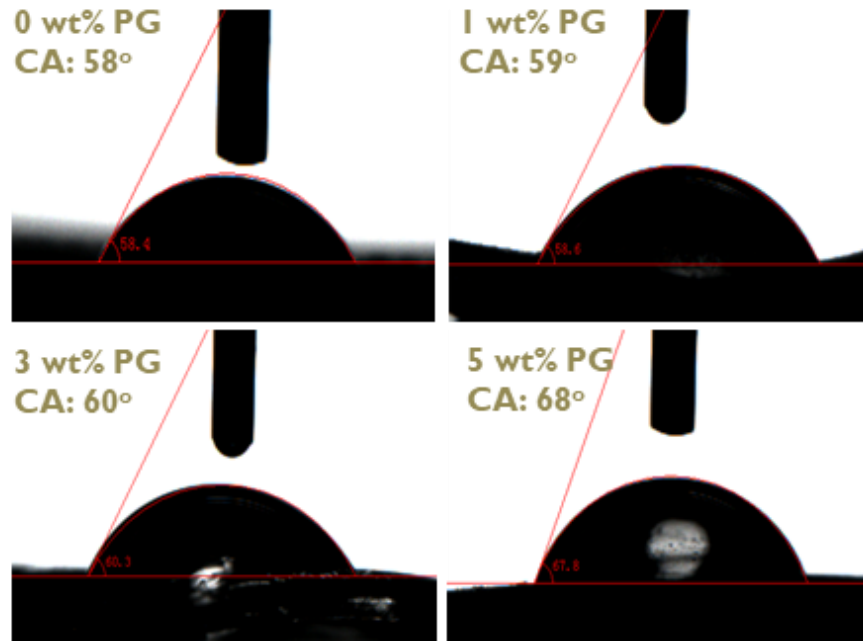


Figure 4-7: Water contact angle of printed substrates cured by different PG concentration resins.

The tensile strength is also measured to investigate the effect of PG on the mechanical performance. The results are shown in Figure 4-8. According to the tensile strength for various concentrations, the increase of PG content weakens the mechanical performance of the 3D printed objects. However, after post UV-curing for 10 mins, the tensile strength can be improved to a certain extent. It is plausible to see that 1 wt% PG has very limited influence on the performance, which is accessible in the application. Therefore, 1 wt% PG is used in the following study.

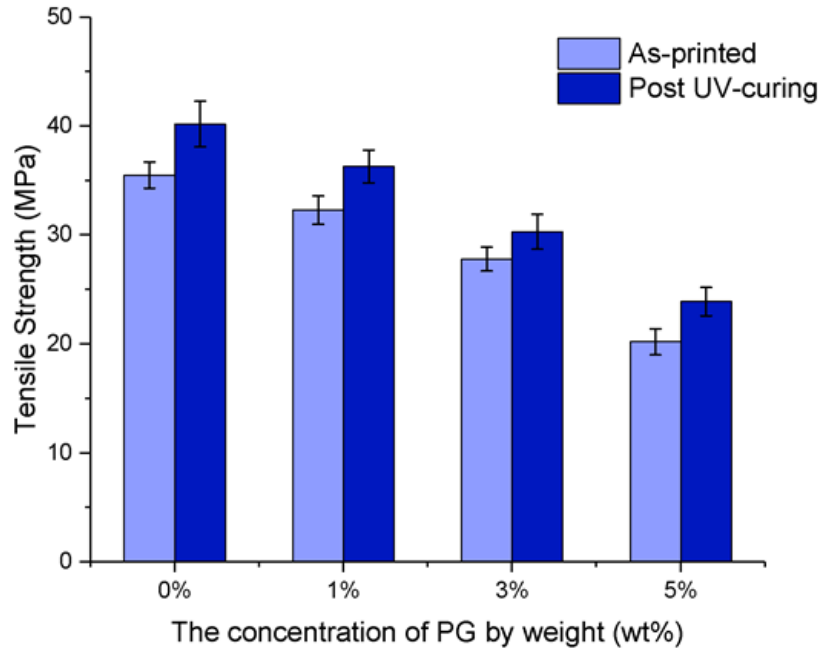


Figure 4-8: Tensile strength of the as-printed and post UV-curing samples.

The strong surface adhesion is one important characteristic of polyphenols. Here the adhesion forces were measured through taking force distance curves with atomic force microscopy (AFM). Detail of AFM measurement is listed in the previous chapter. Results in Figure 4-9 indicate that the adhesion force has doubled after mixing with 1 wt% PG into 3D printing resin.

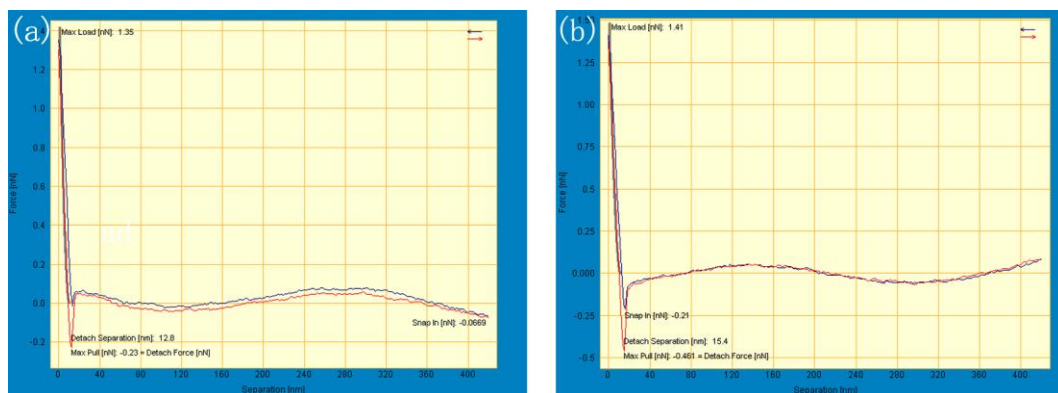


Figure 4-9: Measurement of adhesion forces with atomic force microscopy. Force distance curves for (a) the sample without PG and (b) the sample with 1 wt% PG integrated into the resin.

One crucial advantage of this method over other PD modification-based techniques is the stability of the chemical structure. PD formation is sensitive to the pH value of the environment, and it would be decomposed in acid solution. Because of this, the application of PD is again limited. For example, PD is a good candidate for water treatment due to its excellent adsorption characteristics. However, it is only applicable for alkaline wastewater. Without polymerization reaction, we hypothesize that the pH change did not affect the functionality of PG. To verify this hypothesis, samples coated with PD (hexagon) and as-printed samples using PG-integrated resin (star) were placed into various pH solutions (pH=1, pH=7, and pH=13, respectively). After 7 days, all samples were cleaned by DI water and dried by N₂ gas. In pH = 1 solution, the PD coated sample became transparent, indicating the decomposition of PD film. The color of pH=7 and pH=13 solution changed from transparent to light yellow, and the color of pH=13 solution is darker. It is believed that the polymerization of PG occurs in the alkaline solution. After immersing in a silver nitrate solution, silver was deposited on all samples printed by PG-integrated resin, while for PD coated samples, only the sample being immersed in pH=7 solution possesses the strong metal bonding affinity. Therefore, compared with PD, PG presenting on the surface of printed sample has better stability.

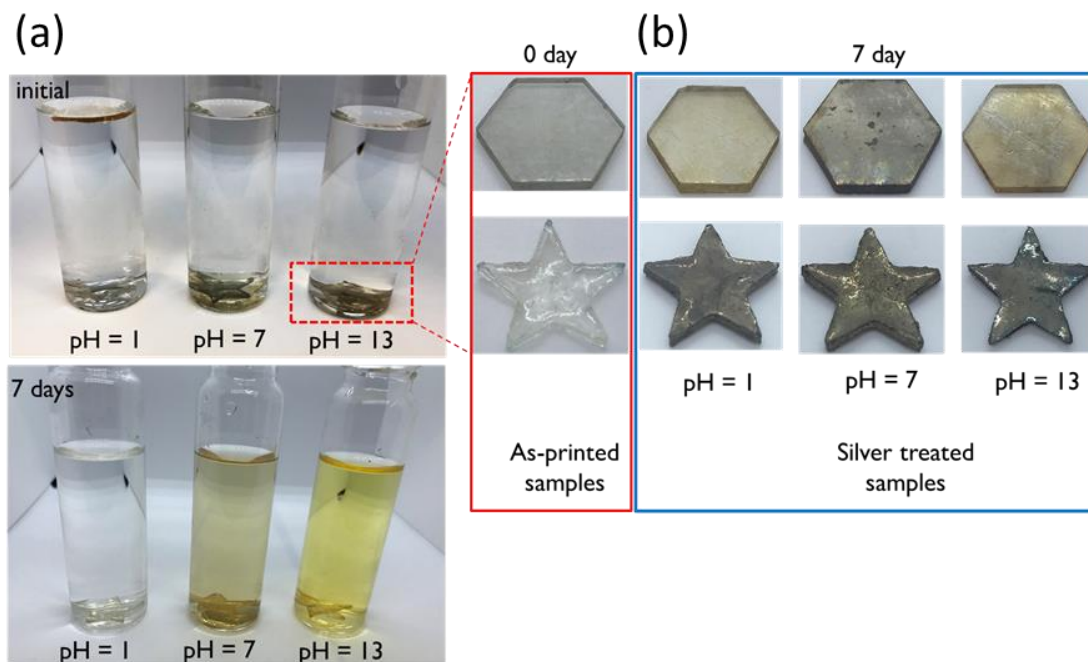


Figure 4-10: (a) As-cured sample and the sample with PD were immersed into pH=1, pH=7, and pH=13 solution, respectively. (b) After 7 days, all the samples are treated with 0.1 mol/L AgNO_3 solution.

4.3.4 3D printing of metallic structures

As printability and functionality of the prepared resins have been proved, it is important to investigate whether this material system is compatible with 3D printer. Thus, 3D printed structures with multiple metals coating were demonstrated in this study (Figure 4-11). Some complex structures, such as microlattice and Eiffel tower, were demonstrated using Formi Clear resin mixed with 1 wt% PG. As-printed Eiffel towers are shown in Figure 4-11c1. From the figures, they all have good surface quality, indicating that the PG-integrated resin provides multifunctional surface while remaining high resolution of stereolithography-based 3D printing process. As Ni can be deposited on the Ag surface and Cu can be deposited on the Ni surface, multiple ELP process can be applied to achieve multi-metals coating. For example, the 3D printed Eiffel tower was first immersed into AgNO_3 solution for silver seeds reduction on the surface. Then, it was placed in Ag, Ni, and Cu ELP solution in sequence. Through controlling the immersion

depth, selective deposition of different metals is demonstrated, and 3D printed objects with different metals coating is fabricated (Figure 4-11c2-c4).

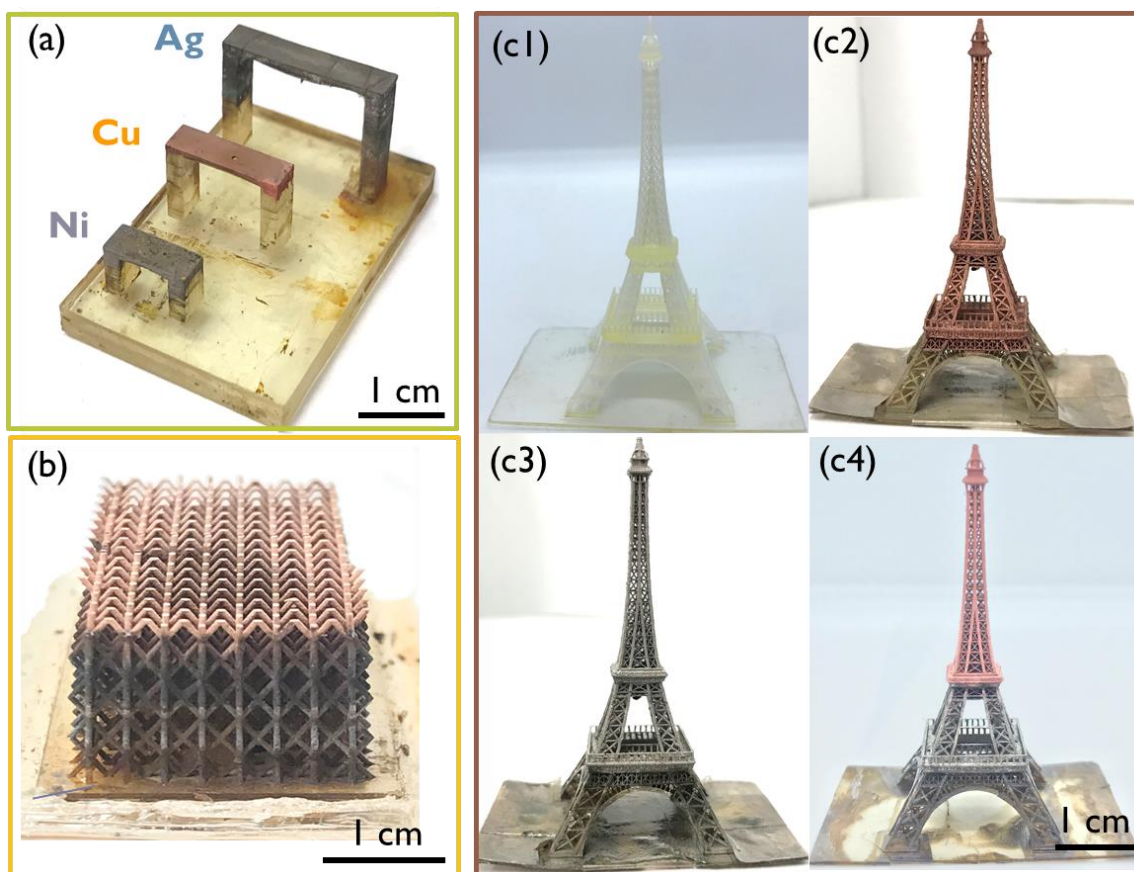


Figure 4-11: 3D printing of complex metallic structures. (a) One part with Ag, Cu, and Ni bridges. (b) Microlattice structure coated with (top to down): Cu, Ni, and Ag. (c1) As-printed Eiffel towers and its metallic structure coated with different metals (top to down): (c2) Cu and Ag, (c3) Ni and Ag, and (c4) Cu, Ni, and Ag.

The effects of the PG concentration on metal deposition were investigated, taking Cu deposition as an example. Upon immersion into AgNO_3 solution, silver seeds were successfully deposited on the surface of the printed objects. Then the Ag^+ -loaded samples were immersed into ELP bath to facilitate Cu particles growth. After 30 mins, all samples were coated with a thin layer of Cu. Figure 4-12 shows that the surface is denser for the samples with higher PG content. For the sample printed by UV resin with 5 wt% PG, it is hardly to observe the grooves in contrast to the samples printed by UV resin with 1 wt%

and 3 wt% PG (Figure 4-12c1). This is because the more PG on the surface can absorb more silver ions on the surface initially. Regardless of PG concentration, a complete copper film was coated on the substrates after sufficient ELP time.

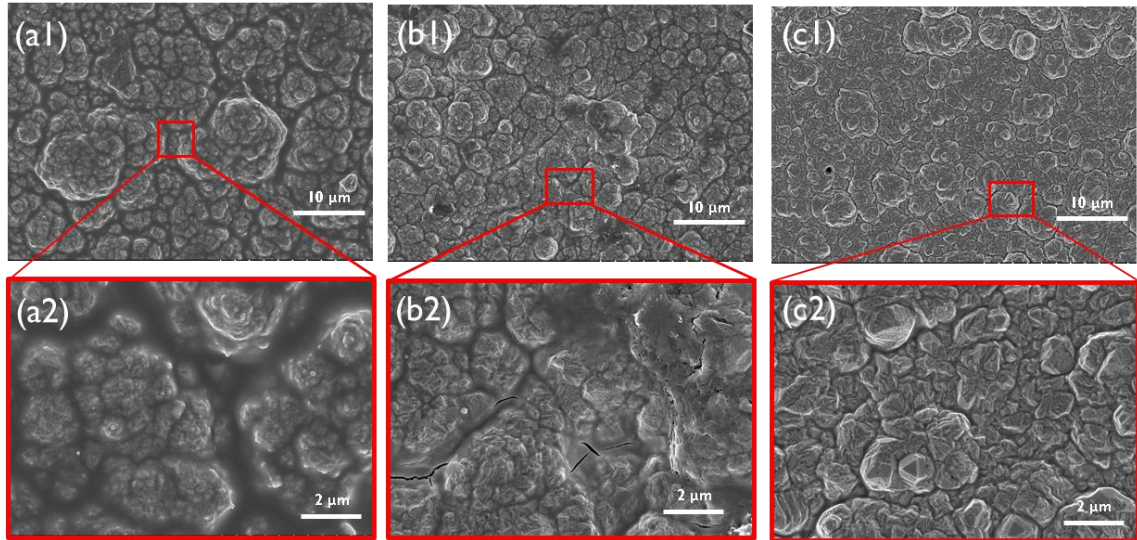


Figure 4-12: Surface morphology for Cu coated substrates printed UV resin with different concentrations of PG: (a) 1 wt%, (b) 3 wt%, and (c) 5 wt%.

The deposition of Cu is further examined with 1wt% PG to study the relationship of deposition time and metal growth (Figure 4-13). The copper growth was clearly observed in Figure 4-13a-c, as more and more Cu particles growing on the surface. At the 30 min, Cu particles fully cover the surface. With the reaction continue, the copper layer further grew into a thickness of 9.27 μm after 240 min (Figure 4-13g). The final sheet resistance is 0.108 Ω/sq , which is about 17.2% to that of the bulk copper. Compared with conductivities obtained by other techniques, the coated metal film by this strategy is consistent, enabling a promising approach to 3D printing electronics.

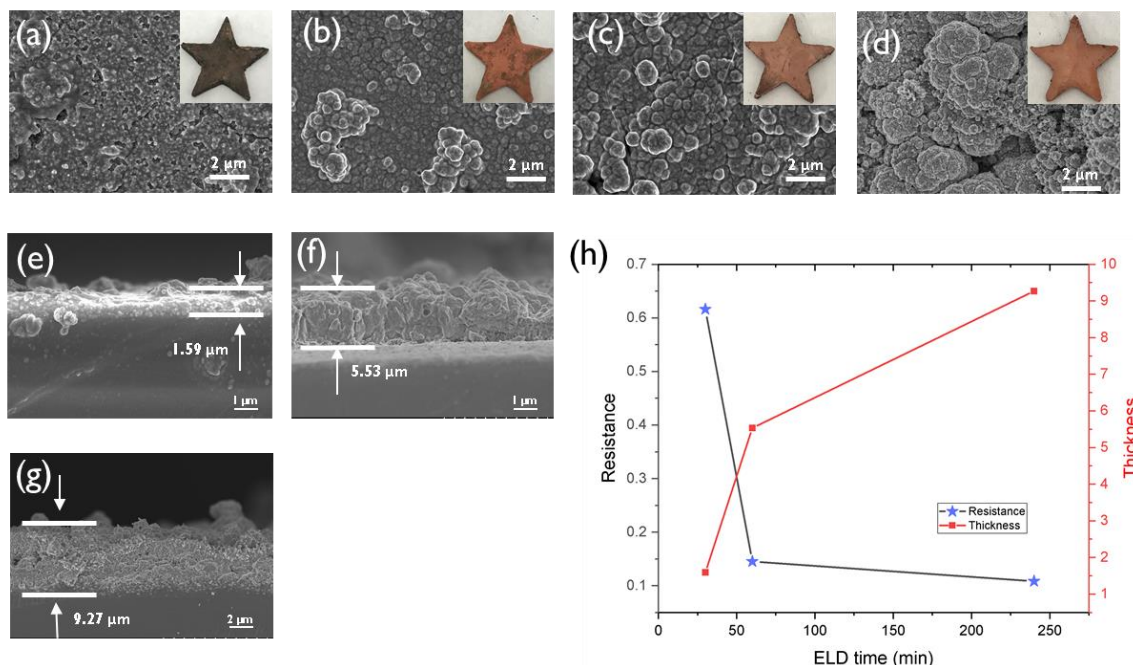


Figure 4-13: SEM used to record the growth of copper particles on the 3D printed object with various ELP time: (a) 10 min, (b) 30 min, (c) 60 min, and (d) 240 min. The inset image shows the Cu-coated object. (e-g) The thickness of the copper film with various reaction time: (e) 30 min, (f) 60 min, and (g) 240 min. (h) Sheet resistance and layer thickness of the deposited copper layer on the substrates with different ELP time. All samples are printed by Formi Clear with 1 wt% PG.

4.3.5 In situ repairing of the 3D printed metallic structures

Due to the PG has a good solubility in acrylate-based resin, it can be distributed throughout the 3D printing material and its printed structure. When the surface was removed, the newly exposed area also possesses catechol groups to allow metals deposition. By repeating ELP process for the damaged area, a new metallic layer can be regenerated on the damaged area. A building with four stairs was used to demonstrate this concept (Figure 4-14a-d). After ELP process, a 3D printed object coated with copper was fabricated. Then the stairs were cut off layer by layer revealing the polymeric area. A 0.1 mol/L AgNO_3 solution was added into the cracked area, followed by adding Cu ELP solution. As shown in Figure 4-14b-d, the damaged area can be recoated a layer of Cu. Regardless of the crack dimension, this regenerating process can finish at the same time.

Moreover, to investigate the influence of in-situ repairing process on conductivity, we repeated this process 10 times. Figure 4-14e demonstrates 1st, 5th, and 10th repairing process. In our study, 10 locations were chosen to scrap away the copper coatings and red box shows the bar with new conductive coating. After 10 times repeating, the bar can still light up the LED by connecting it with a battery. The resistance of the metallic bar has no evident change, ranging from 0.5Ω to 0.8Ω (Figure 4-14f). Therefore, our strategy can be applied to repair the damaged area with any sizes and did not have obvious trail on the resistance.

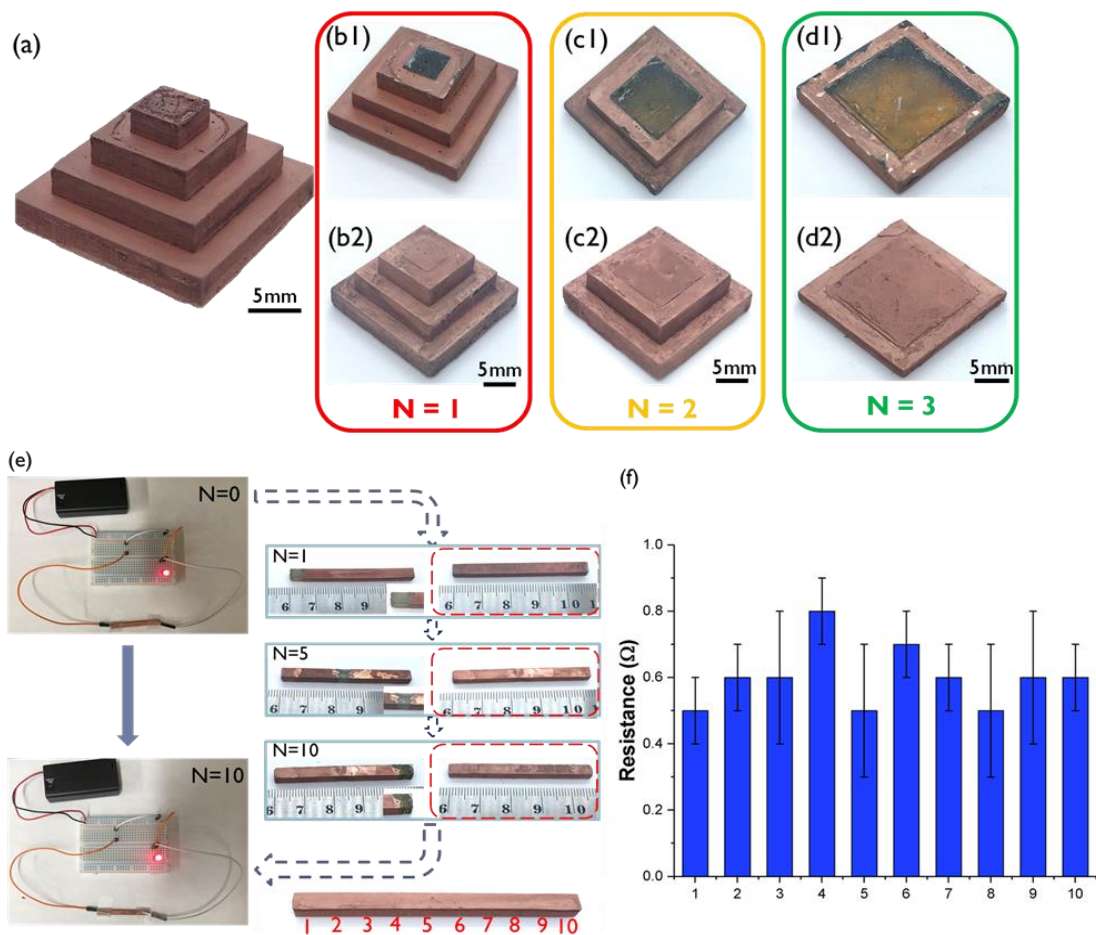


Figure 4-14: In situ repairing of 3D printed metallic structures. (a-d) A metallic structure with three times repairing. (e) After 10 times repairing, the metallic bar is still conductive. 1st, 5th, and 10th repairing processes were shown. NO. 1 – 10 represents different location for every repairing process. (f) The resistance of the metallic bar after various times repairing.

4.3.6 Multifunctional 3D printed electronics fabrication

3D printed objects with metallic layers provides a wide range of applications in electronics, such as actuators, heat-resistance electronics, and flexible electronics. According to the above results, PG-integrated UV resin is promising to be integrated for future applications of 3D printed electronics.

Actuator. 3D printed objects with multi-metal coating was realized as above, which can be used to fabricate actuators reacting to environmental stimuli [4]. Here, a 3D printed strip coated with copper and nickel was fabricated (Figure 4-15a). The composite strip was placed into an oven with one end fixed and the other free to move. The mismatch of thermal expansion coefficient causes internal stresses in the printed object, thus, a deformation can be observed when the ambient temperature was higher than 80 °C, and the largest bending angle can reach to 20° at 140 °C (Figure 4-15b). Multi-metal structures based on PG-integrated resin open the possibility for 4D self-assembling/actuating structures using a simple and facile method.

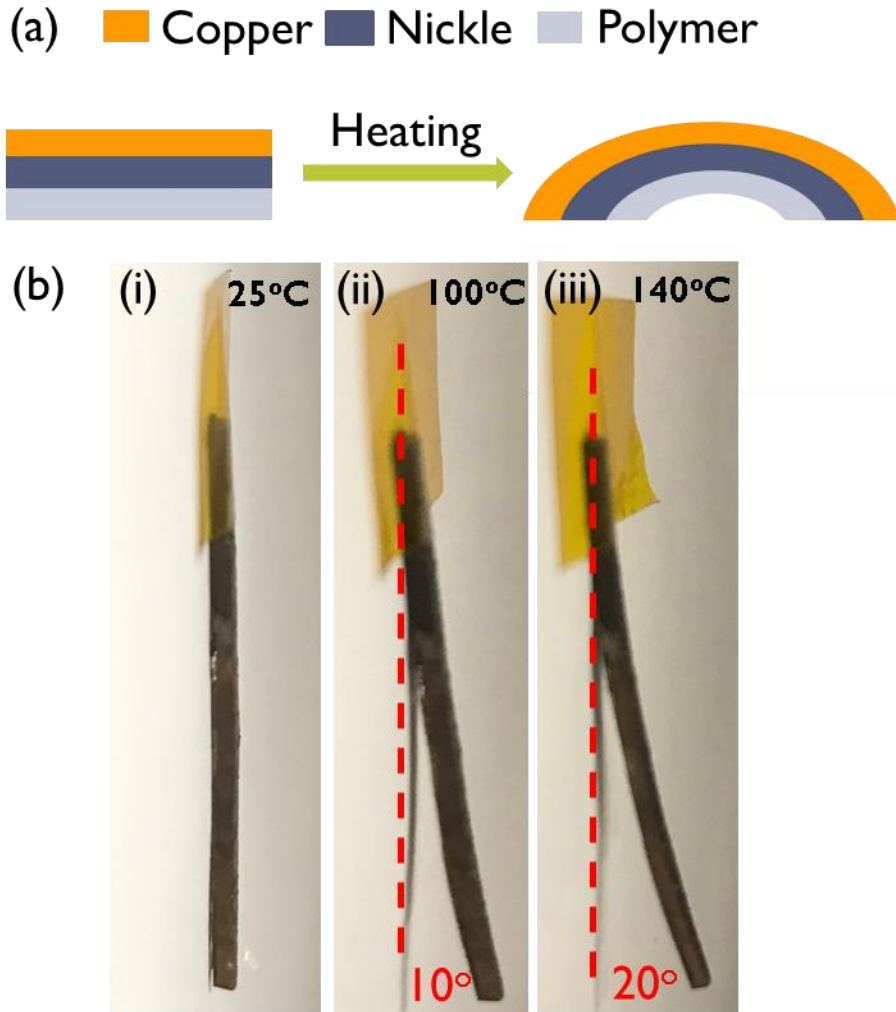


Figure 4-15: Thermo-mechanical response of the polymer-copper-nickel strip. (a) Schematic diagram of the deformation process upon heating. (b) Deformation of the composite strip with perpendicular heating.

Heat-resisting electronics. A big challenge for polymeric structures is that they cannot work at a high temperature environment, especially for the metal-polymer composites, resulting in limited applications in industrial fields. However, with the development of 3D printing materials, such as high temperature UV resins (High Temp resin from Formlab Company), the working scenarios can be largely extended. In our study, High Temp resin mixed with 1 wt% PG was prepared and then printed using a bottom-up SLA 3D printer (Form 1+). Here, a structure with a channel on surface was designed, allowing

selective metallization of printed object. After Cu deposition, the metallic object placed onto a heated bed is used to connect the battery and the LED. When the temperature of the heat bed increases to 220 °C, the conductive pattern can still work, even after 1h (Figure 4-16a). While for the printed object using standard clear resin from Asiga, the cracks and color change was observed after 1 h heating at 220 °C shown in Figure 4-16b. SEM images also confirm the cracks occurred on the sample using clear resin, indicating the high thermal stability of printed electronics based on high-resisting resin. A schematic of heat pad is fabricated, and the temperature field is shown in Figure 4-17.

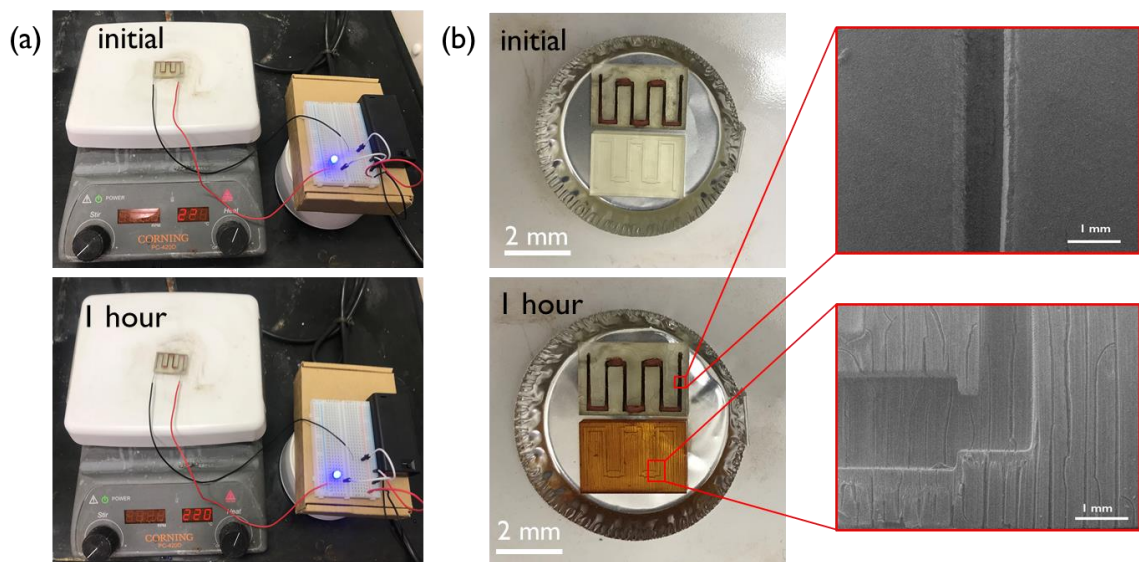


Figure 4-16: 3D printed high-resisting electronic. (a) The metallic structure with circuit is used to connect the battery and LED. The heat bed is set as 220 °C. (b) Another printed sample using Asiga clear resin is used to compare with the sample using High Temp resin.

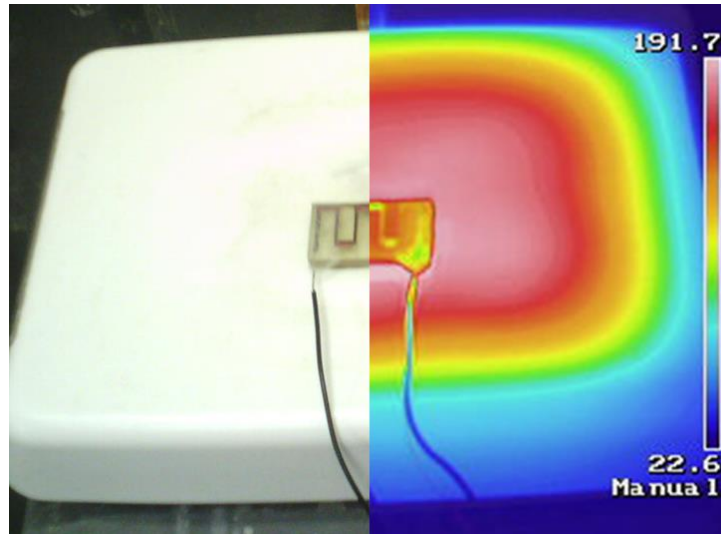


Figure 4-17: Temperature distribution of the heat bed. The real temperature is 191.7 °C.

Flexible electronics. There are exciting opportunities for flexible electronics for applications including sensors, actuators, circuits, electronic skin and displays [5-9]. Coupling flexible UV resin with PG, metallization of 3D printed flexible can be realized. To investigate the stability of the metallic strip, the resistance of the strip after several bending cycles was measured by recording the relative resistivity (R/R_0 , where R represents the conductivity after bending and R_0 represents for the conductivity before bending test). In a bending test, we bended the strips at a fixed angle with the radius in 5 mm. Figure 4-18a shows the relative resistivity for strips with 30 and 40 min ELP changed slightly after 1000 cycles, while there is a largely decrease for strip with 20 min ELP. Moreover, the high conductivity is more easily to retain with a high bending radius (Figure 4-18b). The 3D printed conductive strips also shows high flexibility in Figure 4-18c. The electrical property of the strip was not destroyed by twisting.

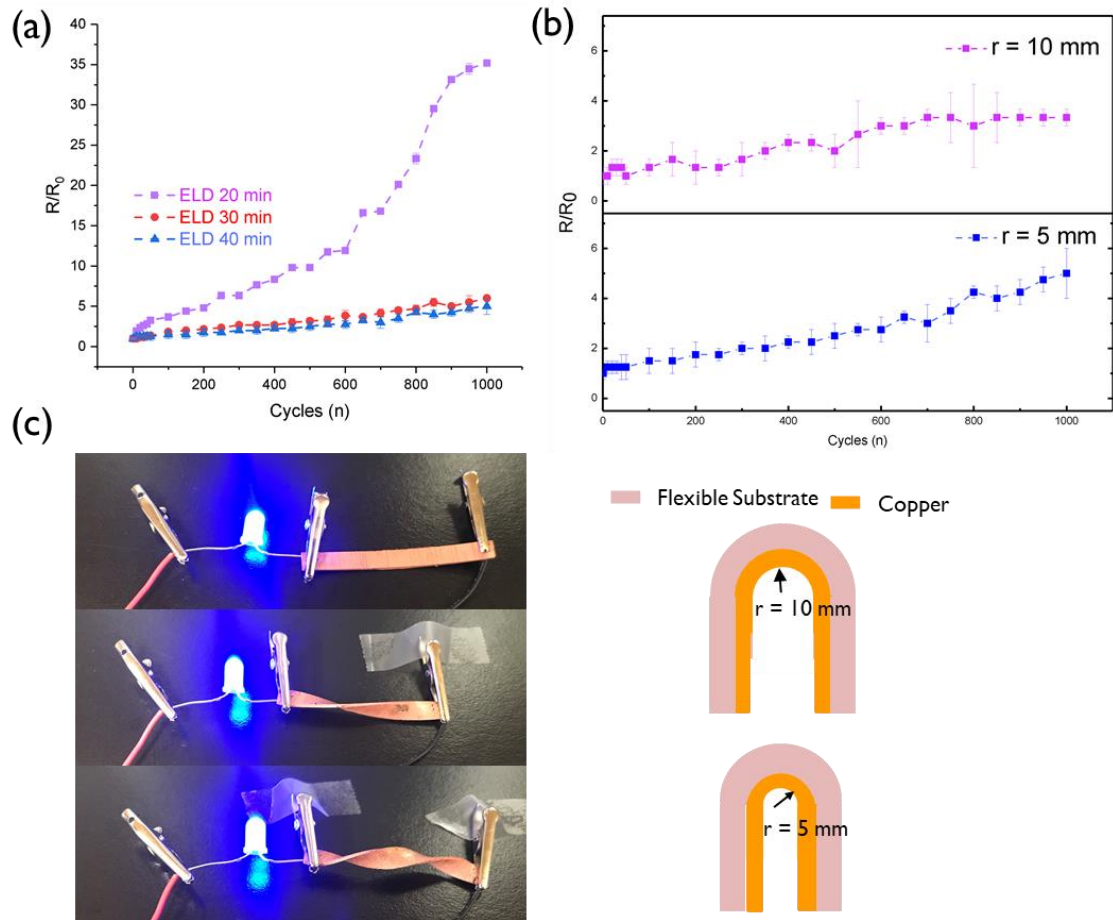


Figure 4-18: Stability and flexibility of printed strips. Relative resistance of the conductive strips with various (a) ELD time and (b) bending radius. (c) Lighting LED when twisting.

Based on the high flexibility and conductivity of the printed structures, two applications were demonstrated: pressure sensor and wearable glove. Taking advantages of 3D printing, the design of the devices is unlimited. Through controlling the immersion area, a conductive circuit with a polymeric substrate was made. With assistance of Velostat film whose resistance changes under pressure, bending can cause the change of the resistance. Arduino chip was used to detect the resistance, and different resistances have their corresponding values which can be used to control LED on/off. Here, the pressure sensor can monitor the bending of a human arm, which is reflected on the three LEDs (Figure 4-19a). For instance, when the bending angle is 135° , all LEDs are turned on. Furthermore, a wearable glove was made. Five pressure sensors were used, and the

movement of each finger can be detected. A simple coding can define different gestures. In this work, a unique gesture can reflect an individual letter, indicating this glove can be treated as a keyboard for computer (Figure 4-19b).

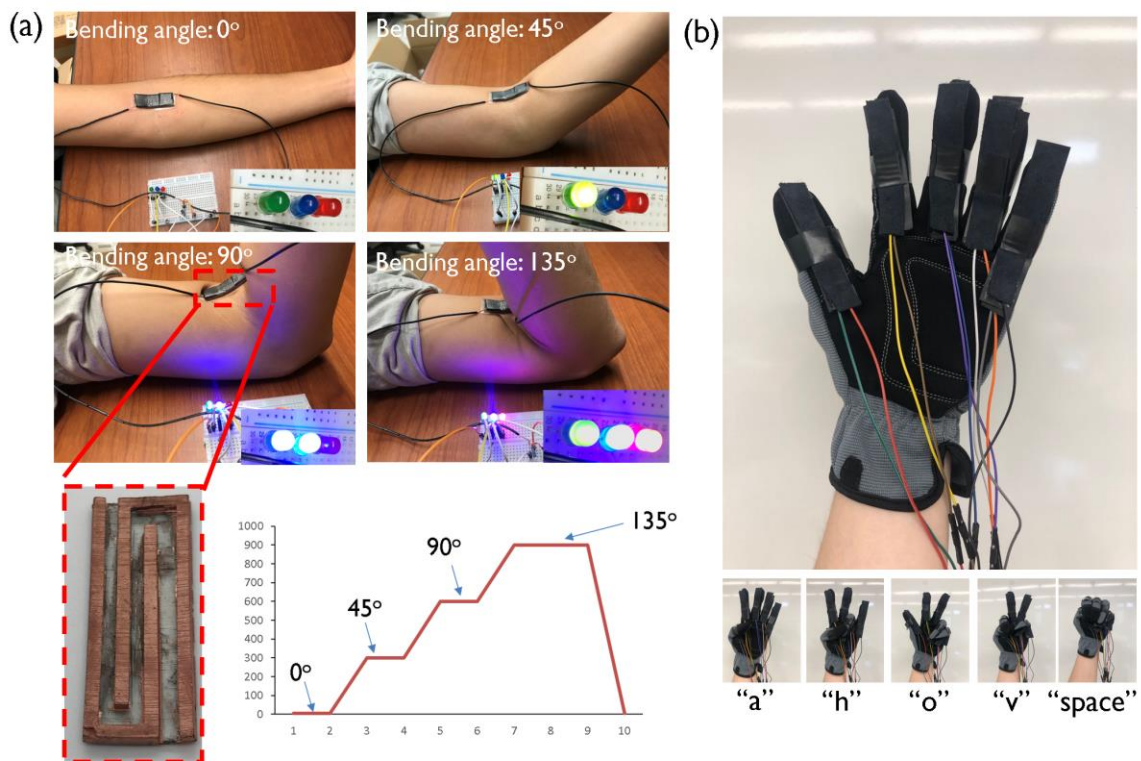


Figure 4-19: 3D printed flexible electronics. (a) Pressure sensor used to detect the arm bending angle. LED lights are used to indicate the bending angle and the corresponding value for different bending angle is shown in the curve graph. (b) Different gestures were designed for different letters.

4.3.7 Water treatment

The existence of catechol groups on the surface of the printed sample are reactive sites of adsorbing heavy metal ions and organic dyes. To verify this, adsorption tests were conducted at room temperature and MB was selected as representative contaminant. Wastewater with high concentrations of MB was used in the experiments. The printed sample was found to exhibit strong adsorption for MB, with uptakes increasing progressively with their concentration (Figure 4-20a,b). The correlation of isotherms

during adsorption followed Langmuir model, suggesting that the adsorption of the organic dye takes place at the binding sites of functional groups. Based on model fitting results, the maximum adsorption capacity (q_m) for MB is 933.07 mg/g. The printed sample adsorption kinetics of MB was examined by investigating the concentration changes of collected samples over time (0–12 h) from each contaminant solution (Figure 4-20b). Equilibrium is reached at around 200 min. The kinetics of the adsorption data was analyzed using both pseudo-first-order and pseudo-second-order kinetic models. The mass changes of contaminants over time exhibit good agreement with the pseudo-first-order kinetic model.

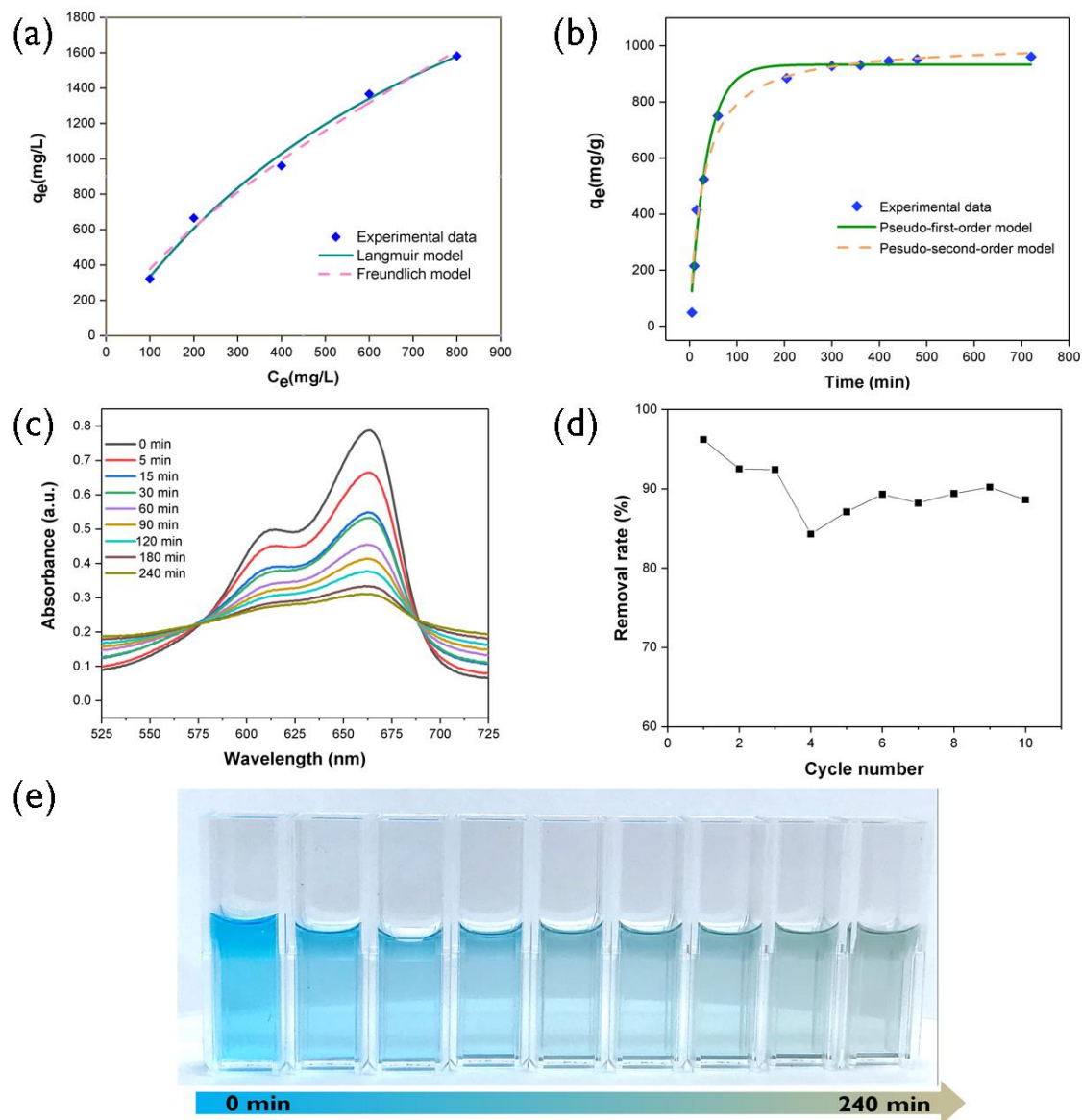


Figure 4-20: (a) Adsorption isotherm plots and curves fitting by Langmuir (solid line) and Freundlich (dot line) models of MB. (b) Adsorption kinetic plots and curve fitting by pseudo-first-order (solid line) and pseudo-second-order (dot line) kinetic models of MB. (c) Time-dependent UV-vis spectra of the MB solution using 3D printed object using PG-integrated resin. (d) Reusability of 3D printed object with PG for MB removal. (e) The photography of the MB solution color change within 240 min.

4.3.8 Surface hydrophilization

Catechol groups presented on the surface also support a variety of reactions with different molecules leading to various functional coatings. For example, catechol group can react with thiols or amines to obtain hydrophobic or hydrophilic surface [10, 11]. Specifically, catechol coated objects are easily to grow functional molecules via the reaction with thiol- or amine-catechol derivatives.

In our work, the surface hydrophilization process was conducted by placing the printed samples into different concentration of DETA solution for 6 h. Here, DETA was adopted to provide amino groups and the influences of concentration of DETA on water contact angle was investigated. According to Figure 4-21, the as-printed sample is hydrophilic, which shows a water contact angle of 54.7°. With the increase of the concentration of DETA to 200 mg/ml, the water contact angle decreased to 1.1°. When further increasing DETA concentration to 250 mg/ml, there is a growth of water contact angle (7.1°), meaning that the abundance of DETA is not good for interaction formation between catechol group and DETA.

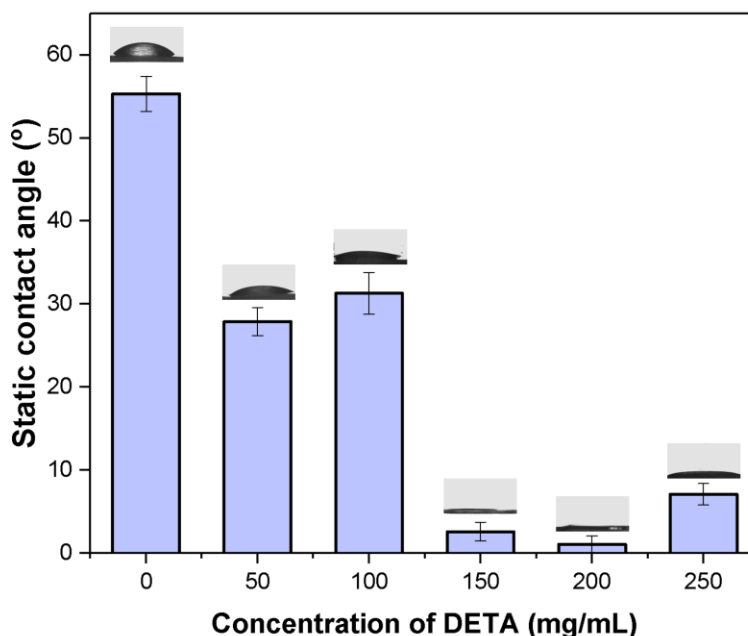


Figure 4-21: Static water contact angles of printed samples treated with different concentration of DETA (0 – 250 mg/ml).

4.3.9 Surface hydrophobization

Similar to surface hydrophilization process, immersion of the printed samples into thiol-containing solution can realize surface hydrophobization. Figure 4-22a shows the preparation process of hydrophobic surface. Silver ions were reduced to silver NPs, which increase the surface micro/nano hierarchical roughness. The Ag-loading samples were further immersed into Oct solution for 0h, 12h, 24h, and 36h, respectively. From the Figure 4-22b, the water contact angle can reach 111° . That is because, firstly, catechol and silver particles react with thiol-terminated molecules through the free catechol-thiol reaction and metal-thiol coordination; then, long-chain was coated onto the printed sample resulting in a hydrophobic surface. The final water contact angle can reach as large as 138.3° .

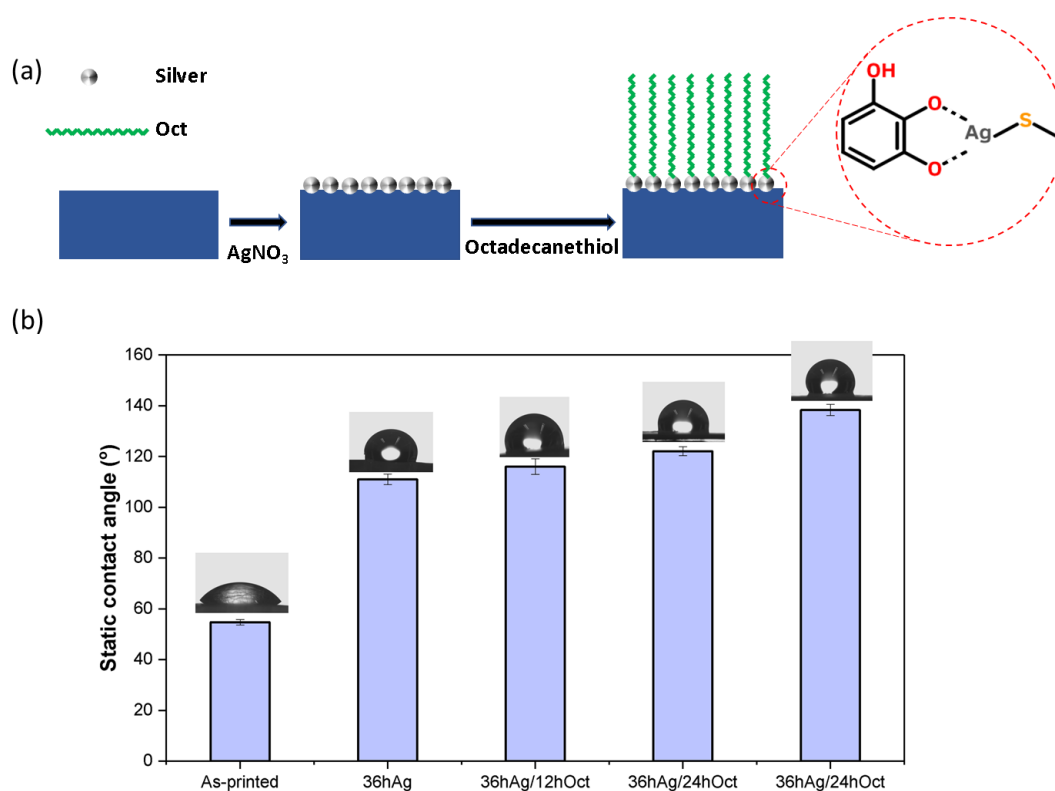


Figure 4-22: (a) Preparation process of the hydrophobic surface. (b) Static contact angle of printed samples with various procedures and reaction time. As-printed sample was used as a control experiment. After 36 h silver nitrate treatment, four samples were immersed into Oct solution for 0h, 12h, 24h, and 36 h, respectively.

4.3.10 Oil-water separation

Microporous mesh-like structures (pore size: 400 μm) were printed by DLP 3D printer. After surface hydrophilization referring to 4.3.8, the water contact angle of the 3D printed mesh was 2.2°. Three types of oil-in-water emulsions were prepared to test the oil/water separation efficiency. The stabilized emulsions contain 1% volume of oil including n-octane, hexane and toluene, respectively. The printed mesh was fixed in the separation apparatus and the emulsion was poured into the surface of the printed mesh. A pre-wetted mesh rinsed with water would not allow oil to pass through as long as the pressure above the mesh is lower than the intrusion pressure. Once the oil phase is expelled, the water pass through the printed mesh driven by gravity very quickly owing to the hydrophilicity of the surface, and the transparent water was collected below the mesh. According to the results in Figure 4-23, the separation efficiency of each emulsion was measured for three times, which was higher than 97%.

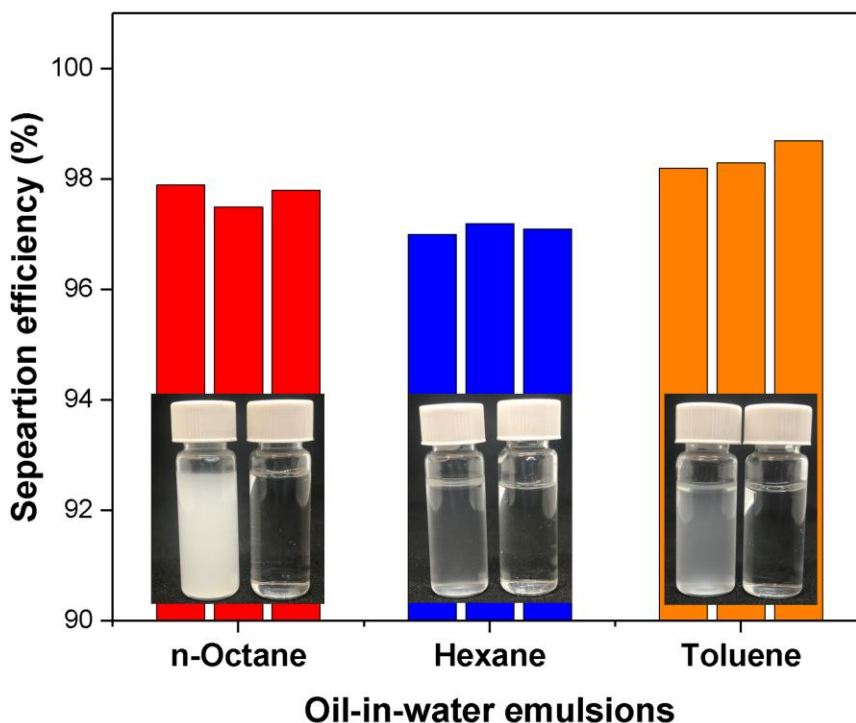


Figure 4-23: Stabilized emulsions composed of n-octane, hexane, and toluene could be efficiently separated. Compared with the milky emulsion, transparent water was collected.

4.4 Conclusions

Polyphenolic compounds are widely existed in the natural plants or fruits. Thanks to its strong solid-liquid interfacial activity, it has been widely used for developing functional coatings. In this study, polyphenols are employed to integrate into 3D printing resin for functional development, focusing on metallization for 3D printed electronics application.

A series of polyphenols are investigated to screen the solubility aiming to comply with lipid resin. Four phenols (PG, Ctl, 4-Methylcatechol, Ethyl 3,4-dihydroxybenzoate) were identified as candidates for 3D printing resin integration, while only two phenols (PG and Ctl) were tested to be functional for metallization use. The printability, chemical stability, mechanical performance and etc. are examined.

It is found that 1 wt% PG is applicable to be integrated into 3D printing resin for various functional development as shown in Figure 4-24. Multiple metal layer was deposited to demonstrate an actuator application; high temperature heater and flexible electronics application were also demonstrated; water treatment capability was demonstrated for heavy metal ion removal use; finally, surface hydrophilization and hydrophobization were realized.

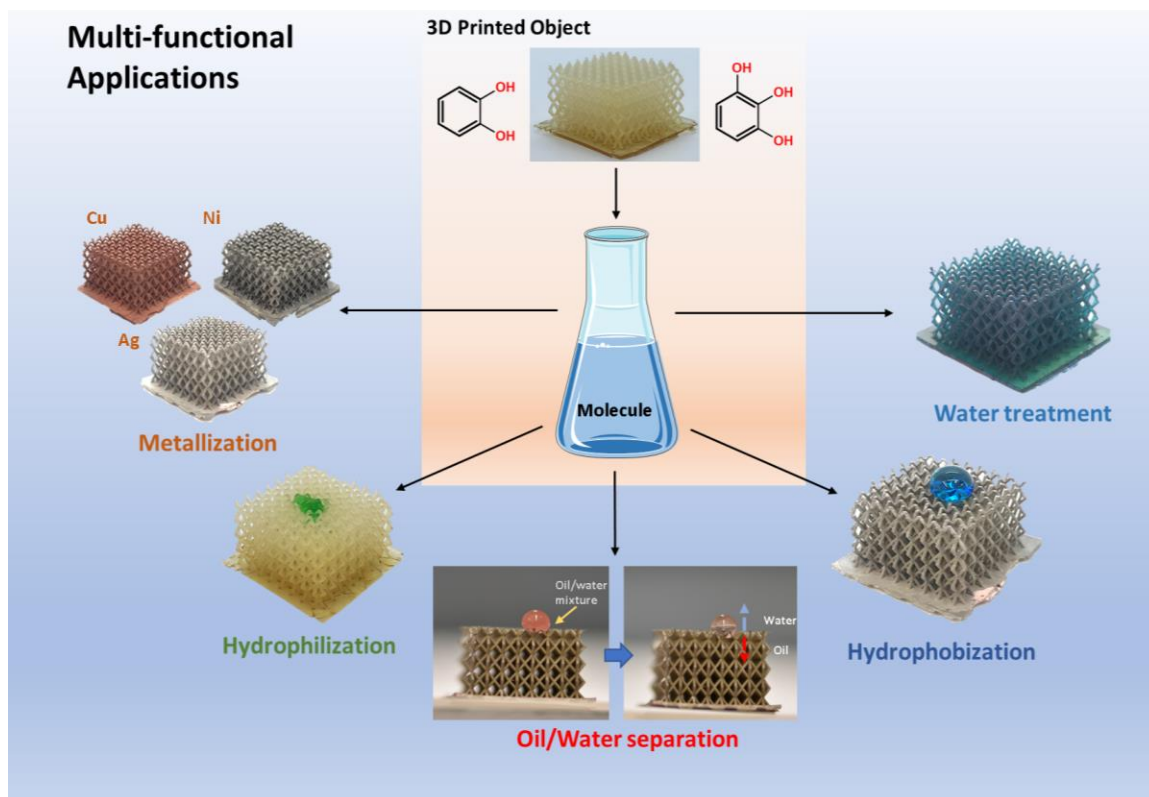


Figure 4-24: Various applications based on i3DP II.

In summary, polyphenolic compounds are excellent candidate for integration into 3D printing, towards to functional 3D printing application. Thanks to its natural source, it is great for future sustainable manufacturing.

References

1. Barrett, D.G., T.S. Sileika, and P.B. Messersmith, *Molecular diversity in phenolic and polyphenolic precursors of tannin-inspired nanocoatings*. Chemical Communications, 2014. **50**(55): p. 7265-7268.
2. Xu, L.Q., K.-G. Neoh, and E.-T.J.P.i.P.S. Kang, *Natural polyphenols as versatile platforms for material engineering and surface functionalization*. 2018. **87**: p. 165-196.
3. Sileika, T.S., et al., *Colorless multifunctional coatings inspired by polyphenols found in tea, chocolate, and wine*. Angewandte Chemie (International ed. in English), 2013. **52**(41): p. 10766-10770.
4. Chen, X., et al., *Multi-metal 4D printing with a desktop electrochemical 3D printer*. Scientific Reports, 2019. **9**(1): p. 3973.
5. Gao, W., et al., *Flexible electronics toward wearable sensing*. Accounts of chemical research, 2019. **52**(3): p. 523-533.
6. Ji, Z., et al., *Multimaterials 3D printing for free assembly manufacturing of magnetic driving soft actuator*. Advanced Materials Interfaces, 2017. **4**(22): p. 1700629.
7. Bauer, S., *Flexible electronics: sophisticated skin*. Nature materials, 2013. **12**(10): p. 871-872.
8. Valentine, A.D., et al., *Hybrid 3D printing of soft electronics*. advanced Materials, 2017. **29**(40): p. 1703817.
9. Wang, Z., et al., *Rapid fabrication of multilayer microfluidic devices using the liquid crystal display-based stereolithography 3D printing system*. 3D Printing and Additive Manufacturing, 2017. **4**(3): p. 156-164.
10. Burzio, L.A. and J.H. Waite, *Cross-Linking in Adhesive Quinoproteins: Studies with Model Decapeptides*. Biochemistry, 2000. **39**(36): p. 11147-11153.
11. LaVoie, M.J., et al., *Dopamine covalently modifies and functionally inactivates parkin*. Nature Medicine, 2005. **11**(11): p. 1214-1221.

Chapter 5

5 3D Co-printing of 3D electronics with a dual light source technology

Chapter 2 – 4 follow the thinking of i3DP II and optimized the initiators step by step, providing effective strategies for metallization polymeric 3D structures, but there is concern that the introduction of active groups causes the entire surface to be metallized. Highly selective metallization process is still required to develop. This chapter reports a new strategy - 3D Co-printing technology by collaboratively employing two photopolymerization processes - to fabricate 3D electronics selectively either deposited on a free-form surface or embedded within a bulk structure. The 3D Co-printing technology only involves one printing material, which works for both the construction of polymeric structure and the metallization process of conductive circuits because of the introduced metal precursor in photosensitive resin. Due to the existing of metal precursor, metal NPs can be efficiently photosynthesized after laser scanning. 3D Co-printing technology addresses the challenge of conventional methods requiring multiple deposition processes. The resultant trace which is composed of NPs exhibits a superior resistivity as low as $\sim 6.12 \mu\Omega \text{ m}$. The resistivity is further controllable ranging from 10^{-6} to $10 \Omega \text{ m}$ through adjusting the material formulation and processing parameters. The validation and demonstration in this study verify the proposed 3D Co-printing as a high-efficiency and low-cost co-printing approach which opens a new avenue of making 3D electronics.

5.1 Introduction

i3DP II proposed and optimized in Chapter 2 – 4 provides effective strategies for metallization polymeric 3D structures, but there is concern that the introduction of active groups causes the entire surface to be metallized. Conductive patterns require additional manual labor for patterning. There remains a need for a selective metallization able to print conductive trace on 3D printed structures. A wider range of electrical applications based on 3D printing techniques will require advances in both 3D printing techniques and material selection.

Recently, a new approach to 3D printing conductive structures was proposed. Incorporating silver nitrate into a photocurable UV resin, silver NPs were in-situ generated on the surface of the printed objects via light [1] or heating [2]. Based on the similar material formulation, Wang et al. developed a blue laser projection printing method to fabricate complex 3D objects. After thermal sintering, silver NPs appeared on surface of the printed objects [3]. As only one material was used, it directly reduces the complexity of 3D process and the in-situ generation of metal NPs also eliminates the poor adhesion from different materials deposition. However, the above methods can only provide a conductive part without a specific pattern to function as a circuit, since the methods using lamp or oven will cover all exposed body/surfaces. Moreover, the obtained resistivity was very high ($\sim 1 \times 10^5 \Omega \text{ cm}$), limiting the wide range of applications. Thus, we propose a method using a second laser to achieve selective metallization on the 3D printed objects with good conductivity. Using a laser to in-situ generate metal patterns during 3D printing process has been rarely studied to date, although laser has been used to print various functional parts by incorporating with tailorable photocurable resins through changing the reactive formulations or adding functional additives [4-7]. It is desired to directly realize the metallization process during printing to achieve 3D circuit. Through developing photopolymer systems, new 3D printing materials allow the construction of complex structures and printing of conductive traces simultaneously, addressing the challenges brought by the multimaterial deposition.

In this study, we develop a 3D co-printing technology by integrating two light systems—digital light processing (DLP) and laser scanning—to fabricate 3D electronics. Sophisticated polymer structure was fabricated by DLP with a high resolution based on the spatially-controlled solidification, and every layer can be cured within seconds [8]. Then, the second light source, a laser system with a controllable scanning speed, is performed to selectively reduce the precursor-contained polymer into conductive material via in situ nucleation and sintering of metal NPs. The laser is applied here as a robust and reliable tool to precisely control the conductivity of metal traces via laser photothermal metallization. Specially, the proposed 3D co-printing technology only works with a single 3D printing resin containing monomer, metal salts and photoinitiator, which avoids the difficulty brought by multimaterial printing processes. As only one material is

required, this method eases the fabrication procedures and can be further extended to fabricate arbitrary-shape electronics in a cost-effective and time-saving manner. In this study, the effects of the laser on the diameter and distribution of the generated silver NPs were investigated in detail, and then experiments were conducted to analyze the influence of different material formulations and processing parameters such as laser power and scanning speed on resistivity. Typical printed 3D electronics circuits by this 3D co-printing technology were demonstrated. Remarkable advantages such as easy-to-use, scalability and flexibility have been clearly showed according to the experimental results.

5.2 Experimental section

5.2.1 Material preparation

The printing resin is photopolymer-based, consisting of oligomer, photoinitiators and additives. Polyethyleneglycol diacrylate (PEGDA) with three different molecular weight (250, 550, 750 g mol⁻¹) were prepared as photocurable oligomer; typical photoinitiator - 2,4,6-trimethylbenzoyldiphenyl phosphine oxide (TPO) - was adopted due to its high performance in the near UV spectrum. Silver nitrate was added as a metal precursor for forming conductive traces. All the above chemicals were purchased from Sigma-Aldrich and used without further purification. Moreover, the second type of photocurable oligomer, 4-acryloglmorpholine (ACMO), was used to compare with PEGDA. ACMO was purchased from Lihou company.

Different amounts of silver nitrate (5, 10, 15, 20 phr) were dissolved into each type of PEGDA, resulting in 12 formulations of resin. We use PEGDA molecular weight and concentration of silver nitrate to denote each resin type. For example, PEGDA250-5% were prepared by 250 g mol⁻¹ PEGDA with 5 phr silver nitrate. The resultant 12 photosensitive resins were tested in the developed 3D printer.

5.2.2 Setup of 3D Co-printing

A hybrid 3D co-printing printer is developed by coupling DLP stereolithography process with laser-induced metallization process, as Figure 5-1a. The 3D Co-printer consists of three main components: DLP projector, laser emitter and building plate; DLP projector

provides a near UV light for curing PEGDA layer by layer; the laser emitter is mounted between DLP projector and the building plate, and is used to selectively scan the solidified layer to generate conductive patterns. After finishing one layer, the building plate moves down to allow the construction of new layer. Figure 5-1b schematically describes the working principle of 3D co-printing process of 3D electronics: UV source from DLP projector is used for structure building; the laser emitter then precisely prints circuitry on polymeric surface based on thermal-chemical reduction reaction. Noted here that the additional laser emitter can provide higher light intensity compared to that of DLP projector light (otherwise extremely long exposure time (>30 minutes) is required to finish one layer of conductive pattern). Thus, the optical energy from laser emitter can be directly converted into heat with high selective and controllable local temperature via photothermal reaction (Figure 5-1c). When reaching the reaction temperature, the nucleation of the silver NPs undergoes an in-situ growth in the laser scanning area, thus creating a conductive pattern. With a high reaction rate, the dielectric polymer is transferred to conductive the silver path in real time.

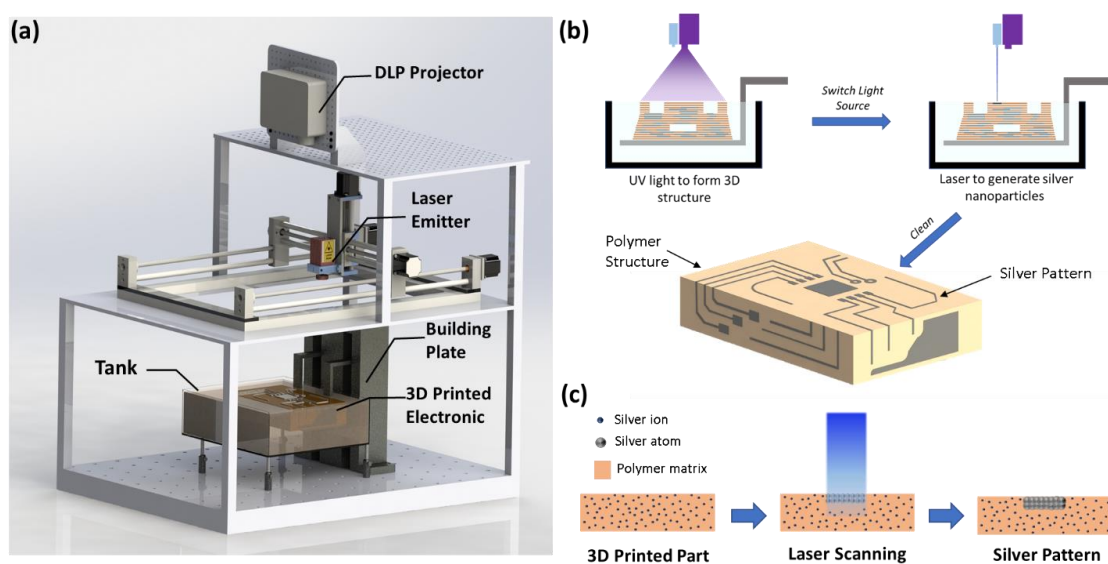


Figure 5-1: (a) Schematic diagram of home-made 3D printing machine. (b) 3D co-printing process by two laser systems. (c) The laser-reduced mechanism of silver nanoparticles in 3D printed structure during laser scanning process.

5.2.3 Characterization

Resistance was measured using a digital multimeter. The morphological characterization of the silver NPs into photopolymerized matrices were carried out by a scanning electron microscopy (SEM, Hitachi S-4500). Another SEM equipped with an Energy dispersive X-ray (EDX) is also used for compositional analyses.

5.3 Results and discussion

5.3.1 Developing material system with metal precursor

To evaluate the suitability of photopolymers for developing the customized 3D printing resin, two kinds of material system were tested with two oligomers, PEGDA and ACMO. They both have good compatibility with AgNO_3 and can formulate as an aqueous solution to load various concentration of AgNO_3 .

ACMO is a thermoplastic resin. With 15 wt% AgNO_3 , we have prepared a UV curable resin for the test. After the resin is cured with UV light, a second laser with various power was employed to reduce the silver ions. Although silver lines were successfully observed on the substrate (Figure 5-2a), all the printed tracks are nonconductive. EDX results in Figure 5-3 clearly reveal that the atomic concentration of silver did not change with the laser parameters, but almost kept constantly (15%). The increasing of the power did not improve the growing of silver NPs. Additionally, there is a groove with smooth surface without burning. The reason is ACMO, as a thermoplastic resin, got melted at high laser power. The fast diffusion of the polymer encapsulates the silver NPs, limiting their growth and prohibit their conductivity. Thus, the type of ACMO resin is unsuitable for this study.

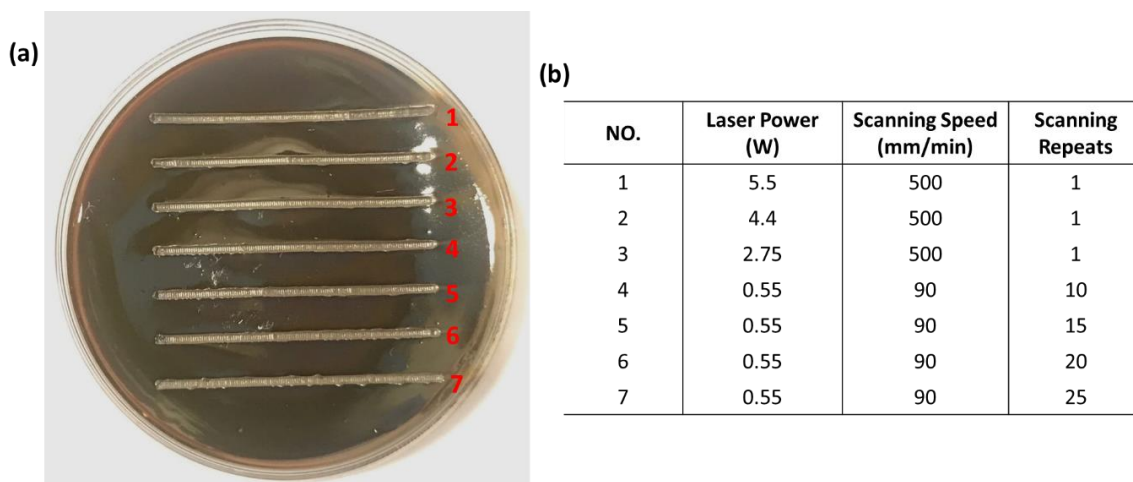


Figure 5-2: (a) The printed tracks on the cured substrate using ACMO. (b) Processing parameters used for NO. 1 – 7 line.

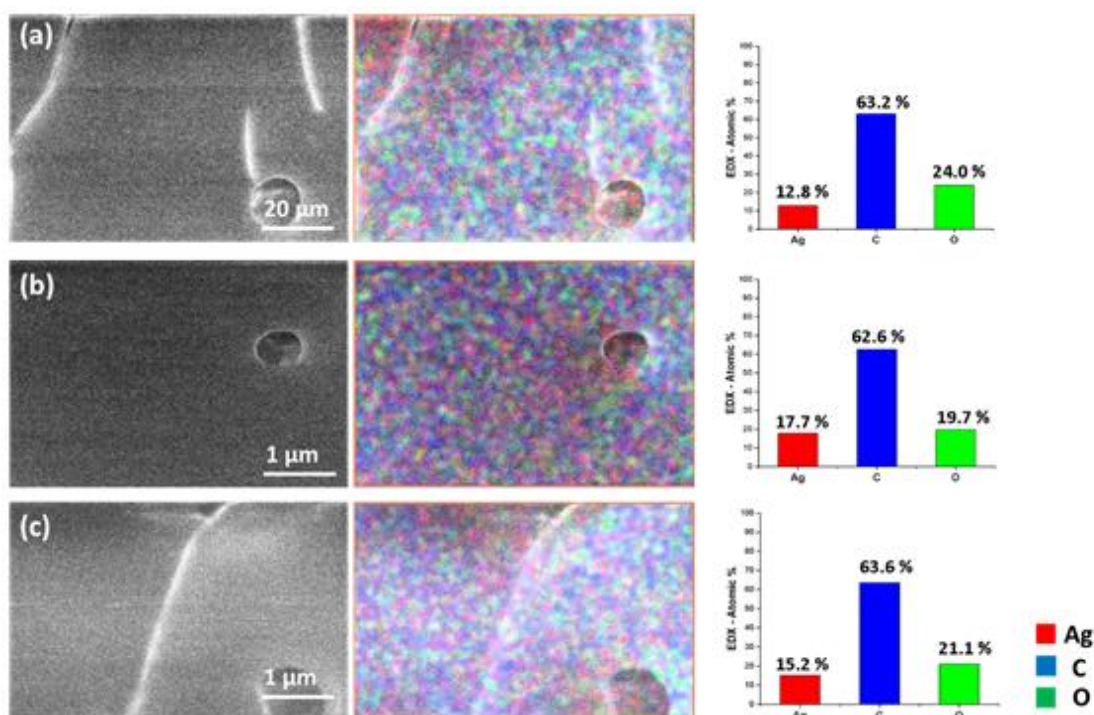


Figure 5-3: SEM images and EDX of silver tracks scanned by different laser power: (a) 5.5W, (b) 4.4W, and (c) 2.75W. The scanning speed is 500 mm/min and the prepared UV resin is based on ACMO.

In this study, water-soluble PEGDA with three different molecular weight, PEGDA250 (250 g/mol), PEGDA550 (550 g/mol), and PEGDA750 (750 g/mol) were mixed with four concentrations of AgNO_3 , resulting 12 formulations. An exemplar prepared resin, PEGDA with 15 wt% AgNO_3 , was shown in Figure 5-4. To test the printability of these formulations, disk shape samples of 80 mm in radius and 8 mm in thickness were prepared (Figure 5-5). The additive of AgNO_3 can keep its printability when the amount of the silver nitrate is below 20 phr. It is observed that the color of the sample becomes light yellow or reddish brown, but 3D printed objects with pure PEGDA are clear. The color change of the printed samples was resulted from the presence of silver NPs. That is because during the DLP process, the UV coming from the projector not only can polymerize the liquid photopolymer, but also reduces a small percentage of silver ions forming to silver NPs through electron transfer [9, 10].

Herein, owing to the requirement of the insulating property for the 3D structure, the solidified structure via photocrosslink should be non-conductive, which is confirmed through the measurement of the resistance for all printed samples. From Figure 5-5, the sample with PEGDA550 and PEGDA750 were transparent, whereas the color of PEGDA250 disks became brown and opaque, indicating that PEGDA with low molecular weight has a high efficiency of photoreduction of silver ions. Both size and distribution of the photo-reduced silver NPs cause color change, for PEGDA250-5% and PEGDA250-10%, the color is much deeper. From the results we can see that PEGDA with lower molecular weight is not proper for this application. The PEGDA250-15% and PEGDA250-20% cases show the distribution of the silver nitrate is inhomogeneous. Therefore, PEGDA with higher molecular weight are more suitable for 3D co-printing technology as its good printability and smaller amount of silver NPs generation without change of the electrical insulating property of printed samples.

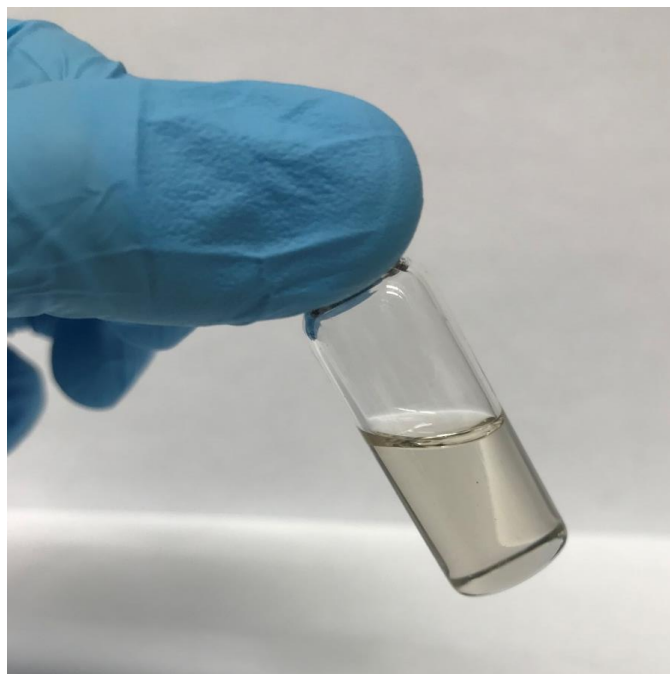


Figure 5-4: The prepared UV resin (PEGDA) with 15 wt% AgNO₃.

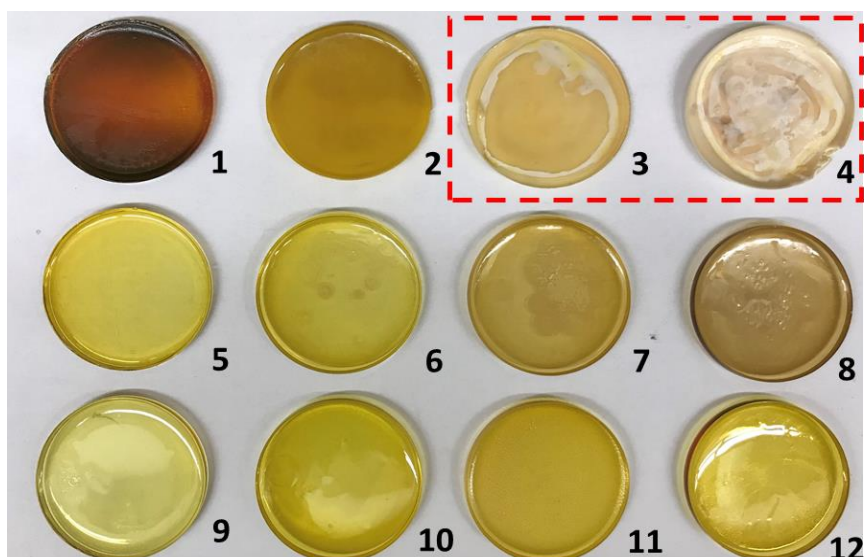


Figure 5-5: The printed sample with various AgNO₃ percentage (5 – 20 phr) and materials (PEGDA- 250, PEGDA – 550, and PEGDA- 750): (1)PEGDA250-5%, (2)PEGDA250-10%, (3)PEGDA250-15%, (4)PEGDA250-20%, (5)PEGDA550-5%, (6)PEGDA550-10%, (7)PEGDA550-15%, (8)PEGDA550-20%, (9)PEGDA750-5%, (10)PEGDA750-10%, (11)PEGDA750-15%, and (12)PEGDA750-20%.

5.3.2 Photoreduction of silver NPs

Figure 5-6 illustrates several printed silver lines with a sequence of repeat times based on PEGDA750-15%. A low power (0.55w) laser with scanning speed of 1.5 mm/s is applied. It is noted that there was no obvious change for scanning below 10 scans. Thus, more scans were applied and studied. From SEM images (Figure 5-6b-e)), no burned and porous structure were observed. Silver lines after repeating scanning show a bulging effect, causing significant difference in width. The width of the line changes from 0.22 to 0.56 μm , and the edge broadens. This could be in part due to the local temperature profile from the center of the laser spot to the edges. Silver NPs at the center of the lines can absorb higher intensity light owing to high intensity of the laser at the center of the spot; more heat is generated than at edges. With the increase of repeating scans, the conductive silver pattern was thick to reflect the laser irradiation, and silver NPs in the hotter area flows toward to the colder edges. Some hollow structures were also produced due to the water evaporating during laser heating process. To a certain extent, the increasing of scans can eliminate the hollow structures (Figure 5-6b(ii) and Figure 5-6c(ii)). Thus, low energy gave rise to generation of silver NPs without burning of the substrate.

The diameter and distribution of silver NPs can be observed on the SEM images. The silver NPs are generally spherical shape with a diameter of 60 nm. With the increases of the scanning repeats, more silver NPs show up on the substrates, but after 20 scanning cycles, the amount of the silver NPs seems no obvious increase. At 20 and 25 repeating scanning, a few nanoparticles clearly started to melt together, resulting in enlarged contacts between nanoparticles. These phenomena also confirmed from the EDX analysis and resistance measurement. EDX results reveals the presence of silver along with carbon and oxygen, and the atomic concentration of Ag increases with the increase of the repeating scanning numbers (Figure 5-7). In Figure 5-6f, the resistance of the silver line underwent a significantly improvement from 10 scans to 25 scans. However, although density of the silver NPs increased, the size of the silver NPs remained constant, a mean diameter of about 60 nm. Since the laser-induced temperature is still very low for every time, the silver NPs cannot further grow and sinter. The conductive silver line formed from 20 scans was also sufficiently thick to reflect the laser irradiation, thus preventing

the further heating. Moreover, the energy induced by the laser scanning is not enough for polymer removal. Due to the insulating polymeric matrix and dispersed silver NPs in it, the metallized tracks possess poor conductivity. We can conclude that the diameter and distribution of silver NPs in the cured polymer rely on the laser power. In other words, both diameter and distribution of the generated silver NPs on the surface could be well controlled through adjusting laser power, scanning speed and repeat times.

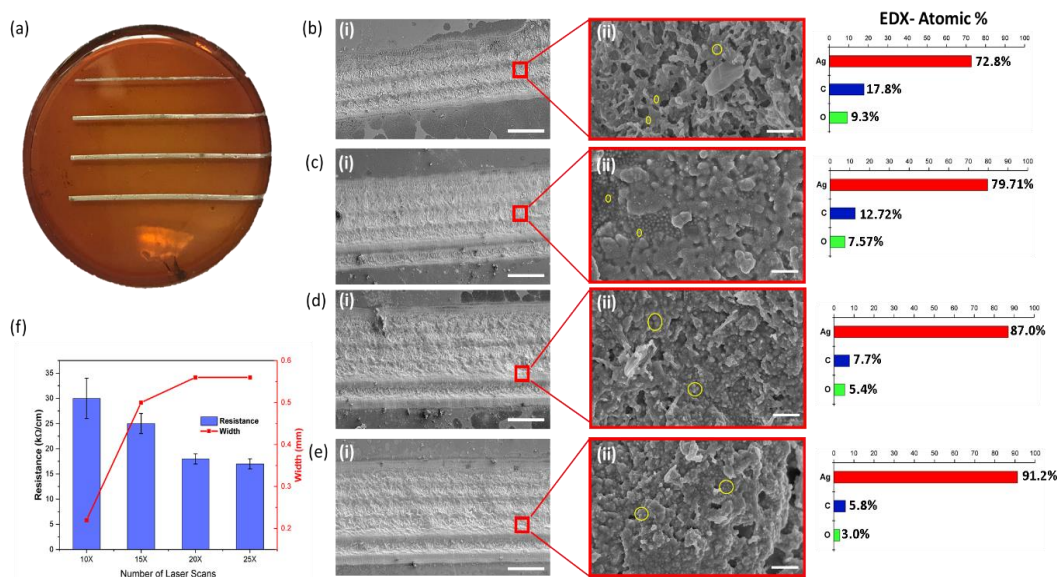


Figure 5-6: Laser metallization process with various number of scans from top: 10x, 15x, 20x, and 25x, respectively. SEM images and EDX results for silver lines with (b) 10 scans, (c) 15 scans, (d) 20 scans, and (e) 25 scans. (f) The resistance and width of the four silver lines.

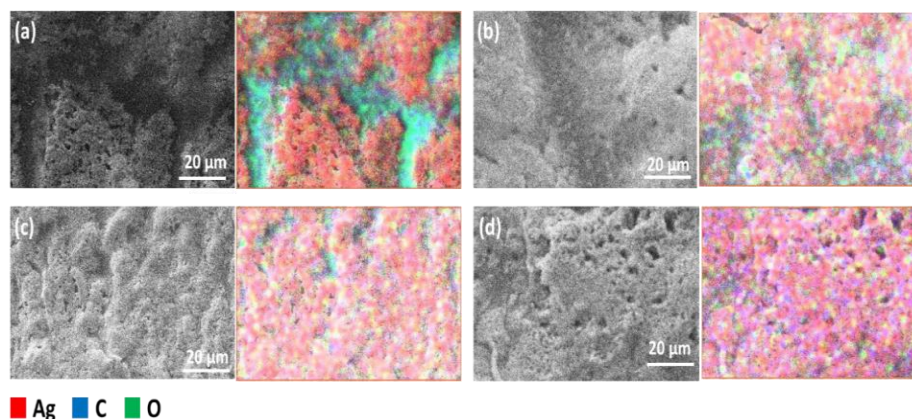


Figure 5-7: SEM images and EDX element mapping of Ag, C and O with different repeating scans: (a) 10, (b) 15, (c) 20, and (d) 25. 3D printing material is PEGDA750-15%.

On average, the resistance obtained from 25 scans was about 17 k Ω /cm. This value is comparable with the results using light and thermal treatment for a few hours, but it cannot meet requirements for most electronics fabrication. As known, the growth and sintering of silver NPs is strongly temperature dependent. Photo-crosslinkable formulations containing silver nitrate was irradiated under UV light at the light intensity 50 mW cm⁻²; with the increase of exposure time to 60 minutes, the mean diameter of single silver nanoparticle increases, and the mean distance between silver nanoparticles decreases [11]. However, because of the insufficient power of light, the surrounding polymeric matrix prevents the metal NPs from a close contact, resulting in a discontinuous trace with low conductivity. In our previous studies, with a low power DLP projector, even after 24 hours exposure the silver NPs were not observed on the printed objects surface. To further improve the conductivity of the printed tracks, higher energy should be applied to facilitate the growth of silver NPs and remove the insulating polymer.

Although low power laser can reduce silver ions into silver nanoparticle and it can protect the polymeric structures, long time exposure is always required for repeated scanning. In addition, the conductivity is very limited, prohibiting for wide applications. Thus, low energy with repeated scanning is unable to provide highly conductive silver tracks.

5.3.3 Optimization of conductivity of 3D printed electronics

From the low power laser study, we understand that one of the key limitations is that the polymer matrix is limiting the conductivity improvement, even with enough silver NPs being reduced. Thus, other than considering laser-induced reduction, the heating of the polymer is also the key to the conductivity improvement. To find suitable processing parameters for the following experiments, numerical simulation using COMSOLTM was conducted. Figure 5-8 illustrates the finite element modeling of laser heating the PEGDA (750 g mol^{-1}) substrate. The heat transfer module is isothermally surrounded by air ($T = 300 \text{ K}$), and the heat source is a Gaussian heat source with a radius of $75 \text{ }\mu\text{m}$. The temperature profiles at the center of the laser spot with different laser powers and irradiation times are shown in Figure 5-8a. The laser-induced temperature can reach to 333.14°C at a power of 5.5 W within 0.3 s , while much longer time is needed with a laser power below 3.5 W . Figure 5-8b displays the temperature profiles at the scanning speed of 10 mm/s and 20 mm/s with the laser power of 5.5 W and 3.85 W , separately. Through controlling the scanning speed, the heating depth and the temperature of the focused laser spot area can be optimized as needed. Thus, a higher laser power with adjustable scanning speed is setup to tune the affected depth of heating on the printed object at the target temperature. At first, we assume that when a target temperature is reached locally, the polymeric structures lose their polymeric shells and NPs further grow until direct physical contact with each other. As the decomposition temperature of the matrix material is about 200°C , the selective metallization of non-conductive polymeric structures can be achieved with high conductivity when the laser-induced local temperature is above 200°C . According to the primary results from the numerical computing, scanning parameters of laser scanning speed ($100 - 1200 \text{ mm/min}$) and power ($3.3 - 5.5 \text{ W}$) were selected in the following experiments.

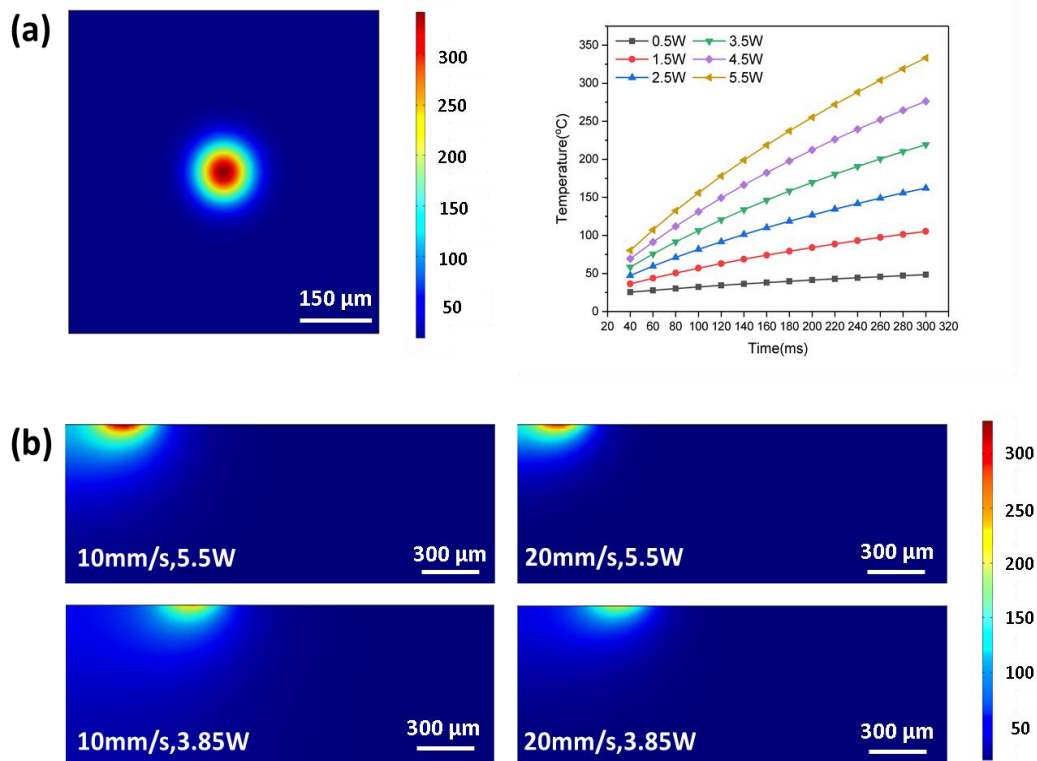


Figure 5-8: Finite element simulation of laser heating the printed object. (a) Temperature (degree centigrade) changing of samples under different laser powers and irradiation times. 9b) Simulation of temperature profiles as laser scanning speeds of 10 mm/s and 20 mm/s with 5.5 W and 3.85 W inputted power. The radius of laser focusing on the surface is 75 μm.

Once the processing parameters were investigated and optimized, the electrical properties of laser-reduced silver NPs with different materials and scanning parameters can be evaluated. In this study, straight lines were printed using a series of power and speed on different samples. Technically, when enough energy was deposited, the printed line with silver mirror effect can be observed. Then, the resistivity of the lines with silver mirror appearance were measured and calculated. The relationship between resistivity and various parameters shown in Figure 5-9a indicates that all the parameters affect the conductivity of the printed pattern. Specifically, the resistivity of the PEGDA250-5% and PEGDA250-10% are in the order of magnitude of 1 Ωm, while PEGDA550 and PEGDA750 have the similar electrical performance with different processing parameters,

ranging from 10^{-6} to $10 \text{ } \Omega\text{m}$. The low conductivity of the samples with low molecular weight was caused by its poor mechanical properties. The printed sample of PEGDA (250 g mol^{-1}) is fragile and the increasing of fine cracks occurs with the increase of the power, leading to discontinuous traces. Additionally, for PEGDA550 and PEGDA750, the decreasing speed from 1000 mm/min to 300 mm/min would improve the conductivity. At the same power, the lowest resistivity is always obtained with the speed in the range of 300 to 400 mm/min . An abrupt resistivity change of four orders of magnitude was observed (Figure 5-9b) for PEGDA750-10% case when the speed increases an additional of 100 mm/min . This phenomenon explains that the laser heating decreases the medium distance between the NPs, and there is a threshold of local temperature to form an efficient percolating path.

In our experiments, the best resistivity ($6.12 \text{ } \mu\Omega\text{m}$) was obtained from PEGDA750-15% at the power of 5.5W and the scanning speed of 300 mm/min . The result is advantageous to the resistivity ($5,280 \text{ } \Omega\text{m}$) from reported method using photoreduction [10], which is extremely high and is not feasible for a practical application let along the time-costly fabrication process. Figure 5-9b further reveals the effects of the silver content, speed and power on the resultant resistivity. The resistivity of 5 and 10 phr silver nitrate are unstable. Take the power of 5.5 W for example, the resistivity of the printed trace using PEGDA750-5% changes from $2.8 \text{ } \mu\Omega \text{ m}$ to nonconductive when the speed increases from 600 mm/min to 700 mm/min . For PEGDA750-10%, the resistivity increases of four order of magnitude when the speed changes from 700 mm/min to 800 mm/min . On the contrary, the resistivity of PEGDA750-15% and PEGDA750-20% mainly varies from 10 to $70 \text{ } \mu\Omega \text{ m}$, which meets our expectation that the higher silver content will bring a better conductivity. However, shock heating to a decomposition temperature for a short time can induce a large supersaturation of silver atoms on the polymer surface when the amount of silver nitrate is above 15 phr, so further improving silver nitrate percentage cannot significantly develop the electrical property.

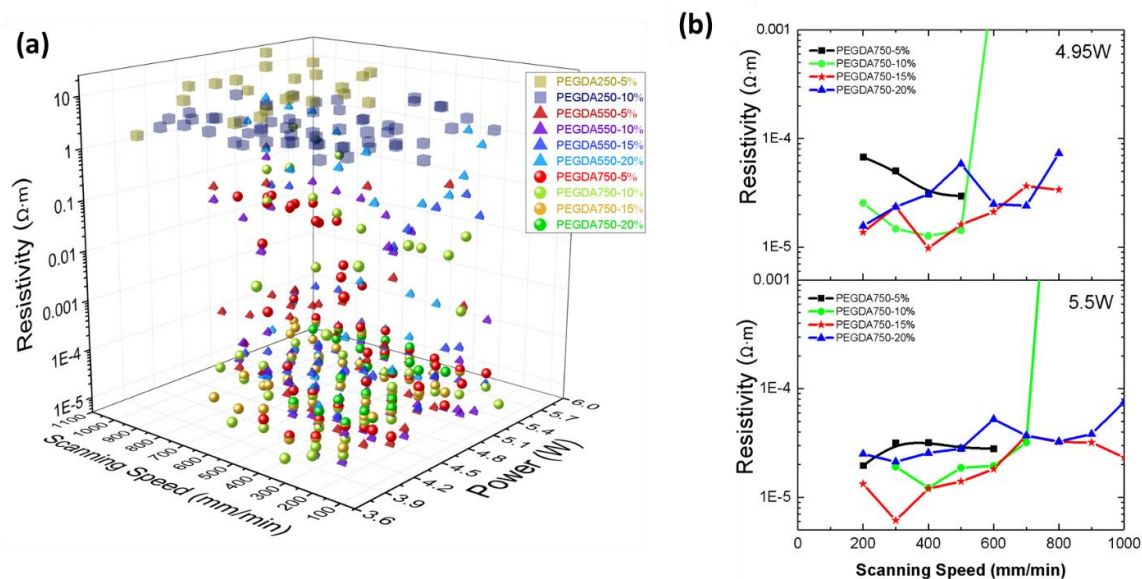


Figure 5-9: (a) Resistivity of the laser reduced and sintered silver conductive path with different powers, scanning speed, and molecular weight of PEGDA. (b) Resistivity of the silver conductive path on printed sample using PEGDA (750 g mol⁻¹) at 4.95W and 5.5W with various scanning speed.

As the printed conductive trace is defined by its microstructure, the size and distribution of the silver NPs on the printed objects were investigated by SEM to understand the relationship between the laser parameters and resistivity. The silver NPs morphology of PEGDA750-15% at different laser scanning parameters is shown as Figure 5-10. After selective laser metallization, the formation of silver NPs in the 3D structure was confirmed and an etched groove was clearly observed. In Figure 5-10a–f, at different laser scanning power, the spherical silver NPs were dispersed along the groove at the same scanning speed of 500 mm/min. According to silver NPs morphology, the resistivity of printed traces should decrease with the increasing power, which is in a good agreement with the measured resistivity of various power at the 500 mm/min in Figure 5-10. It is also noteworthy that important morphological differences, such as size, shape and distribution, clearly appears between various power, and the increase of the power results in a burned and highly porous surface, and large unstructured aggregates.

Since the increasing power brings severe damage on the 3D structure, the energy induced by the selective scanning laser were further optimized by adjusting the power and speed (Figure 5-10f–h). The speed effect is evident - wrapped structure and micro cracks were found in Figure 5-10g,h, respectively. With high scanning speed, the laser did not affect the morphology of the surface, and large aggregated NPs did not show, leading to a poor conductivity. In addition, Figure 5-10i is the sample with a post treatment at 100°C in air for 1 hour. The resistivity of the sample with thermal treatment is similar with the trace irradiated by the laser scanning at the power of 5.5 W and the speed of 1500 mm/min, indicating that comparing with the traditional heating method, selective laser metallization provides an efficient approach to generate conductive patterns. Therefore, during printing conductive traces by photosynthesis process with a secondary light source, the induced energy has a great impact on silver NPs size and distribution, which determines the conductivity of the printed traces.

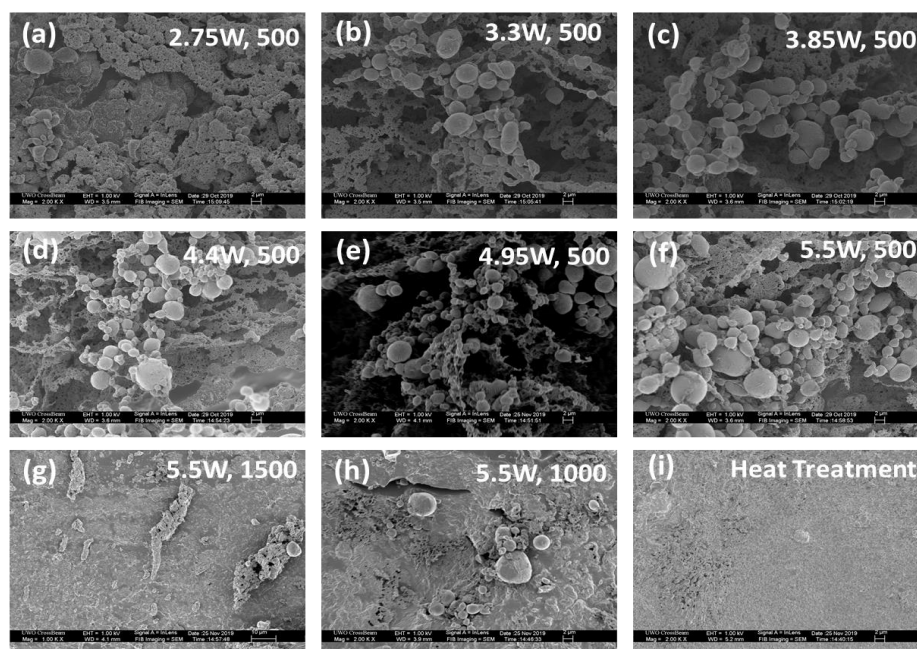


Figure 5-10: The SEM images of sintered Ag nanoparticles with different conditions. (a – f) Ag nanoparticles reduced and sintered by the laser at powers of 2.75 W, 3.3 W, 3.85 W, 4.4 W, 4.95 W, and 5.5 W with scanning speed 500 mm/min. (g – h) Ag nanoparticles reduced and sintered by the laser at scanning speed of 1000 mm/min and 1500 mm/min with 5.5W power. (i) The surface of the sample treated 1 h at 100°C in air.

In summary, the laser-induced temperature determines the silver NPs dimension and the removal of the polymeric substrate, which improves the conductivity as the silver NPs aggregation. Through the analysis of experimental results, the growth mechanisms of silver NPs in solid material was better understood. Temperature induced by the laser has been considered of great importance on conductivity since the conductivity of printed silver traces is defined by its microstructure and different particle sizes and distributions can be obtained by varying the laser processing parameters. During 3D co-printing process, 3D printed polymer structure, which can immobilize and stabilize photosynthesis silver NPs, has been demonstrated to be effective substrates for in situ generation of conductive patterns. The silver atom absorbs energy from the laser, allowing the nuclei to diffuse through the polymer matrix and grow into large particles. At a lower laser power when the induced temperature is below decomposition temperature of the solidified polymeric substrate, the localized fast heating triggers metal atom nucleation and subsequent growth, while fast quenching slows down silver NPs diffusion and freezes the particles in the polymer. When more thermal energy is deposited, particles further grows and reaches a silver mirror aspect. As shown in Figure 5-6, the amount of silver NPs was little after one scan with low energy, and with the increasing scans, more silver NPs were generated. However, owing to the existence of the polymer, both the motion and the growth of particles is retarded. When the selective area is heated above the decomposition temperature, the disappear of the polymeric material provides enough space for particles growing and sintering. Because of the gravity, the silver nuclei diffuse in space not on the surface, and the larger particle aggregation brings a better conductivity.

5.4 Demonstrations of 3D printing electronics

To highlight the ability of the proposed 3D co-printing approach on fabricating volumetric electronics, various applications were demonstrated (Figure 5-11). The samples containing multiply embedded conductive patterns were printed. In Figure 5-11a, two conductive circuits were placed in the different layer to control the illumination of a red and a green LED, respectively. Figure 5-11b shows an electronic circuit on the

surface with a RFID circuit embedded. Each circuit embedded in the sample were printed within one minute, avoiding conductive material deposition and conversion process. Furthermore, the printed traces can also connect circuits at the different layer (Figure 5-11f), and complicated patterns were printed (Figure 5-11d,e). A resistance of 7.7Ω between two points proves that the good conductivity was obtained in 3D co-printing fabrication process. Meanwhile, benefiting from in situ generation of silver NPs, selective laser metallization enables conformal printing of silver mender lines on arbitrary shapes. Here, a small 3D electrically antenna on hemispheres surface is shown in Figure 5-11c. All these features may enable several applications, including flexible, implantable and wearable antennas, and sensors.

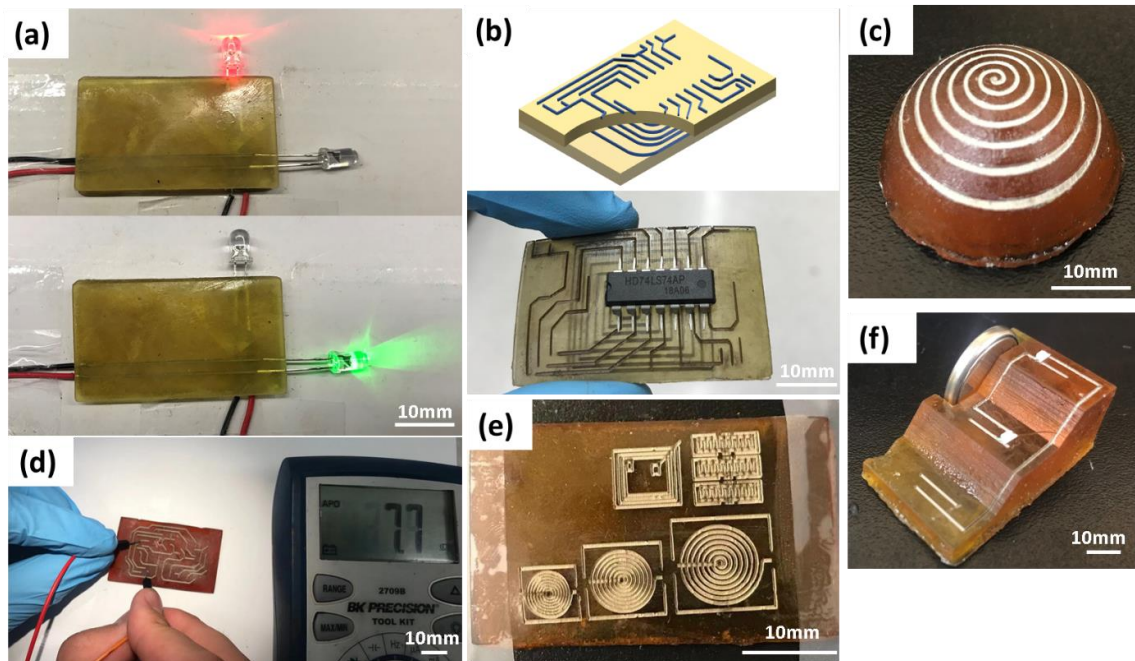


Figure 5-11: 3D printed electronics. (a) 3D printed film with conductive tracks in two different layers connecting a red LED and a green LED to power sources, respectively. (b) A RFID is printed inside a film with a chip on the surface and its 3D model. (c) A printed antenna. (d) the resistance between two points. (e) A printed film with RFID, MIM (metal-Insulator-Metal) capacitors, and inductors. (f) A structure connecting different circuits at the different layer.

5.5 Conclusions

In this study, 3D co-printing technology was proposed to fabricate 3D electronics using single material in our designed apparatus, which consists a dual light system for structure printing and conductive circuit printing. Selective laser metallization process converts the customized nonconductive polymer into conductive patterns, which can be formed both on the surface and in the structure to form a 3D circuit, eliminating the need for post treatment. Through controlling the laser power, the in-situ generation of silver NPs almost completes once the laser irradiates the surface, which vastly speeds up the fabrication process and enables printing a large number of layers containing conductive patterns possible.

Factors that influenced the performance were investigated and optimized in this study, including the formulation of the materials, laser power, scanning speed and etc. A low resistivity of $6.12 \mu\Omega \text{ m}$ was achieved with the high power and low speed of laser. This performance was much better than that from the UV irradiation or heating in the oven for long time. Additionally, the metallic traces can be printed on arbitrary structures in a simplified manner, offering a wide application in electronics market, such as electrical devices, sensors, wearable electronics and antennas.

With the dual light source system, the newly developed 3D printer can produce embedded silver circuits, which has enabled an unprecedented fabrication capability of 3D printing electronics based on one single material. This 3D co-printing technique is efficient, inexpensive, compact, and can even be applied to generate different size of silver NPs in 3D printed structures through properly adjusting the parameters.

References

1. Fantino, E., et al., *3D printing of conductive complex structures with in situ generation of silver nanoparticles*. *Advanced Materials*, 2016. **28**(19): p. 3712-3717.
2. Fantino, E., et al., *In Situ Thermal Generation of Silver Nanoparticles in 3D Printed Polymeric Structures*. *Materials*, 2016. **9**(7): p. 589.
3. Wang, X., et al., *Blue Laser Projection Printing of Conductive Complex 2D and 3D Metallic Structures from Photosensitive Precursors*. *ACS Applied Materials & Interfaces*, 2019. **11**(24): p. 21668-21674.
4. He, R., et al., *Fabrication of complex-shaped zirconia ceramic parts via a DLP-stereolithography-based 3D printing method*. *Ceramics International*, 2018. **44**(3): p. 3412-3416.
5. Na, K., et al., *Effect of solution viscosity on retardation of cell sedimentation in DLP 3D printing of gelatin methacrylate/silk fibroin bioink*. *Journal of Industrial and Engineering Chemistry*, 2018. **61**: p. 340-347.
6. Wang, X., et al., *i3DP, a robust 3D printing approach enabling genetic post-printing surface modification*. *Chemical Communications*, 2013. **49**(86): p. 10064-10066.
7. Yin, X.-Y., et al., *Monolithic Dual-Material 3D Printing of Ionic Skins with Long-Term Performance Stability*. *Advanced Functional Materials*, 2019. **29**(39): p. 1904716.
8. Macdonald, N.P., et al., *Comparing Microfluidic Performance of Three-Dimensional (3D) Printing Platforms*. *Analytical Chemistry*, 2017. **89**(7): p. 3858-3866.
9. Chiolerio, A., L. Vescovo, and M. Sangermano, *Conductive UV-Cured Acrylic Inks for Resistor Fabrication: Models for their Electrical Properties*. *Macromolecular Chemistry and Physics*, 2010. **211**(18): p. 2008-2016.
10. Chiolerio, A. and M. Sangermano, *In situ synthesis of Ag-acrylic nanocomposites: Tomography-based percolation model, irreversible photoinduced electromigration and reversible electromigration*. *Materials Science and Engineering: B*, 2012. **177**(4): p. 373-380.
11. Roppolo, I., et al., *Dual step irradiation process for in situ generation and patterning of silver nanoparticles in a photocured film*. *RSC Advances*, 2016. **6**(18): p. 14832-14843.

Chapter 6

6 Conclusions and future directions

For functional 3D printing application, a bioinspired approach is developed to engineer new 3D printing materials with active additives, including dopamine, modified-dopamine and natural plants derived polyphenols. The active chemical groups on the printed surfaces enables 3D printing of functional materials/devices possible, focusing on metallization application. Further, a dual-light 3D co-printing technology is developed to realize selective metallization process.

6.1 Conclusions

A bio-inspired additive, dopamine, was firstly employed by 3D printing materials to realize functionalization. Due to the hydrophilic nature of dopamine, dopamine aqueous solution can be dissolved into water-soluble UV resin with a high concentration. This catechol-functionalized UV resin can efficiently deposit metal particles, such as silver, copper and nickel, on the surface of the 3D printed objects. According to the experimental results, the high metal-binding ability of the catechol groups was verified. Also, the amine group was confirmed improving the silver deposition and growth. It is interesting to note that a high conductive silver layer was formed ($0.1246 \Omega/\text{sq}$) through silver nitrate treatment using UV resin with dopamine solution. The coexistence of catechol and amine group has facilitated silver deposition and growth. This strategy provides a simple solution to develop a water-soluble resin with metallization capability.

A robust and universal additive was further developed to be adopted in a wide range of 3D printing materials. Since acrylic resin is the mostly used materials for stereolithography-based 3D printing, we improved the solubility of dopamine in acrylic resin through chemical modification. The synthetic dopamine, DMA, has an excellent solubility in acrylic oligomer up to 6 wt%. After photopolymerization of UV resin with DMA, the catechol group presented on the surface allows silver ions reduction effectively, serving as the catalyst for ELP process to deposit robust metal layers. It is proved that the modified dopamine is highly effective to make 3D printing UV resins

practical in the fabrication of functional materials, and show great potential in the fields of electronics.

Noting previous success with dopamine, catechol group was identified as the functional group for multifunctional coating precursors. Plant phenol and polyphenol possessing a remarkable abundance of catechol and gallol groups are of interest to the research community. Through screening of natural (poly)phenols, two phenols (PG and Ctl) were selected as candidate initiators due to their good solubility in all types of resins and capability of silver ion reduction. It is proved that 1 wt% of PG is sufficient to reduce silver ions for metallization purpose, and the printability of PG-integrated is well maintained. With the assistance of 3D printing technology, actuator, heat-resisting electronics, and flexible electronics were manufactured. Besides the application of electronics, the introducing of catechol group can also be used for water treatment and tailoring the surface properties.

I3DP II technology provides a simple yet robust method to tailor the surface properties of the 3D printed objects. In this study, the initiators can be compatible with most 3D printing materials, developing functional 3D printing material in a simple method. Coupling with fabrication capability of the original materials, the integrated initiators enable a wide range of functionalities after the secondary reactions. As the existence of the catechol groups in the highly cross-linking network, the initiators are stable in various environment with superior adhesion and all the functionalities can be re-obtained.

So far, following the thinking of i3DP II, three categories of additives were proposed to integrate the active chemical groups into 3D printing materials. However, the introduction of active groups causes the entire surface to be metallized, which is conflicted with the fabrication of electronics that patterning of circuits by selective metallization are required. It is therefore required to develop a highly selective metallization process. In this study, we reported a new strategy - 3D Co-printing technology by collaboratively employing two photopolymerization processes - to fabricate 3D electronics selectively either deposited on a free-form surface or embedded within a bulk structure. The 3D Co-printing technology only involves one printing

material, which works for both the construction of polymeric structure and the metallization process of conductive circuits because of the introduced metal precursor in photosensitive resin. Due to the existence of metal precursor, metal NPs can be efficiently photosynthesized after laser scanning. 3D Co-printing technology addresses the challenge of conventional methods requiring multiple deposition processes. The resultant trace which is composed of NPs exhibits a superior resistivity as low as $\sim 6.12 \mu\Omega \text{ m}$. The resistivity is further controllable ranging from 10^{-6} to $10 \Omega\text{m}$ through adjusting the material formulation and processing parameters. The validation and demonstration in this study verify the proposed 3D Co-printing as a high-efficiency and low-cost co-printing approach which opens a new avenue of making 3D electronics.

6.2 Future work

One of the major difficulties in 3D printed electronics is the conductivity because of the poor conductivity of printing materials. More and more challenges in the fields of material types and processing challenges in the process of 3D integrated objects. Therefore, the compatible material sets should be explored and created to provide the adequate functionality and manufacturability for the product invention by designers. Besides, repairing is especially important concern for traces that are embedded within a structure and not on the surface. It is believed 3D printing will be applied to more and more functional electronics and the related products, and it will provide a powerful tool for innovative product development, although there is still a long way to go for either high-value added products or industrial-level applications. Further potentials of 3D printing electronics need still to be explored and investigated.

In terms of 3D printing materials for electronics, phenol and polyphenols have attracted considerable interests as their important biological activities, and intriguing chemical and physical properties. Especially, they are derived from natural plants or fruits, which can be sources in the by-product in the biomass production. Thus, the application is attractive for a sustainable economy. More functionalities of the polyphenols integrated strategy for 3D printing functional materials can be developed. In addition, other kinds of surface modification technologies can be further extended.

At last, a catechol-integrated 3D printing material will be applied into the 3D co-printing techniques, so as to realize selectively ELP process for the printed objects. From previous study, the self-polymerization of polyphenolic compounds can be accelerated by UV irradiation [1, 2], and phenol degradation can be realized with UV irradiation and the presence of an oxidant agent [3]. The effects of the UV light on catechol group chemical properties allow the adaptation of the catechol-integrated UV resin into 3D co-printing technique, resulting in selective metal deposition.

References

1. Behboodi-Sadabad, F., et al., *Bioinspired Strategy for Controlled Polymerization and Photopatterning of Plant Polyphenols*. *Chemistry of Materials*, 2018. **30**(6): p. 1937-1946.
2. Behboodi-Sadabad, F., et al., *UV-Triggered Polymerization, Deposition, and Patterning of Plant Phenolic Compounds*. *Advanced Functional Materials*, 2017. **27**(22): p. 1700127.
3. Li, H., et al., *Catechol degradation on hematite/silica–gas interface as affected by gas composition and the formation of environmentally persistent free radicals*. *Scientific Reports*, 2016. **6**(1): p. 24494.

Curriculum Vitae

Name: Junfeng Xiao

Post-secondary Education and Degrees: North China Electric Power University
Baoding, Hebei, China
2009-2013 B.A.

The University of Western Ontario
London, Ontario, Canada
2014-2015 M.A.

The University of Western Ontario
London, Ontario, Canada
2016-2021 Ph.D.

Honours and Awards: The third-class scholarship
2010-2011, 2011-2012

Honorable title of Advanced Individual in Volunteer Service
2011-2012

Third prize in National University Student Social Practice and Science Contest on Energy Saving and Emission Reduction
2011-2012

Related Work Experience Research Assistant
The University of Western Ontario
2015-2016

Publications:

Xiao, J., Zhang, D, Guo, Q., & Yang, J. “Dopamine assisted metallization process in water soluble 3D printing resin”, *Additive Manufacturing*, under review.

Xiao, J., Zhang, D, Yin. X., Guo, Q., & Yang, J. “A modified-dopamine customized UV resin for Electroless metallization in 3D printing”, *Research*, under review.

Xiao, J., Zhang, D, Yin X., Guo, Q., & Yang, J. “Metallization and functionalization of 3D printed polymers assisted with Polyphenols”, *Advanced Materials*, under review.

Xiao, J., Zhang, D, Guo, Q., & Yang, J. “3D Co-printing of 3D electronics with a dual light source technology”, *Advanced Functional Materials*, under review.

Zhang, D., **Xiao, J.**, Bai, Y., Guo, Q., Zheng, M., Liu, M., ... & Yang, J. (2020). Introducing Bioinspired Initiator into Resins for In Situ Repairing of 3D-Printed Metallic Structures. *ACS Applied Materials & Interfaces*, 12(43), 49073-49079.

Zhang, D., **Xiao, J.**, Guo, Q., & Yang, J. (2019). 3D-printed highly porous and reusable chitosan monoliths for Cu (II) removal. *Journal of Materials Science*, 54(8), 6728-6741.

Wang, Y., **Xiao, J.**, & Chen, X. (2019). New structure of pneumatic networks actuators for soft robotics. *The Journal of Engineering*, 2019(13), 273-277.

Zhang, D., **Xiao, J.**, Yu, W., Guo, Q., & Yang, J. (2018). Hierarchical metal/polymer metamaterials of tunable negative Poisson's ratio fabricated by initiator-integrated 3D printing (i3DP). *Nanotechnology*, 29(50), 505704.

Cai, X., **Xiao, J.**, Zhang, H., Zhang, Y., Hu, G., & Yang, J. (2018). Compact acoustic double negative metamaterial based on coexisting local resonances. *Applied Physics Letters*, 113(24), 244101.

Zhang, D., **Xiao, J.**, Moorlag, C., Guo, Q., & Yang, J. (2017). Development of ultralight, super-elastic, hierarchical metallic meta-structures with i3DP technology. *Nanotechnology*, 28(45), 455708.

Zhang, D., **Xiao, J.**, Qiu, Y., Yang, J., & Guo, Q. (2017). Initiator-integrated 3-D printing of magnetic object for remote controlling application. *IEEE Transactions on Magnetics*, 53(5), 1-9.

Yin, X. Y., Zhang, Y., **Xiao, J.**, Moorlag, C., & Yang, J. (2019). Monolithic Dual-Material 3D Printing of Ionic Skins with Long-Term Performance Stability. *Advanced Functional Materials*, 29(39), 1904716.

Wang, Y., Liu, Y., **Xiao, J.**, & Huang, H. (2018). Choice of Shaping Linkage-Methods on Pascal Limacon Gears. *Recent Patents on Mechanical Engineering*, 11(3), 225-231.

Peng, T., Guo, Q., Yang, J., **Xiao, J.**, Wang, H., Lou, Y., & Liang, X. (2019). A high-flow, self-filling piezoelectric pump driven by hybrid connected multiple chambers with umbrella-shaped valves. *Sensors and Actuators B: Chemical*, *301*, 126961.

Fantino, E., Roppolo, I., Zhang, D., **Xiao, J.**, Chiappone, A., Castellino, M., ... & Yang, J. (2018). 3D printing/interfacial polymerization coupling for the fabrication of conductive hydrogel. *Macromolecular Materials and Engineering*, *303*(4), 1700356.

Cai, X., Zhao, S., Hu, M., **Xiao, J.**, Zhang, N., & Yang, J. (2017). Water based fluidic radio frequency metamaterials. *Journal of Applied Physics*, *122*(18), 184101.

Yin, X., Zhang, Y., Guo, Q., Cai, X., **Xiao, J.**, Ding, Z., & Yang, J. (2018). Macroporous double-network hydrogel for high-efficiency solar steam generation under 1 sun illumination. *ACS applied materials & interfaces*, *10*(13), 10998-11007.